Data driven predictive modelling for Archean lode gold potential, Bubi greenstone belt, southwest Zimbabwe.

Gilbert Mhlanga

March, 2002

Data driven predictive modelling for Archean lode gold potential, Bubi greenstone belt, southwest Zimbabwe.

by

Gilbert Mhlanga

Thesis submitted to the International Institute for Geo-information Science and Earth Observation in partial fulfilment of the requirements for the degree in Master of Science in *Mineral Resources Exploration and Evaluation*.

Degree Assessment Board

Thesis advisor	Dr. E. M. J. Carranza
	Prof. M. Hale
Thesis examiners	Prof. M. Hale (Chairman)
	Dr. A. B. Westerhof (Member)
	Dr. S. Barrit (Member)
	Dr. H. de Boorder (External Examiner), I. v. A. U Utrecht

INTERNATIONAL INSTITUTE FOR GEO-INFORMATION SCIENCE AND EARTH OBSERVATION

ENSCHEDE, THE NETHERLANDS

Disclaimer

This document describes work undertaken as part of a programme of study at the International Institute for Geo-information Science and Earth Observation (ITC). All views and opinions expressed therein remain the sole responsibility of the author, and do not necessarily represent those of the institute.

Abstract

Predictive models for Archean lode gold potential in the Bubi greenstone belt were developed using probabilistic spatial data analysis and integration. Datasets used include gold deposits records, geological maps, structural maps, aeromagnetic and ASTER imagery. Geological features indicative of Archean lode gold potential were extracted from the geoexploration data-sets for use as inputs in the predictive model, based on the conceptual model for Archean lode gold deposits. The indicative geological features include lithological units, proximity to the granite-greenstone contact, shear and deformation zones, foliation and s-fabric, fold axes, hydrothermal alteration zones and aeromagnetic lineaments (conduits for mineralizing fluids). Hydrothermal alteration zones, associated with gold mineralization were extracted from ASTER data using the Crosta technique. The syn-to late-tectonic granitoid intrusions supplied the heat and/or hydrothermal fluids, responsible for gold mineralization while the rest of the structures acted as depositional sites for the gold deposits. The known gold deposits show spatial association with the geological features. Quantitative analysis of the spatial associations between the gold deposits and the different geological features was carried out. A total of 201 gold deposits occur in the study area. The 147 small deposits were used for predictive modelling while the 51 large deposits were used for model validation. The input maps were buffered and the optimum distance of spatial association determined by calculating the studentized contrast. The seven feature maps were converted to binary predictor patterns and used as evidential layers for predictive modelling of gold potential. The binary patterns were integrated in combinations of three in order to avoid over prediction due to integrating conditionally dependent patterns. Five maps of posterior probability, representing mineral potential were created. All the mineral potential maps include the lithological units and granite-greenstone contact binary patterns in combination with the foliation and s-fabric, shear and deformation zones, fold axial traces, deep seated discontinuities and alteration binary patterns respectively. The five mineral potential maps define broadly coincident favorable areas (up to 53% of the study area is indicated as having at least some favorability). The models correctly predict between 60% and 86% of the validation deposits. New target areas were generated, especially in the northern parts of the greenstone belt. Field checks and follow up work are recommended in these areas. It is also recommended that stream sediment geochemical sampling be carried out and the results incorporated in the predictive model.

Keywords

Conceptual mineral deposit model, Archean lode gold deposits, greenstone belt, Bayesian probability, weights of evidence, spatial association, mineral potential

Acknowledgements

I would like to thank all the people who contributed in various ways to the successful completion of this work. I am indebted to Prospecting ventures Limited (Zimbabwe), particularly the then manager Mr C. Z. Murahwi for purchasing most of the data-sets required for the research. I am grateful to the Netherlands government who provided funding through the Netherlands Fellowship Programme, the Zimbabwean government for endorsing my application for a fellowship and Mr W. Magalela of Rock Steady Geo-consult for encouraging me to pursue further study abroad.

My gratitude goes to my co-supervisors Prof. M. Hale and Dr. E. M. J. Carranza who meticulously went through all my work and gave invaluable advice. I acknowledge Dr. A. B. Westerhof, Drs. B. Desmeth and Drs. F. van Ruitenbeek of the Mineral Resources Exploration and Evaluation Division (ITC) and Professor C. V. Reeves of the Geophysics Division (ITC) for their comments on my work. All ommisions, errors and oversights in this work are my sole responsibility

I acknowledge the support and encouragement of my friends and colleagues in the ITC student community. Last but not least, to my wife Rosweeter and all members of my family, I say thank you for your support, understanding and long-suffering.

Dedicated to Nomagugu Samantha Mhlanga and her siblings.

Contents

List of Tables

List of Figures

Chapter 1

Background

1.1 Introduction

Zimbabwe produces an average of 15 to 20 tonnes gold per annum, contributing significantly to world gold production. Most of this production comes from Archean age lode gold deposits. A lode deposit is defined as a mineral deposit consisting of veins, veinlets, disseminations, or planar breccias. These deposits occur in consolidated rocks as opposed to placer deposits. Historically, the mined deposits were high grade (about 6 to 35 g/t Au). Developments in bulk mining and extraction technologies have permitted the exploitation of lower grade deposits (1 to 5 g/t Au). The sale of gold in the international markets generates much needed foreign currency for the country. The mining industry is therefore an important component of the Zimbabwean economy. It contributes 8 % to GDP and employs approximately 6000 people [35].

In Zimbabwe the oldest rocks belong to the Archean craton. The gold deposits are dominantly hosted by these ancient rocks. The Zimbabwe lode gold deposits have produced $>$2200 tonnes gold [32]. The Archean rocks comprise greenstone belts that are separated by extensive areas ($>$70 %) of granites and gneisses. The main lithostratigraphic divisions of the Bulawayo-Bubi greenstone belt and the location of the study area on the Zimbabwe craton are shown on Figure 1.1.

In greenstone belts, gold mineralization occurs mainly as vein type or shear zone hosted disseminations. Most of the larger deposits are found within the greenstone belts or their contacts with the granitoids. The occurrence of gold deposits in second and third order structures is well known. Examples exist from most greenstone belts of the world, including the Bulawayo-Bubi greenstone belt [28].

Area selection in mineral exploration is based on the presence or absence of specific geological features or geophysical and geochemical features that reflect geological features. Conceptual genetic models for Archean lode gold mineralization are thus important for setting criteria for modelling areas that are likely to host gold deposits [2]. Conceptual modelling research, mainly in Australia and Canada, has resulted in the recognition of features that

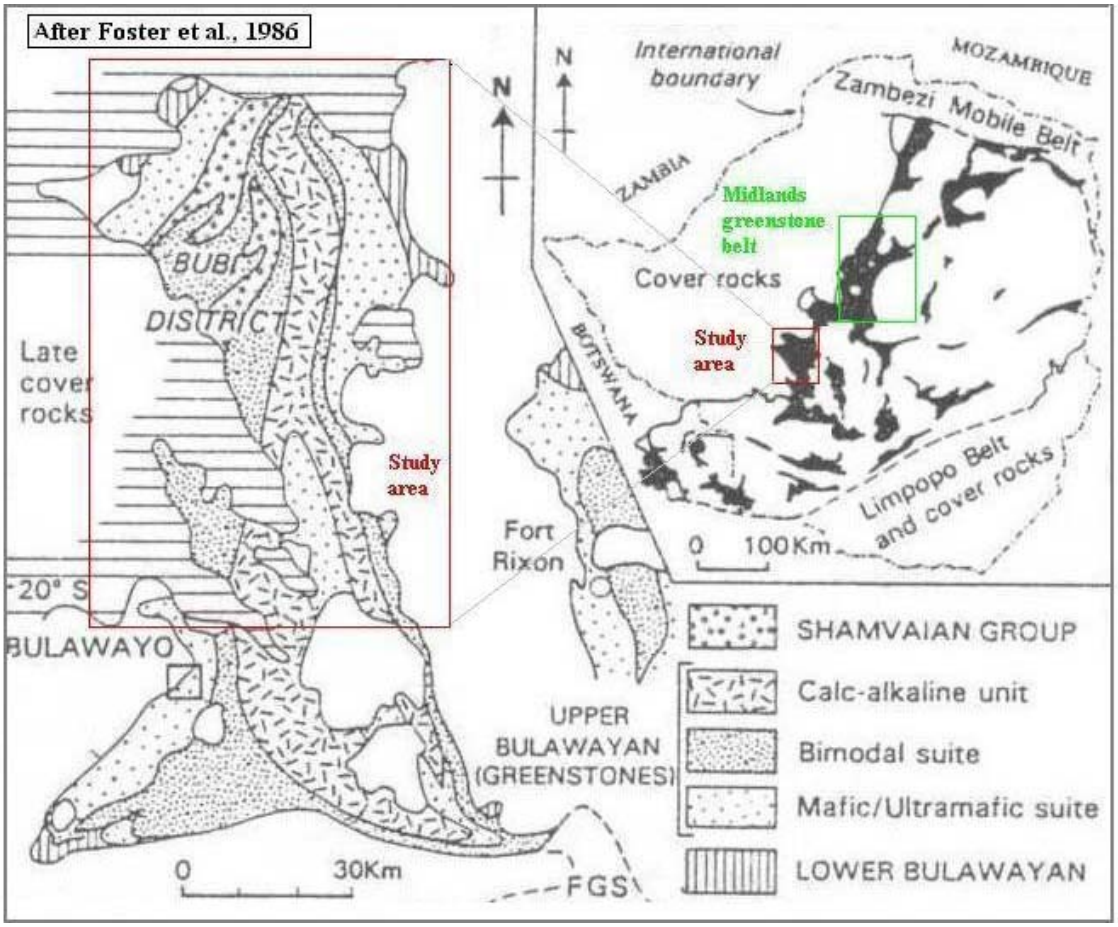

Figure 1.1: Main stratigraphic divisions of the Bulawayo-Bubi greenstone belt; inset map; Zimbabwe craton showing location of study area and the Midlands greenstone belt.

are common to Archean gold mineralization. Gold mineralization tends to take place late in the deformation history of the individual greenstone belts, irrespective of the host rocks. The gold occurs as quartz-carbonate lode deposits associated with hydrothermal alteration haloes. The gold occurs in association with a variety of sulphide minerals. Arsenopyrite is the most common sulphide mineral in meta-sedimentary host rocks, whereas pyrite or pyrrhotite are more typical in metamorphosed igneous rocks [12]. Close to and at the surface, the sulphide minerals are oxidized to iron oxides. Albite, sericite or fuchsite, chlorite, scheelite and tourmaline are common gangue minerals in greenschist host rocks. In addition to structural and lithological guides, hydrothermal alteration haloes formed during the emplacement of the gold deposits and the iron oxide enriched zones resulting from the oxidation of sulphides are valuable guides in the search for gold deposits. More research is required for a more complete formulation of Archean lode gold mineralization conceptual models as these are still not well understood [16, 12].

Spatial information analysis and integration in a GIS environment facilitates the process of selecting areas that are most likely to host mineral deposits [2]. Application of GIS in gold exploration has the potential for large exploration cost savings in that areas of obvious unsuitability can be easily recognized and eliminated leaving areas that show favorable conditions.

1.2 Problem definition

1.2.1 Background

A large proportion of Zimbabwean gold production comes from the Midlands greenstone belt, where intensive studies on gold mineralization were carried out during the early nineteen nineties. The Midlands Goldfield Project, a programme of structural mapping, gold exploration and training of personnel was carried out in Zimbabwe between 1989 and 1993. The project was subsequently extended by sixteen months so that the research could be extended to cover all the major greenstone belts of the Zimbabwe craton. Techniques applied during the project included remote sensing, particulary the use of satellite and aeromagnetic imagery , together with structural analysis techniques [27, 24]. GIS modelling was not included during the Midlands Goldfield Project. The major output of the project was a compilation of the regional structural framework of the Midlands greenstone belt.

1.2.2 Motivation for this research

Identification of areas prospective for gold mineralization within the Bubi greenstone belt will stimulate foreign investment in the area resulting in job creation in gold mining and downstream industries in Zimbabwe. This will contribute to economic development and improve living standards of the local people in the impoverished rural areas.

An investigation of the usefulness of GIS-based predictive modelling in the study area is considered important due to the following observations:

- Most gold deposits with field recognizable surface expressions in the Zimbabwe greenstone belts have already been found and exploited. There is therefore a need to find new deposits, or to identify extensions of known ore bodies by re-mapping existing mining camps.
- Modern mining and extractive techniques now permit efficient exploitation of large, low grade deposits which have been overlooked, or simply not considered as viable propositions in the past.
- The success of the Zimbabwe gold mining industry has largely been sustained by a high gold price, improved benefaction methods and exploration or development in and around existing mines. No important gold camps have been discovered in the recent past.

1.2.3 Research Problem

The Midlands greenstone belt is the only one that was intensively studied during the Midlands Goldfield Project [27, 25]. The rest of the Zimbabwe greenstone belts, including the Bubi greenstone belt were studied in far lesser detail. However, it is believed that there is still potential for finding more gold deposits within these greenstone belts particulary in the northwest Bubi area within the Bubi greenstone belt, where low-grade high-tonnage gold deposits were discovered within known gold camps (eg. the Isabella-Motapa gold camp in the northwestern part of the study area) during the 1990s.

The Bubi greenstone belt has been a major gold producer since the beginning of modern mining in Zimbabwe, around the turn of the last century. The biggest producer in the area to date is Lonely mine (34.93 tonnes @ 17.5 g/t). The greenstone belt attracted a lot of exploration capital in the 1990s. Parties involved included a Canadian junior, Casmyn (Lonely and Turk mines, production of 34.93 and 16.52 tonnes gold respectively, up to 1992) and two majors, Anglo American (Isabella and Motapa mines, production of 0.56 and 9.47 tonnes gold respectively, up to 1992) and Ashanti (Lonely mine) [26]. In all the exploration and mining campaigns within the Bubi greenstone belt, application of computer based GIS techniques were minimal. In order to sustain exploration investment in the Bubi greenstone belt, there is need to integrate data in order to delineate other prospective areas.

Accurate and up-to-date geological maps are essential in the search for minerals, as they represent the most basic information for directing exploration activities. The geological map of the central part of the Bubi greenstone belt was produced in 1928 and is therefore outdated. The existing geological maps are of different quality, with lithological units having been mapped differently along strike in some cases. The geological maps of the area will be up-dated before integration with the rest of the spatial data.

1.3 Research objectives

This study seeks to generate a rapid, efficient and cost effective way of locating gold deposits in the study area using computer aided spatial data analysis and integration in a GIS environment.

The main objectives of this research are:

1. to define geological features that are spatially associated with Archean lode-gold deposits using a conceptual model and extract these geological features from the data-sets of the Bubi greenstone belt.

2. to quantify the spatial associations between known gold deposits and the geological features and use the quantified spatial associations to develop models capable of predicting areas favorable for Archean lode gold mineralization.

1.4 Resources

1.4.1 Available data

The available data for this study comprises:

1. **Topographic data**
   Scale 1:50 000, Obtained from the Surveyor general's Office, Zimbabwe.
2. **Geological literature and maps**
   Obtained from the Zimbabwe Geological Survey (ZGS).
   - Gold deposits data. Point map at scale 1:100 000.
   - Geological descriptions, grade and tonnage data for individual mines.
   - Landsat TM imagery. Structural interpretation map of Landsat TM scene 171-073 . Structural interpretation was carried out by the British Geological Survey Remote Sensing and Image Analysis Group as part of the Midlands Goldfield Project [27].
   - Bulletins on the regional geology of the Bulawayo and Lonely mine areas and accompanying geological maps. These bulletins includes brief treatment of mine geology and gold production statistics.
   - Geological maps covering the Gwampa Valley and the Queens Mine areas. There are no descriptive bulletins accompanying these maps.
3. **Digital aeromagnetic data**
   An airborne magnetic survey covering the southwestern parts of Zimbabwe was conducted by Sanders Geophysics Ltd, during the period 1988 to 1989. Line spacing is 1000m with about 150m ground clearance (nominal flight height). Flight line direction is NW-SE, perpendicular to the general strike direction of the greenstone belts in the area. The data was obtained from the ZGS as digital total magnetic intensity data (*.gxf and *.grd files).
4. **ASTER data**
   ASTER level 1B images (with system radiometric corrections applied) where requested from http://edcdaac.usgs.gov/asterondemand/index.html. The images were acquired on 01-09-2001 at approximately 08:24 Hrs and on 04-11-2001 at approximately 08:22 Hrs respectively. Each data set comprises three scenes.

1.4.2 Software

The software used in this study are listed in Table 1.1.

1.5 Research methodology

This study deals with the integration of multiple spatial data sets to map the gold potential of the Bubi greenstone belt. The following steps were carried out in order to achieve the objectives of the study.

Table 1.1: Software used in this study

Activity	Software
Tabular data manipulation	Microsoft Excel
Digitizing and map editing	ILWIS 3.0, surfer
ASTER image processing	ILWIS 3.0
Aeromagnetic Image processing	Oasis montaj
Data analysis and integration	ILWIS 3.0
Typesetting	WinEdt, Latex

1. Review literature pertinent to Archean lode gold deposits.
2. Input spatial data into a geographic information system (GIS).
3. Extract geological features to be used as evidential layers from the data-sets and quantify their spatial associations with small gold deposits (model deposits) by calculating weights and studentized contrasts.
4. Create binary predictor patterns using studentized contrasts and weights calculated in step 3 above.
5. Integrate the binary predictor patterns using the weights of evidence method to produce probabilistic gold potential maps.
6. Validate the gold potential maps by crossing each of them with the large gold deposits (validation deposits) and noting the proportion of the large gold deposits within favorable areas on the gold potential map.

A flow chart of the research methodology is shown on Figure 1.2.

The initial formats of the data and how they were transformed into evidential layers for use as inputs in the predictive models are indicated in the flow chart. Below is a brief description on the processing staeps carried out on the data to create binary predictor patterns.

1. **Mineral occurrence data**.
   The hard copy map of gold deposits was digitized. The gold deposits were separated into small (cumulative production $< 1 - 100$kg) and large deposits (cumulative production > 100kg). The two classes of gold deposits will be used for developing the predictive models and validating them respectively.
2. **Geological maps**.
   Geological maps were digitized as segment maps from scanned paper maps using ILWIS 3.0 software. The four geological maps were digitized separately and then glued together and slightly modified using information from ASTER imagery and airborne magnetics. The glued map was polygonized to produce areas representing different rock units. Faults were digitized as segments from the Gwampa Valley map sheet. The other map sheets have scant structural data.

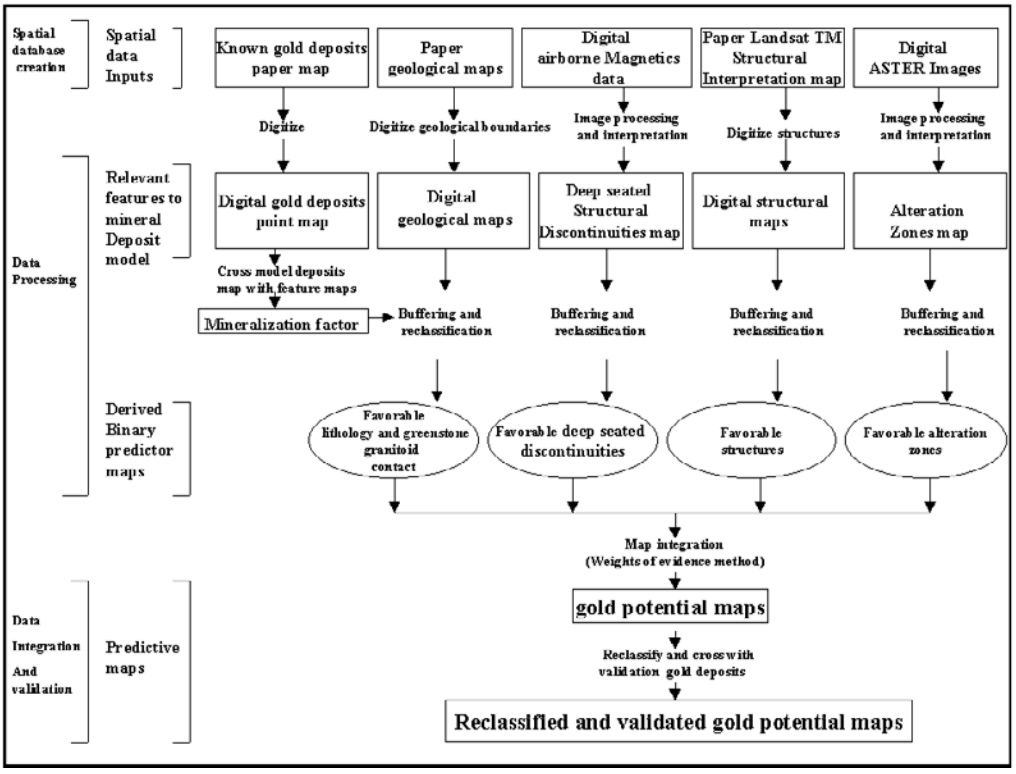

Figure 1.2: Flow chart of methodology for predictive modelling of gold potential.

3. **Airborne magnetic data**.
   Airborne magnetic data were processed to map magnetic lineaments. Magnetic lineaments represent deep seated first order shears. The lineaments were interpreted and digitized as segments.

4. **Landsat TM structural interpretation map**.
   The shear/deformation zones, foliation/s fabric and fold axial traces were digitized as separate segment maps.

5. **ASTER data**.
   ASTER level 1B images were ordered through the internet and geometrically corrected. The Crosta technique was used to map alteration zones. The mapped alteration zones were digitized as segments and polygonized.

1.6 Summary

A GIS (ILWIS 3.0) was used to manipulate and transform the data in order to extract features relevant to Archean lode gold mineralization. The conceptual deposit model for Archean lode gold deposits was used for the identification of features indicative of gold mineralization. The feature maps were converted to binary predictor patterns and were used as evidential layers for predictive modelling of gold potential in the study area. Quantitative analysis of

the spatial associations of the gold deposits and the different geological features was carried out during generation of predictive models for Archean lode gold deposits in the Bubi greenstone belt. Ranked target areas with characteristics favorable for gold mineralization were generated through reclassification of the mineral potential maps. The reclassified mineral potential maps were finally validated using the large gold deposits that occur in the study area.

Chapter 2

Study area

2.1 General information

2.1.1 Location and access

The study area is located in southwestern Zimbabwe. Its southern boundary approximately is approximately 15 kilometers north of the city of Bulawayo. The area lies between latitude 19^o 00' N and 19^o 40' N, and longitude 28^o 30' W and 29^o 00' W, (Figure 1.1). The area is approximately 4500 km^2. The main access route to the area is a tarred road which connects the city of Bulawayo and Victoria Falls, a tourist resort town at the international boundary with Zambia. A network of good, all-weather roads leading mainly to farming settlements and gold mines exists within the area.

2.1.2 Physical features

The area is fairly flat, but the flatness of the landscape is broken in places by isolated hills and ridges composed of resistant rocks, mainly banded iron formation and mafic intrusions. The highest point in the study area is the Ndumba hill (altitude 1500 m). The lowest area is where the Mbembesi river leaves the area (altitude 1200 m).

The study area is part of the Zimbabwe plateau and is drained by five north-westerly flowing rivers, which are all tributaries of the Gwayi river. The southwest part of the area is drained by the Umguza and the Insuza rivers. The Mbembesi river and its major tributary, the Inkwenkwezi river, have sources in the main watershed of Zimbabwe. The two rivers combine within the study area and drain the greater part of it. The Bubi river, whose head waters have been captured by the Longwe river, a tributary of the Shangani river lying approximately 3 kilometers north west of the study area, rises within the study area.

2.1.3 Climate and vegetation

The area is semi-arid, with two distinct seasons, a cool dry season and a hot wet one. The mean temperature for June and July, the coldest months is maximum 21^oC and minimum

7^oC, and for October, the hottest month, the maximum is 33^oC and the minimum is 15^oC. Annual precipitation averages 450 mm. The rainy season is from mid-November to mid-March with some showers and misty periods in June and July. Due to the semi-arid environment, cattle ranching is the major agricultural activity.

The vegetation is savanna type and is closely related to the underlying rock types. The mafic and calc-alkaline greenstones support a variety of brachystegia bush, known locally as igonde and itshabela, while the more felsic greenstones carry acacia and mopane scrub. The granitoids have sparse trees interspaced with stretches of grassland. Human activities have considerably reduced the extent of the natural vegetation. The secondary vegetation resulting from the destruction of the natural vegetation consists of stunted thorny bush.

2.2 Previous geological work

The geological map of Matabeleland (by Fletcher and Espin), published in 1897 shows the Mbembesi river gold belt, flanked by Karro rocks on the south and by granite and gneiss to the northeast. Molyneux made a traverse in the southeast corner of the study area and described the Archean volcanic rocks and the cover red sandstones. He produced a section, which also indicated the granitic rocks. In 1909, Mennel produced a map of the Lonely mine area as an illustration in his publication, The Geology of Rhodesia [8]. The map correctly depicts the greenstone lithologies, banded iron formations, serpentinites, granitic rocks and the forest sandstones. In 1912, Mennel improved on his original map and in 1921 he published, in the Annual report of the Rhodesia Resources Committee, an amendment of the map at a smaller scale. Maufe, Lightfoot and McGregor mapped the Queens Mine area (scale 1:100 000) in 1920. The earliest comprehensive geological map of the central and northern parts of the study area was produced in 1928 (Geology of the country around Lonely Mine, scale 1:119, 000) by the then Rhodesia geological Survey (RGS), based on mapping carried out between 1921 and 1922 by McGregor. A more recent geological map covering the northern half of the study area was produced in 1977 through a compilation of mapping carried out by Muirhead between 1969 and 1972. There is no descriptive bulletin accompanying this map. Garson mapped the area around the Bulawayo area in 1985 and published a descriptive bulletin and a geological map (scale 1:100, 000). In addition to Zimbabwe Geological Survey work in the area, geological research has been carried out by university researchers and mining company geologists under Exclusive Prospecting Orders. The first detailed mine scale geological map in the area was that of the Lonely mine. In 1909 Mennel [8] described the Lonely mine deposits while Weill made a detailed report on the general geology around the mine. As more gold deposits were discovered, mainly at the sites of ancient artesinal workings, mine scale maps and reports proliferated. However, most of this information is not available to the public as it is in private archives.

Between 1983 and 1989, studies on gold mineralization controls in the Zimbabwe craton were carried out as an integral part of a Technical Co-operation Agreement between the UK and Zimbabwe governments. The results of this work, carried out by staff from the British and Zimbabwe Geological Surveys was summarized by Pitfield and Campbell [27].

Pitfield and Campbell followed this with a publication specifically on the Bubi greenstone belt in 1996 [28]. In both publications, remote sensing, particularly Landsat TM imagery and aeromagnetic structural interpretation, played an important role.

2.3 Regional geology

Approximately 60 % of rock outcrop in Zimbabwe consists of the Archean granite-greenstone terrain of the Zimbabwe craton. The Archean craton consists of two units: 1. granitoids, granitic gneisses and migmatites with subordinate amphibolites, epiclastic metasediments and banded iron formation (BIF) and 2. greenstone belts, comprising mainly mafic, ultramafic and felsic volcanics, volcaniclastics, epiclastics, BIF and younger granitoid intrusions. Figure 2.1 shows the Archean Zimbabwe and Kaapval cratons and the surrounding mobile belts while Figure 2.2 illustrates the major tectonic domains and the distribution of greenstone belts in Zimbabwe.

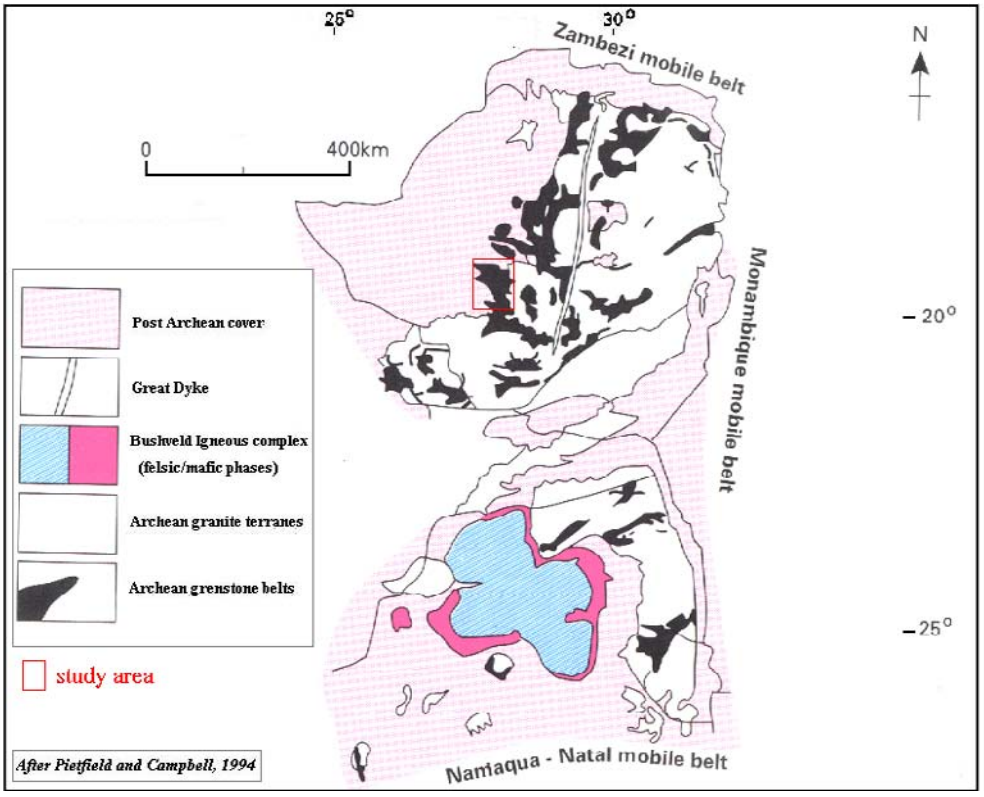

Figure 2.1: Regional setting of the Zimbabwe and Kaapval cratons

Three major phases of greenstone belt emplacement have been proposed in Zimbabwe. The Sebakwian (c. 3.5 Ga), the Lower Greenstones [or Lower Bulawayan] (c. 3.1 - 2.9 Ga) and the Upper Greenstones [or Upper Bulawayan and Shamvaian] (c. 2.7 Ga). The Upper

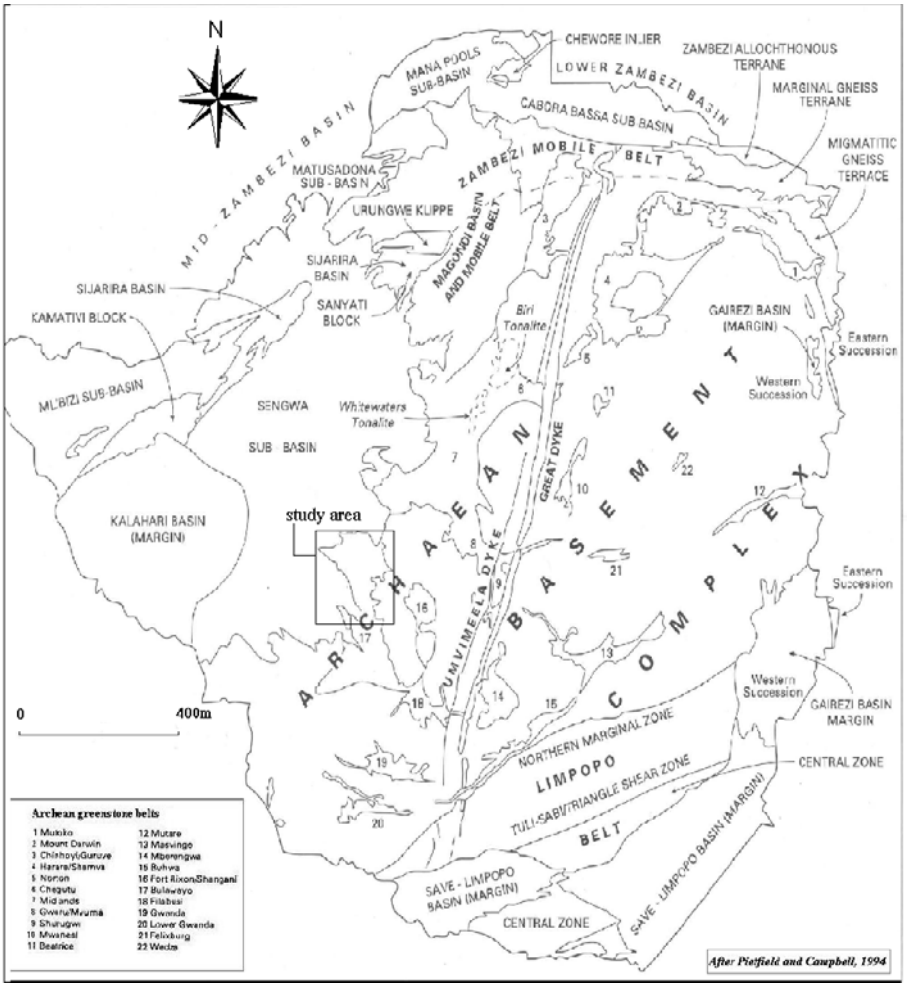

Figure 2.2: Outline of tectonic domains and the distribution of greenstone belts in the Zimbabwe craton.

Greenstones dominate most of the greenstone belts and host all the Archean lode gold deposits in the Bubi greenstone belt. There are limited outcrops of the Lower Greenstones and the Sebakwian. The tripartite subdivisions reflect deformation events at > 3.1 Ga and c. 2.9 Ga, prior to the main regional foliation forming event at c. 2.65 - 2.55 Ga [27]. The main volcanic lithologies of the Upper Bulawayan sequence comprise a lower mafic-ultramafic unit, a bimodal suite and an upper calc-alkaline unit. The internal granitoids and most of the surrounding granitic terrain postdate the upper Bulawayan and comprise the syn-volcanic to late-tectonic, largely tonalitic, Sesombi suite (c 2.7 Ga) and the post tectonic, dominantly monzogranitic Chilimanzi suite (c 2.6 Ga) [37].

Structurally, the greenstone belts are characterized by their arcuate and sigmoidal outlines and internal foliation patterns [26]. Most of the greenstone belts are tight to subisoclinal synforms. Only one penetrative fabric (S1) is regionally developed. Other fabrics and structures occur; mainly in or near deformation zones [27]. Most of the gold only mine-

ralization is broadly contemporaneous with the peak in deformation and metamorphism or coeval with syn-to-late kinematic emplacement of granitoids during the late Archean [28].

2.4 Geology of the study area

2.4.1 Lithostratigraphy

In general terms, the Bubi greenstone belt is like most other greenstone belts in Zimbabwe, a tight, asymmetric, synclinorial structure that is transected by anastomosing shear and deformation zones. The Bubi greenstone belt comprises a succession of tightly folded metavolcanic and metasedimentary rocks flanked by tonalitic and granodiorictic gneisses. The Bulawayan Group comprises more than 90 % of the exposed meta-volcano sedimentary succession.

The Lower Bulawayan Group is limited to two formations comprising felsic volcanics and volcaniclastic rocks, komatiites and komatiitic basalts with interbedded iron formations and polymict clastic sediments (c.2.9 Ga) [37]. These outcrop along the eastern side of the greenstone belt. The Lower Bulawayan Group is uncomformably overlain by the Upper Bulawayan Group comprising basically the same lithologies as the Lower Bulawayan Group but having overall lower metamorphic grade and containing clasts derived from the latter [17]. Figure 2.3 illustrates the geology of the study area.

The Archean basement hosts all the important gold deposits within the study area. Below is a summary of the lithostratigraphic subdivisions in study area. These were compiled from published geological maps [17]. The letter-number symbols shown in brackets after the greenstone formation names below, denote the symbol used in the geological map of the study area [18].

Migmatites and gneisses make up to 70 % of the Zimbabwe Archean craton. They comprise granodiorite gneiss, quartz diorite gneiss and tonalite gneiss, amphibolite and epidiorite and quartz-sericite granulite.

The Lower Bulawayan Group subdivisions from top to bottom are the Bubi Source Formation (Y3), Goodwood Formation (Y2) and the Kenilworth Formation (Y1). The Bubi Source Formation consists of mafic and ultramafic metavolcanics with tuffaceous intercalations. The Goodwood Formation comprises felsic metavolcanics and the Kenilworth Formation, which is the oldest of the greenstone formations comprises epidiorite, amphibolite, chlorite and sericite schists.

Muirhead, (1977) subdivided the Upper Greenstones into two groups, the Middle Bulawayan Group and the Upper Bulawayan Group. This subdivision was based on the change in volcanism from dominantly mafic in the Middle Bulawayan Group to dominantly calc-alkaline in the Upper Bulawayan Group and the existence of a major uncomformity between the two groups in the Bulawayo region to the south of the study area [26].

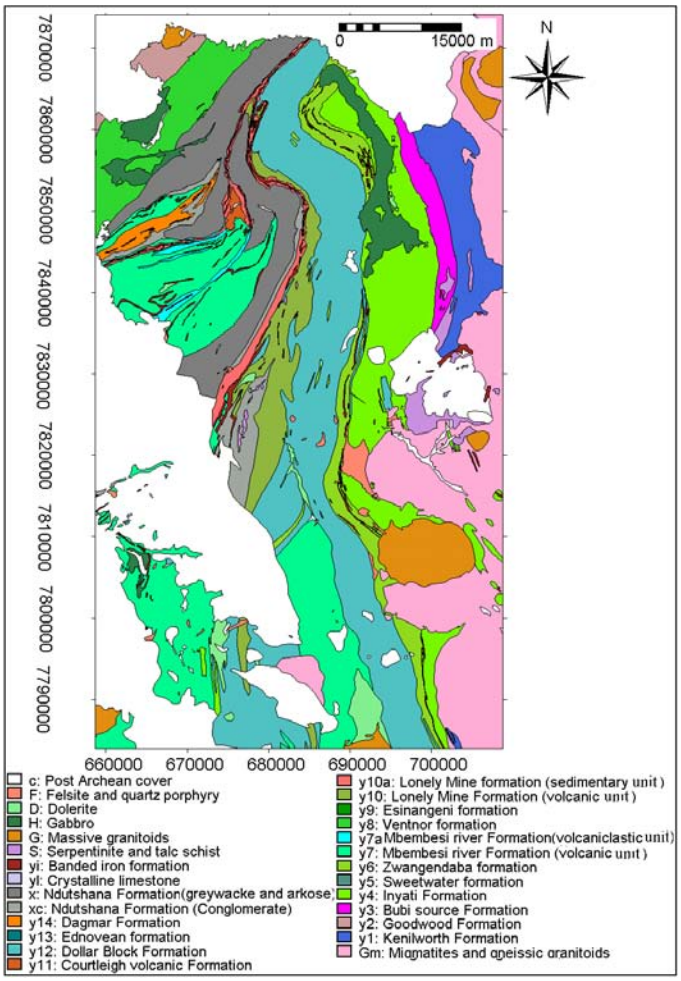

Figure 2.3: Lithological map of the Bubi greenstone belt.

The Middle Bulawayan Group is subdivided into the following formations, from top to bottom: The Lonely mine Formation (Y10), The Esnangeni (Y9), Ventnor (Y8), Mbembesi River (Y7) and Zwangendaba (Y6) Formations and the Sweetwater (Y5) and Inyati Formations (Y4). The Lonely mine Formation is composed of an upper unit of basaltic and andesitic greenstones underlain by shale, slate, argillite and sheared felsic volcanics with BIF intercalations. The Esinangeni, Ventnor, Mbembesi River and Zwangendaba Formations are dominantly composed of basaltic, andesitic, dacitic and rhyodacitic greenstones with intercalations of andesitic and rhyodacitic agglomerates, BIF, jaspilite and chert and limestone. The oldest formations of the Middle Bulawayan Group are the Sweetwater and Inyati Formations. These are dominantly composed of basaltic greenstones with intercalations of rhyodacitic pyroclastics.

The Upper Bulawayan Group comprises the Dagmar Formation (Y14), the Ednovean (Y13) and Dollar block (Y12) Formations and the Courtleigh Formation (Y11). The Dagmar Formation is composed of calcareous grit, arkose and phyllite with intercalations of BIF and

impure limestone. The Ednovean and Dollar block Formations comprise volcanic and pyroclastics rocks of andesitic to rhyodacitic composition. The Courtleigh Formation is composed of dacitic greenstones, chert, tuff, agglomerate and intrusive felsitic rocks.

The Shamvaian Group uncomformably overlies the Upper Bulawayan Group. In the Bubi greenstone belt it is locally referred to as the Ndutshana Formation. This Formation is characterized by siliciclastic metasediments comprising greywacke and polymict conglomerate.

The intrusive rocks in the area belong to various ages. Rock types include, quartz veins, dolerite, serpentinite and talc schist, gabbro, adamellite and pophyritic adamellite, quartz diorite, granophyre, pegmatitic gneiss, tonalite gneiss, granodiorite gneiss, felsite and quartz porphyry.

Post Archean rock formations in the study area are Recent to Pleistocene, Tertiary, Cretaceous and Triassic to Jurassic ages. Recent to Pleistocene formations are represented by unconsolidated material composed of alluvium, colluvium and redistributed Kalahari sand. Tertiary age rocks are referred to as the Kalahari System in Zimbabwe. They consist of Kalahari sandstone overlying a ferricrete horizon. Rocks of Cretaceous age are locally referred to as the Nkai Formation. They are composed of variegated and pipe sandstones, calcareous grit, conglomerate and limestone. Triassic to Jurassic rocks belong to the Karro system. Rock types include sandstone and grit. None of these formations host gold deposits of any economic significance.

2.4.2 Metamorphism

In the Lower Bulawayan group, regional metamorphism is upper greenschist to amphibolite facies. In the Upper Bulawayan Group, regional metamorphism ranges from sub-greenschist facies, where primary textures and structures are well preserved and the rocks lack foliation, to upper greenschist facies, where primary structures are poorly preserved and the rocks are foliated. Metamorphism in the Shamvaian Group is mainly greenschist facies. Metamorphic domains in the study area are shown in Figure 2.4.

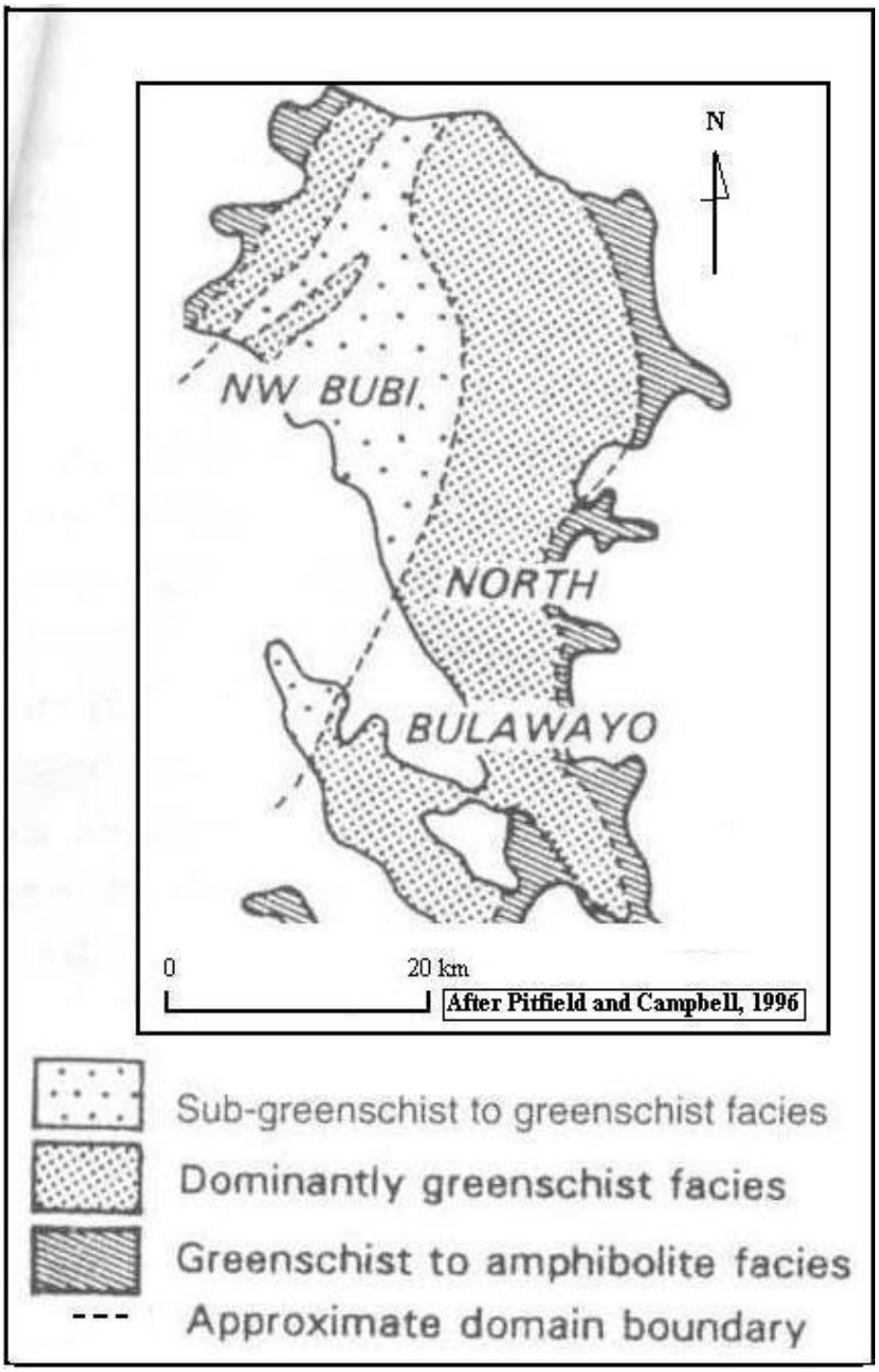

Figure 2.4: Metamorphic domains in the Bubi greenstone belt.

2.4.3 Structure

The structural configuration of the Bubi greenstone belt is largely a result of late Archean deformation and granite emplacement. The area is dominated by an asymmetric southward plunging synclinorium, which is refolded by a major Z- shaped, D2-warp termed the Inunwa inflection [28]. The shear zones are confirmed in the field and in mines as reverse dominated with a variable lateral component of movement [27]. Shear sense indicators show that the NWN to NNW striking shears have a predominantly dextral component while the N-S to NE-SW trending shear zones are mostly sinistral (Figure 2.5). The general pattern of NNW and NNE trending first order high strain zones can be explained in terms of a conjugate shear model similar to the one proposed for the Midlands greenstone belt [27].

In the western part of the Bubi greenstone belt, clastic sediments are interfolded and tectonically juxtaposed with Upper Bulawayan bimodal volcanics. The structure is an axially sheared, strongly asymmetrical periclinal synclinorium with an s-shaped form that is bounded by linear shears to the northwest and southeast [26]. The curvilinear, thrust faulted, fold complex closes northwards against the Courtleigh shear zone. Shear zone hosted gold deposits typically occur in en-echelon or conjugate patterns. Some of these gold deposits are localized within dilational jogs and splays. The shear zones range from brittle-ductile to brittle [26].

To the east, conjugate NNW-trending and NNE-trending shear zones that generally follow the contacts between the Upper Bulawayan calc-alkaline and basaltic/komatiitic volcanic sequences dominate the structure. Kilometer-scale, upright, isoclinal folds occur. The eastern contact of the greenstone belt is largely intrusive with syn-to-late tectonic tonalites and post-tectonic granites [28].

High-strain zones in the study area include: the Gabriela-Mulungwane deformation zone, the Mbembesi shear zone, the Gomoyo deformation zone and the Northwest Bubi shear system. A structural map of the Bulawayo Bubi greenstone belt shown on Figure 2.6.

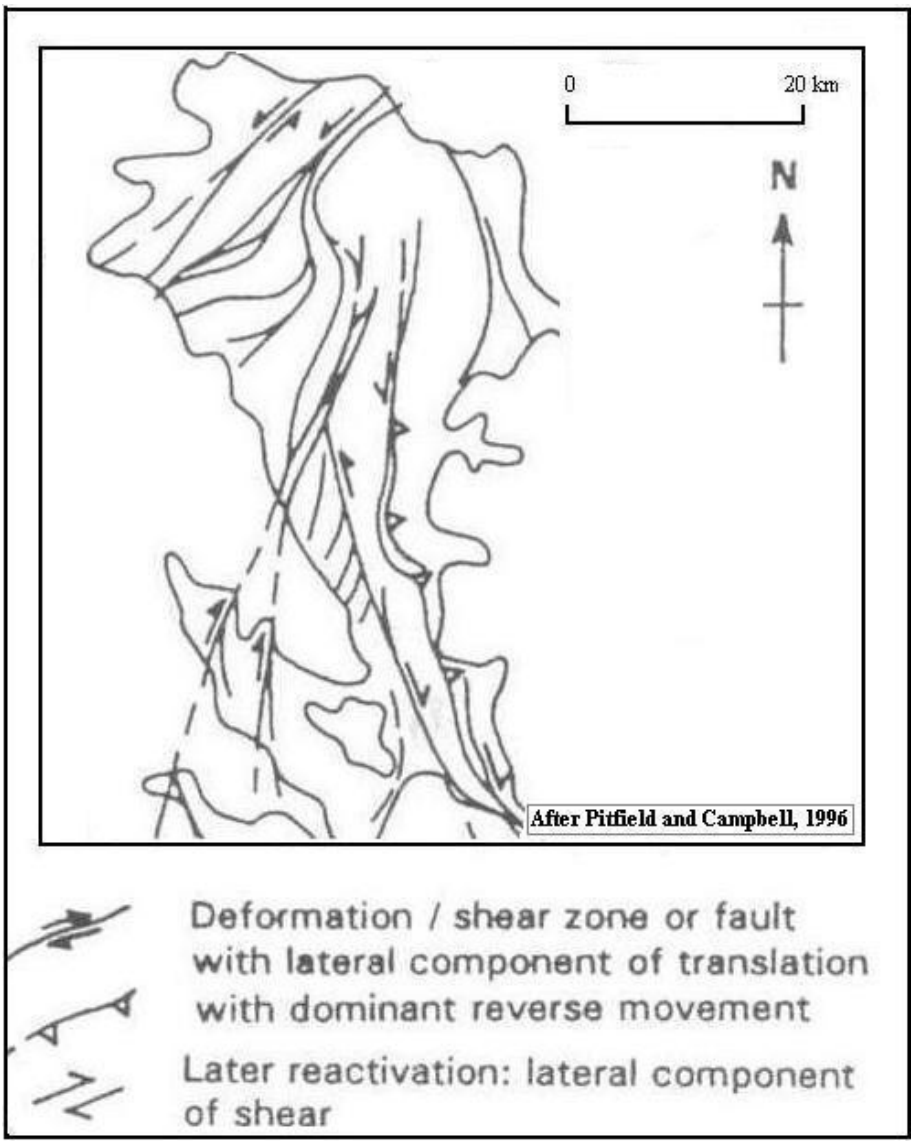

Figure 2.5: Deformation and shear or fault zones with known sense of movement in the Bubi greenstone belt.

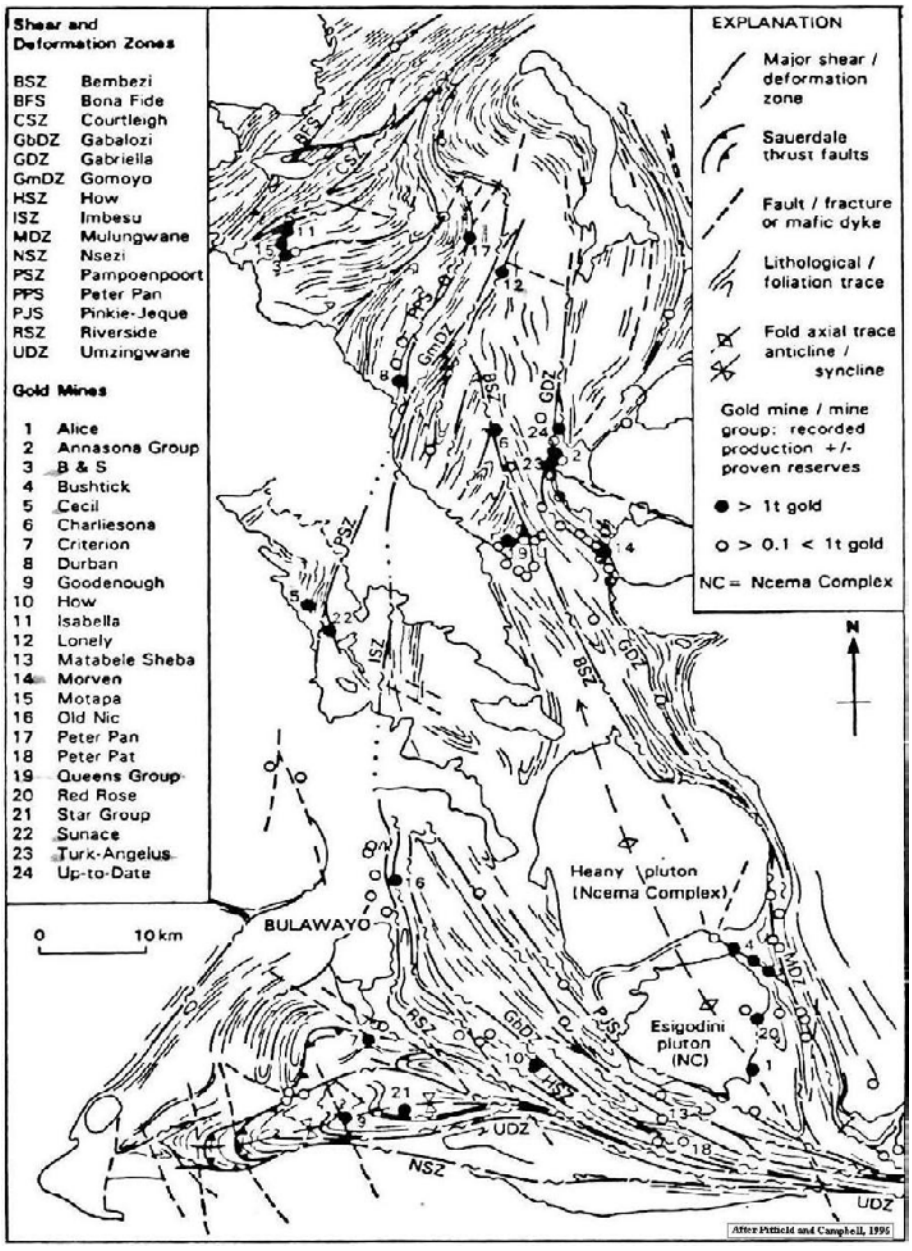

Figure 2.6: Landsat TM structural interpretation of the Bulawayo-Bubi greenstone belt

- **The Gabriela-Mulungwane shear zone**

  The Gabriela-Mulungwane shear zone follows the eastern contact of the Bembezi Valley/Dollar Block calc-alkaline Formations with the Zwangendaba/Inyati mafic Formations and merges with the Umzingwane Deformation zone south of the study area. The N-S striking segments of the deformation zone show sinistral deformation while NW-SE striking segments have a dextral deformation style. These opposing lateral senses of motion could be generated by NNW-SSE directed compression [28].

- **The Mbembesi shear zone**

  The Mbembesi shear zone is a fairly linear feature traceable on Landsat TM imagery from close to the Imbesu-Lonely Mine deformation zone up to the Ncema complex, south of the study area. The shear zone is intruded by undeformed dolerite sheets along the Bembezi river valley [27]. South of Queens Mine, the shear zone follows the western margin of the calc-alkaline volcanics. Kinematic indicators are not conclusive. Folding indicates sinistral movement while z-inflections and tailed porphyroblasts indicate dextral reverse kinematics at a local scale [26].

- **The Gomoyo deformation zone**

  The Gomoyo deformation zone comprise the north-south striking Pampoenpoort and Imbesu shear zones. In the Bembezi river valley, these shears border banded iron formation units and form the margins of the Ndutshna and Lonely Mine Formations. The shears become obscure in the Lonely Mine area around the short limb of the Inunwa inflection. Kinematic indicators show dextral movement with a small reverse component [27].

- **The Northwest Bubi shear system**

  The Northwest Bubi shear system is a series of thrusts associated with the Inunwa inflection. This shear system hosts most of the low grade large tonnage gold deposits discovered during the 1990s within the study area. The Northwest Bubi shear system lies to the west of the Gomoyo deformation zone. From east to west the individual shears are the Peter Pan, Robin Hood, Mfuzi, Calcite, Courtleigh and Bonafide shear zones. All these shear zones except the Bonafide shear zone cut and juxtapose the Ndutshna and Dagmar sedimentary Formations with the middle greenstone metavolcanics. The rock formations in the vicinity of the Northwest Bubi shear system are folded by two synclines with an intervening anticline cored by the Courtleigh Volcanic Formation and Mbembesi River greenstones. Duplexing shears link the Courtleigh and the Calcite shear zones [27]. The Bonafide shear zone is a NE-SW, linear structure bordering a laterally continuous unit of felsic to intermediate volcanics. Movement along this shear zone is dominantly dextral.

  Two distinct structural styles occur in the Bubi greenstone belt. These are side-step and conjugate systems. Subareas typified by the different structural styles are shown on (Figure 2.7). The eastern edge of the greenstone belt has more complex deformation styles with both side-step and conjugate systems occurring. All three structural subareas host Archean lode gold deposits [26].

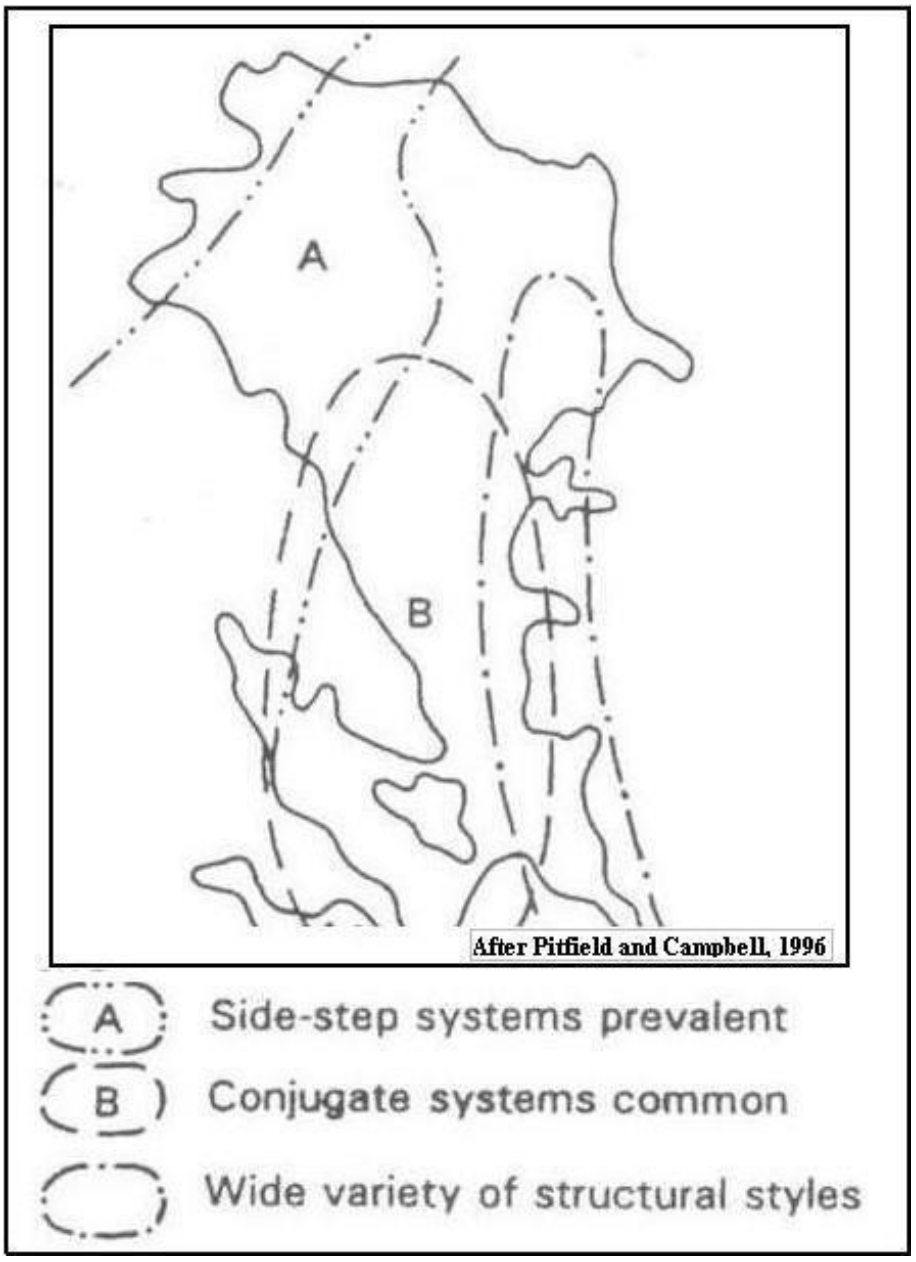

Figure 2.7: Subareas typified by particular structural styles of gold deposits in the Bubi greenstone belt

2.4.4 Conclusions

The Mbembesi River Formation, Dollar Block Formation, Zwangendaba Formation, Dagmar Formation, Lonely Mine Volcanic Formation, Ventor Formation and Ndutshana Formation host most of the gold deposits in the Bubi greenstone belt . The gold deposits generally lie within 5 km of the major shear zones [17]. Greenschist regional metamorphism is commonly associated with the gold deposits. It is believed that the syn-to-late tectonic granitoid intru-

sions supplied the heat source which drove the hydrothermal systems responsible for gold mineralization [26]. Understanding the stratigraphic, igneous, structural and metamorphic history of the study area is important for the generation of predictive models for Archean lode gold deposits.

Chapter 3

Archean lode gold deposits

3.1 Introduction

The major Archean lode gold deposits are situated in late Archean cratons of Australia, Brazil, Canada, India, South Africa, Tanzania and Zimbabwe [3]. They contribute about 18% of world gold production. The gold content of these deposits ranges from less than one tonne to more than 1500 tonnes. Average grades vary from 2 to 50 g/t [32]. The generalized mineralization styles of Archean lode gold deposits are described in the following section. Section 3.3 focuses on Archean lode gold mineralization within the study area.

Structural studies of Archean gold deposits indicate that most of these deposits are localized by dilatant features at shear zone junctions, in drag folded sites, in zones of mashing and contortion of the schist and at or near flexures in the walls of breccia shear zones [9]. Buckling, mashing and contortion are greatest at shear zone junctions. Diapiric intrusives and lithological boundaries with a high degree of competency contrast between the adjacent rock units indirectly control the location of structurally controlled gold deposits by their influence on the development of potentially mineralized structures.

The physical effect of structural disturbance is an increase in volume at the affected junction, creating space for the precipitation of minerals [1]. At the vicinity of flexures, differential movement along the shear zone causes dilation. Drag folding has the same effect. Pressure and chemical concentration gradients were established between the dilation zones and their surroundings [26]. This promoted the migration of mobile elements into these zones where they were subsequently precipitated. To fully understand the mineralized shear systems in greenstone belts, both chemical and kinematic aspects have to be considered. The nature of the shearing, alteration and origin of these extensive shear systems is well documented. However, a lot of research remains to be done on their kinematic and chemical history [32].

Archean lode gold deposits contribute about 18% of world gold production [3]. The gold content of these deposits ranges from less than one tonne to more than 1500 tonnes. Average grades vary from 2 to 50 g/t [32]. The mineralization styles of Archean lode gold deposits are described in section 3.2, genetic aspects are covered in Section 3.3 while Section 3.4 focuses

on Archean lode gold mineralization within the study area.

3.2 Mineralization styles of Archean lode gold deposits

3.2.1 Auriferous deposits in iron formations and tuff beds

Gold deposits in chemical sediments have been interpreted as evidence of syngenetic or exhalative gold [3]. Two categories are recognized; laminated units in volcanic rocks (mainly tuffs) and iron sulphide enriched units in BIF.

Gold deposits in dragged tuff beds and in Algoma-type-iron-formations are mainly diffuse, irregular impregnation zones with amphibolitization, biotitization, chloritization, pyritization and development of pyrite and arsenopyrite. Carbonitization is uncommon except where an original carbonate facies existed. Concordant and discordant quartz veins, lenses and irregular bodies are widespread in gold deposits hosted by iron formations but are rare in those hosted within tuffs. The quartz bodies in both the iron formations and tuffs were probably derived from sedimentary chert [3].

Examples of Archean lode gold deposits hosted by iron formations in greenstones (volcanics) or mixed greenstone and greywacke-argillite occur in the Canadian Shield (Crow river and Pickle Lake areas, Geraldton and Beardmore areas) and Zimbabwe (Wanderer mine). Examples hosted in sheared tuffs occur at the Madsen mine, Red Lake, Ontario and Hemlo, Ontario [6]. The latter is hosted by tuffs.

3.2.2 Shear zone hosted, replacement type auriferous deposits

In replacement (metasomatic) gold ore deposits such as the Campbell and A.A. White Mines in the Red Lake District, Ontario, Canada and the Golden Mile deposits, Kalgoorlie, Australia, quartz veins are a minor component [3]. The ore zones consist of silicified mafic rock containing disseminated pyrite and arsenopyrite replacing and forming stringers in the mafic host rock. Disseminated gold occurs in association with iron sulphides in magnetite rich iron formations. World class examples are the Lupin Mine and Cullaton Lake Mine (B-zone) in the Northwest Territories [3]. Most replacement gold deposits exhibit irregular zoning and abundant crack-seal fractures illustrating polycyclic episodes of mineralization related to shear deformation. Ore mineralogy varies from simple to complex in different deposits, e.g., at How mine, Zimbabwe, mineralization is dominated by disseminations of gold carrying pyrite in felsites and tuffs and fabric replacements in tuffs [11]. In the Maria Lazara gold deposit, Goias State, Brazil, the mineralogy is more complex. The gold mineralization at the Maria Lazara gold deposit occurs within mylonitized basalts. The dominant sulphide is arsenopyrite (up to 60%) with subordinate pyrite, chalcopyrite, pyrrhotite and galena. Bismuth minerals also occur [29].

3.2.3 Auriferous deposits in shear zones that transect the Archean volcanic flows

Two types of Archean gold deposits within shear zones that transect volcanic flows occur. These are deposits in extensive, carbonitized shear zone systems and deposits within shear zones that brecciate and fault intrusive rocks.

1. **Auriferous deposits in extensive, carbonitized shear zone systems**.
   Auriferous deposits in extensive carbonatized, shear zone systems are of two general sub-types: veins and irregular, complex bodies [3].

   - Vein type auriferous deposits.
     Quartz vein hosted gold mineralization occurs within the greenstone lithologies and the surrounding granitoids. Quartz vein deposits are characteristic of spur shears and cross over shears between master shears. The vein deposits are usually high grade but with limited tonnages compared to disseminated and replacement type deposits. Metamorphic grade of host lithologies is usually greenschist facies. The gold occurs as disseminations often associated with pyrite, chalcopyrite and arsenopyrite. The mineralization was emplaced during or just after regional deformation and metamorphism [26]. The veins are variable in size, ranging from mm scale veinlets to meter scale veins. Alteration haloes are of limited extents, generally in the immediate vicinity of the ore bodies.

   - Auriferous deposits occurring as irregular, complex bodies.
     These deposits are characterized by silicification, sericitization and sulphidization (mainly pyrite and arsenopyrite). The deposits generally occur within master shears systems. Local lenses, veins and restricted stock-works of quartz of two or more generations are common. Alteration zones from within the ore body outwards are as follows: a) a silicified, quartz-sericite-pyrite-arsenopyrite zone (The ore body); b) a carbonate-sericite-pyrite schist zone; c) a chlorite-carbonate schist zone; and d) a chlorite schist zone which is the principal component of the shear zone [3].

2. **Auriferous deposits within shear zones that brecciate and fault intrusive rocks**.
   Common host lithologies are quartz-feldspar porphyry, syenite, granite, diorite and gabbro. The ore bodies are stockworks and/or diffuse, irregular impregnations. In some ore bodies, the whole stockwork constitutes the ore while in others the whole intrusive is mined. Alteration varies with lithology. In granitic rocks, sericitization, silicification, feldpathization and pyritization occur. In intermediate, mafic and ultramafic rocks, carbonitization, sericitization, serpentinization, development of talc, and pyritization prevail [3].

3.3 Genesis of Archean lode gold deposits

3.3.1 Wall rock alteration

Wall rock alteration in Archean lode gold deposits is mainly due to the introduction of fluids rich in carbon-dioxide (CO_2), potassium, water and silica. The last is either introduced or mobilized from the country rocks. Pervasive carbonate alteration is common in sub-amphibolite facies rocks. Carbonate alteration is characterized by an ankerite-dolomite-magnesite core, with an outer zone of calcite, associated with chlorite, biotite, sericite, tourmaline, quartz veining and silicification [3].

Wall rock alteration overprints metamorphic assemblages in greenschist facies settings, indicating that metamorphism was earlier [9]. In amphibolite facies settings, the timing of wall rock alteration is still to be resolved [23].

Elements characteristically associated with Archean gold mineralization include As, W, Ag, Te, and B with low base metal and molybdenum concentrations [14]

3.3.2 Timing of mineralization

There is no agreement on the absolute age of Archean lode gold mineralization [9, 1]. Estimations have been made relative to deformation, metamorphism and intrusive events. Radiometric dating using the U-Pb system on zircons in felsic intrusions in Canada indicate that the gold mineralization was probably broadly synchronous with the emplacement of syenite and lamprophyre of late alkaline intrusions. Archean gold mineralization is therefore related to late deformation accompanying peak metamorphism and post-dates most granitoid, felsic porphyry and lamprophyre intrusions [32].

3.3.3 Mineralizing fluids

Fluid inclusion studies on Archean gold deposits indicate that the mineralizing fluid was dominantly a water and CO_2 (10 to 25 mole % CO_2) mixture. The fluids are typically low salinity (< 2 wt % NaCl equivalent), neutral to slightly alkaline and reducing [32]. Minimum gold depositional P-T conditions are 200 to 400^o (normally 250-350^o) and 0.4-4.5 kb (normally 1 to 3 kb). Low salinity and high CO_2 are attributed to metamorphic sources [9]. The fluid composition is comparable to fluids generated under amphibolite facies conditions [7]. The fluids are probably generated by CO_2 saturation in water or a CO_2 rich silicate melt [13]. Isotope studies indicate that the fluid source is either metamorphic or hydrothermal. To date, there is no conclusive evidence for the source of mineralizing fluids. Current knowledge points to either a magmatic or a metamorphic source [9]. The fluids are most probably a mixture from the different sources. Gold precipitation is effected by a number of mechanisms, including, increase in the fugacity of oxygen destabilizing sulphur complexes, change in pH, reaction of sulphur complexes with iron in mafic host rocks forming iron sulphides and reaction with organic matter in carbonaceous sediments [7]. Gold transport in the ore fluids that formed the diopside and diopside-K-feldspar class deposits (T$> 550^o$) would contain the $AuCl_2^-$ complex whereas the $Au(HS)_3$ complex may have been important in the lower temperature($< 270^o$),

less alkaline mineralizing fluids [22].

3.4 Gold mineralization in the study area

3.4.1 Introduction

Gold mines within the Bubi greenstone belt are spatially distributed in distinct clusters and linear groups along shear zones. The most important of these are the Lonely, Motapa, Durban, Turk, Queens, and Surnace groups. There is a strong spatial relationship between these mine clusters and certain lithologies, first and second order structural features and lineaments interpreted from Landsat TM imagery and granitoid intrusions. There is also more localized, but close spatial relationships with low angle thrust imbrications, kilometer scale folding and felsic intrusions [27].

3.4.2 Structural control

Most Zimbabwe gold deposits are spatially associated with deformation zones, or with folds between major deformation zones. Regional metamorphism is associated with deformation. Metamorphic grade in known deposits is greenschist or less commonly, amphibolite facies. Deposits in higher metamorphic conditions are rare.

A large proportion of Archean lode gold deposits occur within shear zones. Particular favorable sites for gold mineralization within shear zones include: (a) second order shear veins and conjugate shear sets; (b) sites within shear zones with duplexing, inflection, en echelon segmentation and pressure shadows; (c) sites where the intensity of deformation is relatively stronger as indicated by foliation and s-fabric. An example which has been studied in detail is the Habour Lights Mine, Western Australia where the intensity of mineralization related alteration is spatially associated with deformation intensity [12]. In Zimbabwe, many shear-hosted Archean lode gold deposits occur in the shallowly dipping sections of the shear zones [27]. Within folds, gold mineralization occurs in fold noses, along fold axes and in sheared fold limbs. Foliation and s-fabric are also spatially associated with some deposits within the study area.

Examples of some structural styles exhibited by Archean lode gold deposits at outcrop scale are illustrated in Figures 3.1, 3.2, 3.3, 3.4, 3.5, and 3.6. In Figure 3.1, hydraulic brecciation occurred after ductile shearing and before the emplacement of the mineralized quartz vein. In Figure 3.4, pale brown, arsenopyrite/gold bearing cherty layers alternate with pyrite/pyrrhotite bearing amphibolite facies minerals. In Figure 3.5 the gold is associated with a pyrite-pyrrhotite-chalcopyrite-galena mineral assemblage. In Figure 3.5, the banding is parallel to the shear fabric, sulphides include arsenopyrite, pyrite, pyrrhotite and chalcopyrite.

Figure 3.1: Ultramafic hosted quartz vein. Phoenix Mine main reef, Zimbabwe.

Figure 3.2: Boudinaged auriferous quartz veins related to late stage compression, Goodenough Mine, Zimbabwe.

Figure 3.3: Quartz impregnation and replacement mineralization, C1 lode, Turk Mine, Zimbabwe.

Figure 3.4: Banded replacement style mineralization within amphibolite facies alteration assemblages, Venus ore-body, Acturus mine, Zimbabwe.

Figure 3.5: Quartz vein with coarse gold, Hanover Mine, Zimbabwe.

Figure 3.6: Banded sulphide and quartz replacement mineralization in Shamvaian sediments, Kimberley Mine, Zimbabwe.

3.4.3 Control by granitoid intrusions

Granitoid intrusions indirectly control the location of Archean lode gold deposits by their effect on the development of potentially mineralized structures during diapirism. The actual structures hosting the mineralization are shear zones and folds. In Zimbabwe greenstone belts, tonalite-trondjhemite-granodiorite plutons intruded the greenstone belts during the late Archean deformation (c. 2.65 Ga) [27]. Some gold deposits are genetically related to these intrusive rocks. The gold deposits tends to occur in concentric, normal and radial strike

slip faults and shears. Lateral balloning and forceful intrusion may also generate concentric compressional structures (reverse and strike slip faults and compressional fabrics). Many gold deposits in the Bubi greenstone belt tend to occur close to the granite-greenstone contact, irrespective of the age and nature of the granitoids. This is attributed to the competency contrasts between the granitic rocks and the greenstone belt lithologies during deformation resulting in favorable structural traps for gold mineralization.

3.4.4 Stratigraphic control

Gold-bearing shear zones are commonly sited along lithological boundaries between greenstone lithologies, where there is a high degree of competency contrast between the adjacent rock formations [30]. An excellent example occurs within the Motapa Mining Lease in the study area where two mineralized shear zones follow the contacts of the more competent metabasalt and less competent muscovite schist/andesitic agglomerates. An example of these low cost, open pit mines is shown in Figure 3.7. Low strain lithologies surrounded by high strain lithologies are probably favorable for stratabound gold mineralization [28]. This is due to prevailing fluid pressure gradients. Due to lithogeochemical control on gold precipitation, many gold deposits are stratabound [9].

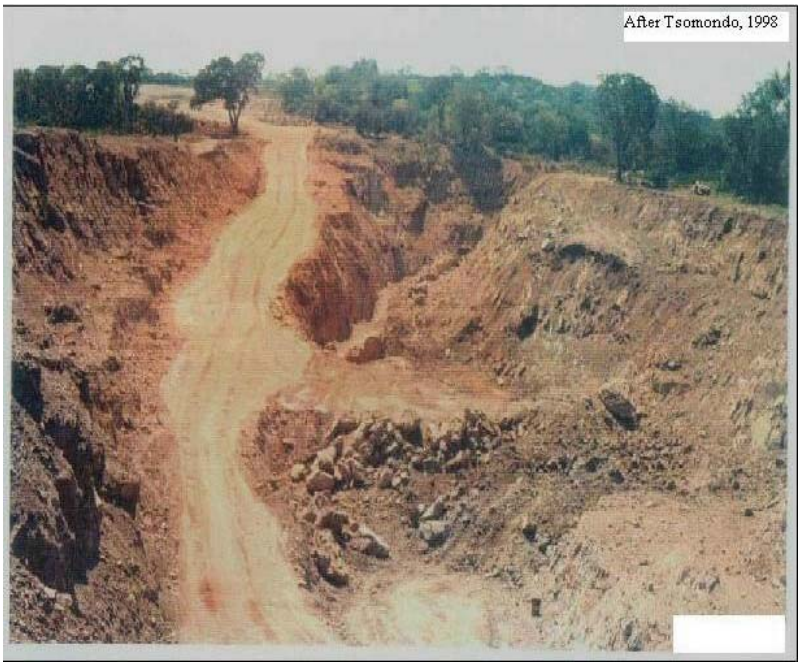

Figure 3.7: Motapa Mining Lease, Club Section Pit, looking east at the access ramp and the ore that is remaining the pit. Note the contrasting soil color marking the contact zone between the basalts and andesites.

3.4.5 Hydrothermal alteration

Most of the gold deposits are associated with hydrothermal alteration and/or iron oxide enrichment related to sulphide weathering. The presence of silicified, carbonatized, K-enriched, and pyritized zones indicate hydrothermal activity. Fuchsite may be a guide in ultramafic rocks [15]. Iron oxide enrichment zones related to normal weathering are widespread within the study area, limiting their usefulness in gold exploration.

3.4.6 Conclusions

Archean lode gold mineralization within the Bubi greenstone belt are associated with the following geological features:

- **Structure.**
  Mineralization is usually associated with second-order shear veins and conjugate shear sets and sites within shear zones where duplexing, inflection, en-echelon segmentation and pressure shadows occur. Regional metamorphism in known deposits is greenschist or less commonly, amphibolite facies. Deposits in higher metamorphic conditions are rare.
- **Granitoids.**
  Granitoids indirectly control the location of Archean lode gold deposits by their effect on the development of potentially mineralized structures during diapirism regional deformation.
- **Lithostratigraphy.**
  All major Archean rock types, especially the iron rich varieties are potentially host to economic gold mineralization. Highly favorable sites for hosting gold deposits are lithological boundaries, where there is a high degree of competency contrast between the adjacent rock units.
- **Hydrothermal alteration.**
  Alteration is an indication of potentially mineralized areas. Areas of iron oxide enrichment, resulting from the weathering of sulphide minerals that potentially host gold deposits are a guide, though the iron oxides may result from the normal weathering processes. [15].

Chapter 4

Area selection criteria for Archean lode gold deposits

4.1 Introduction

Area selection is based on the presence or absence of specific geological features or alternatively geophysical and geochemical features that reflect geological features. These features (”area selection criteria”) are used to distinguish prospective ground from less or non prospective ground. In areas with known mineral deposits, prospectivity can be determined by the presence of features which elsewhere in the area are known to be associated with mineral deposits. Quantitative spatial associations of known mineral deposits with geological features is the basis of data driven modelling for mineral potential.

Similarities between mineral deposits enable them to be classified. These similarities include lithology, structure, hydrothermal alteration patterns, geophysical signature and other features common to one class of mineral deposits. Mineral deposit modelling attempts to understand the processes, ore controls or metallotect and environments leading to economic accumulation of minerals so that analogues can be sought in the field. Ore controls operate on a variety of scales from regional to local. As a result, area selection criteria and the use of ore deposit models must take into full account the scale and timing of metallogenic processes to be successful [36]. Two types of ore deposit models can be distinguished. These are; the empirical (or descriptive) model and the theoretical (or metallogenic or conceptual) model. Theoretical mineral deposit models are built on the basis of empirical models.

The empirical model attempts to explain observational data, which characterize a particular deposit class within a coherent physico-chemical framework and is based on the idea that conformity in features is a product of conformity in processes [36]. The theoretical model on the other hand reflects the reasoning and conclusions of economic geologists on how ore deposits form. The theoretical model attempts to interpret the data through a unifying theory of genesis.

Conceptual mineral deposit models provide guidelines for mineral exploration work. For GIS-based mineral potential mapping, conceptual mineral deposit models provide the theoretical framework for deciding which features to enhance and extract as evidence [2]. In this study, selection of geological features favorable for gold mineralization is based on the conceptual model for Archean lode gold deposits. The major value of a conceptual model is that it directs the geologist to questions that would otherwise remain unasked [36].

4.2 Conceptual models for Archean lode gold deposits

4.2.1 Introduction

The emplacement of gold deposits is linked to the regional structural, metamorphic and intrusive igneous history of the greenstone belts [3]. Sketches illustrating the development of Archean volcano-sedimentary terrains are shown on Figure 4.1. It is generally accepted that economic Archean lode gold deposits formed during stage 3 of Figure 4.1 in the evolution of greenstone belts. Shear deformation and alteration are broadly coeval and linked to batholith emplacement. A two stage genetic model for Archean lode gold deposits is generally accepted. This involves the formation of a pre-tectonic proto-ore and the remobilization and concentration of this into dilatant zones during progressive metamorphism and deformation to form the structurally controlled gold mineralization [34].

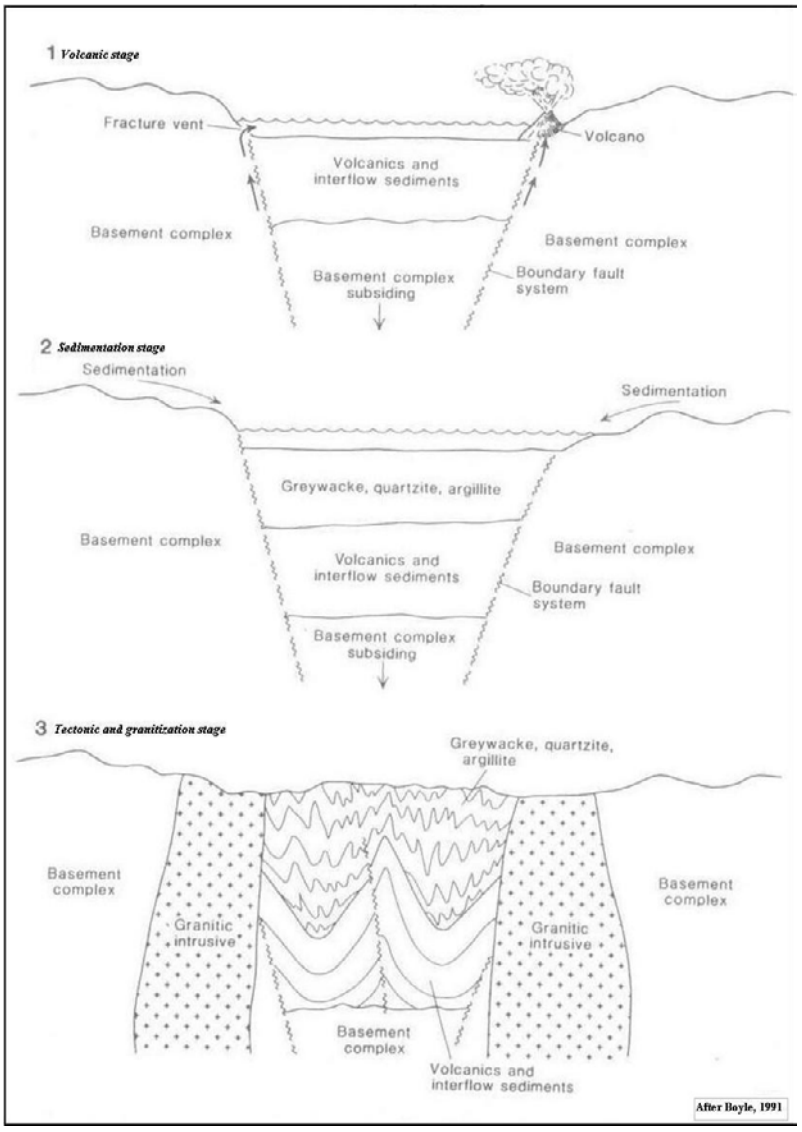

Figure 4.1: Sketches illustrating the development of Archean volcano-sedimentary terrains.

4.2.2 Pre-requisites for the formation of Archean lode gold deposits

The essential pre-requisites for the formation of a gold deposit are as follows:

- Genesis of a large volume of gold bearing hydrothermal fluid. Probable sources of this fluid are magmatic, metamorphic and mantle. Researchers still have to determine which hydrothermal fluid contained most of the gold [27].

- Genesis of fluid pathways which focused the fluid during regional deformation. These have to be deep-seated, ductile shear zones passing up into brittle-ductile shears to enable large volumes of hydrothermal fluids to circulate.

- Induced flow of fluids. Fluid flow up shear zones is principally along pressure gradients and or due to convection.
- Transport of the fluid through a depositional environment and subsequent precipitation of the gold. Precipitation of the gold is in response to physico-chemical changes. These include temperature decrease, increase in $f0_2$ destabilizing sulphur complexes, reaction with iron in mafic rocks, decrease in sulphur (%) and pH changes. Depositional sites are typically syn-kinematic, second order dilatational sites within or adjacent to major shear zones. Lithology is also an important physical variable controlling dilation.
- Precipitation of the gold. This is estimated to have occurred at temperatures of c. 350^0C and at pressures of $2+\_1.5$ kb [depths 2-11km] [21].

4.2.3 The volcanic syngenetic remobilization model

According to this model, gold is concentrated in the crust by volcanic-related processes, principally chemical precipitation in exhalative sediments and Algoma type banded iron formations. The wall rock alteration is assumed to be related to this primary process. Gold and associated minerals are remobilized from sediments by post-depositional processes, which include compaction and diagenesis of auriferous sediments, deformation and metamorphism and the deformation-metamorphic processes associated with the emplacement of igneous rocks. Early pre-metamorphic mineralization and related synvolcanic hydrothermal alteration produced initial auriferous sulphides and an advanced argillic alteration. This event is suggested by highly aluminous rocks closely spatially associated with mineralized zones and by textures preserved through the overprint of metamorphic textures [34]. Another model for Archean lode gold deposits emphasizes a syngenetic origin for the widespread anomalous gold values, similarity of the geological environments to currently active submarine exhalative systems, and the association of gold deposits with chemical sedimentary strata.

At Bousquet mine, Abitibi greenstone belt, Quebec, Tourigny et al. (1989) were unable to find direct evidence for stratiform synvolcanic gold mineralization. However, they proposed that it is probable that the first stage in the mineralization process could have been related to subvolcanic hydrothermal activity beneath the sea floor with gold and sulphide mineralization and host rock alteration occurring in and adjacent to major faults [34]. In general, Archean lode gold deposits typically have low contents of tin and Cu-Pb-Zn relative to their host rocks. The occurrence of stannite at Bousquet mine, which is characteristic of many volcanogenic massive sulphide deposits in the Canadian Precambrian Shield suggests that tin was initially concentrated in the host rocks by volcanogenic exhalative processes and was later remobilized together with gold during metamorphism and deformation into the present ore bodies [34].

The syngenetic model has a number of weaknesses. In many Algoma -type iron formation-hosted deposits, primary magnetite has been replaced by gold-bearing iron sulphides suggesting epigenetic processes. It is not possible to relate the geometry of the altered host rocks or the geochemical gradients in the alteration zones to the type of footwall alteration that may be expected in a deposit emplaced at surface. Pyritic-gold ore bodies originally considered to be

synvolcanic (eg., Bousquet district, Abitibi greenstone belt) have been re-evaluated as dominantly structurally-controlled due to their geometrical aspects and their highly deformed host rocks [34]. Replacement features in Archean lode gold deposits could be explained as normal diagenetic features and contact areas between sulphide-rich ore and carbonate wallrock as facies boundaries [19].

4.2.4 The metamorphic epigenetic remobilization model

This model states that mineralizing fluids are generated by decarbonation and dehydration reactions at the base of the greenstone sequences in amphibolite facies conditions [3]. Deformation zones serve as conduits to the mineralizing fluids. The fluids rise to zones of lower P-T conditions where they are at disequilibrium with the surrounding rocks resulting in mineral precipitation. The mineralization is controlled in part by transition across metamorphic boundaries. The post-metamorphic gold is considered to be contemporaneous with retrograde alteration of metamorphic assemblages formed during late deformation. Mineral assemblages formed include kaolinite-pyrophyllite-diaspore replacing syntectonic andalusite pophyroblasts in felsic rocks [34]. In mafic rocks, retrograde alteration forms carbonate, chlorite, muscovite, pyrite and gold. These assemblages are interpreted as epigenetic because they overprint the greenschist metamorphic assemblages.

The metamorphic epigenetic remobilization model is compatible with important features of gold deposits, which require that the deposits be formed at depth. The distribution of the deposits and associated alteration zones in tabular deformation zones of regional extent and reflection of P-T conditions of regional metamorphism by the geochemistry of alteration assemblages of the deposits indicate formation of the mineral deposits under metamorphic conditions [32]. One model proposed for iron formation-hosted gold states that the mineralization may have formed due to deformation, focusing metamorphogenic or magmatic hydrothermal fluids, from depth, into a chemically and structurally favorable depositional environment (brittle-ductile transition zone), late in the orogenic cycle. This theory is consistent with both the cross-cutting relationships and radiometric dating for the gold mineralization [15].

4.2.5 Conclusions

Genetic models are revised in the light of new experimental and field data. Currently, it is generally agreed that the emplacement of gold deposits is linked to the regional structural, metamorphic and intrusive igneous history of the greenstone belts. It is generally accepted that Archean lode gold deposits formed late in the development of Archean granite-greenstone terrains. A two stage genetic model for Archean lode gold deposits is generally accepted. This involves the formation of a pre-tectonic proto-ore (volcanic syngenetic remobilization model) and the remobilization and concentration of this into dilatant zones during progressive metamorphism and deformation (metamorphic epigenetic remobilization model) to form the structurally controlled economic gold mineralization [34].

4.3 Exploration criteria for Archean lode gold deposits

Exploration criteria for Archean lode gold deposits are defined on the basis of the conceptual genetic model for Archean lode gold deposits and an understanding of the geological setting of Archean greenstone belts. Pitfield and Campbell, [28, 26, 27, 25, 24] have identified 4 main exploration criteria for Archean lode gold deposits in Zimbabwe. These are structural, stratigraphic, granitoid diapirism and hydrothermal alteration criteria.

4.3.1 Structural criterion

Favorable areas with respect to shear zones

The vicinity of shear zones and faults are generally favorable sites for gold deposits, especially structurally anomalous segments. These include pronounced inflections, splays, shear zone intersections, imbricate splays at shear zone terminations, en-echelon segmentation, duplexes and folding within or adjacent to shear zones [27]. Favorable areas with respect to shear zones and faults are shown on Figure 4.2. The target areas are high-lighted on the figure.

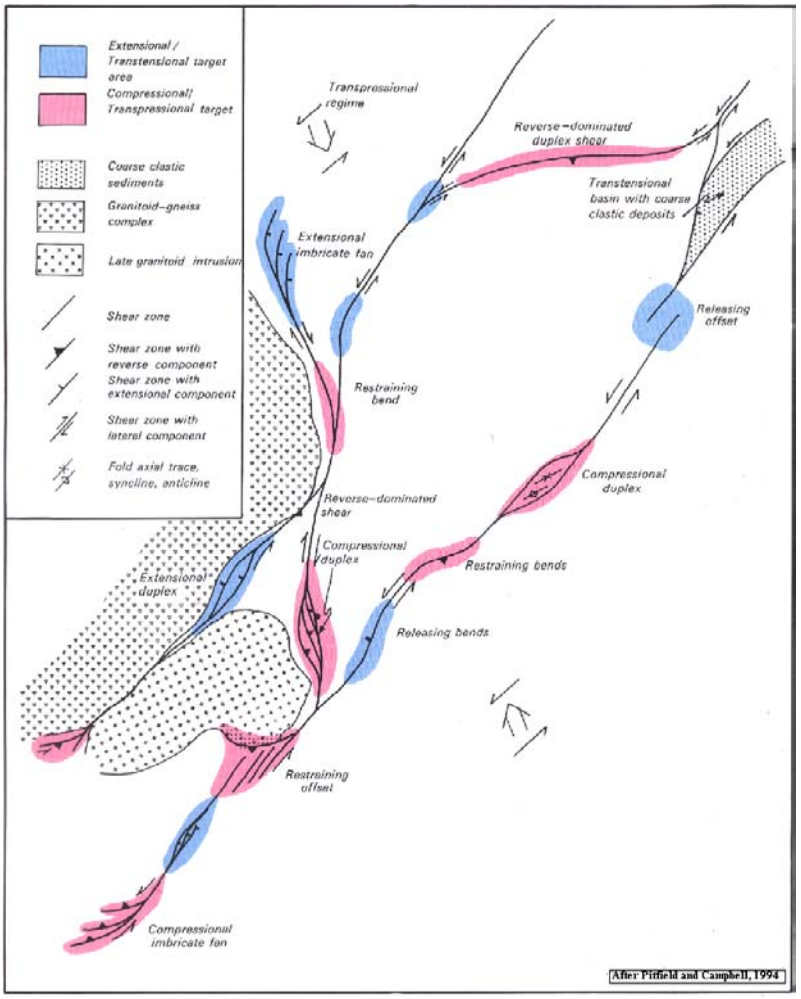

Figure 4.2: Idealized structural configuration associated with shear zones.

Favorable areas with respect to folds

Fold noses in particular and associated axial shearing are favorable sites for gold mineralization. Other favorable sites include areas of limb shearing and limb asymmetry. Association of fold axes with synvolcanic intrusions, especially felsic intrusions, suggesting volcano-tectonic structures are also potential hosts for gold deposits, as well as folding of inter-bedded felsic rocks with greenstones or BIF and fold axes parallel to the nearby granitoid margins. Figure 4.3 shows potentially mineralized sites with respect to fold structures. The potential fold controlled gold deposit targets are highlighted.

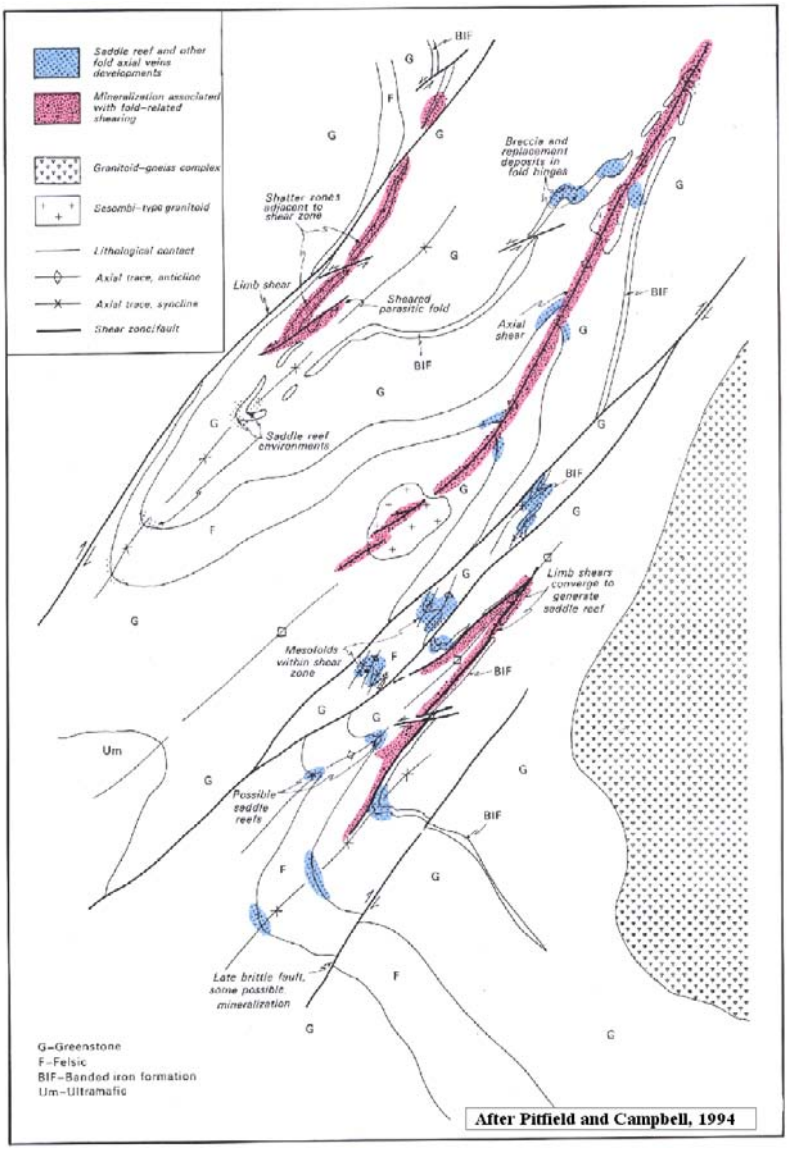

Figure 4.3: Idealized structural configuration associated with folding.

4.3.2 Stratigraphic criterion

The following stratigraphic settings are potential host to Archean lode gold deposits: proximity to the margin of the greenstone belt; proximity to the margin of granitoids within the greenstone belt; and alternating felsic and greenstone lithologies and their contacts. Contacts between BIF and ultramafic units with other rock types are particularly favorable. Areas of clastic rocks associated with shear zones are also potentially mineralized. The latter indicate possible transtensional or transpressional tectonics. Areas of lithological contrast, especially in or adjacent to shear zones are favorable sites for Archean lode gold mineralization.

4.3.3 Granitoids criterion

Contacts between rocks with contrasting competency (e.g., felsic/greenstone) striking parallel to granitoid margins are potentially gold bearing. Radial faults and shear zones relative to the granitoids, concentric arrays of felsic intrusions near granitoids, domal structures near granitoids, particularly along strike from exposed granitoids are all potential host sites for Archean lode gold deposits. Figure 4.4 shows the spatial association of granitoid intrusions with Archean lode gold target areas. The potential granitoid related gold deposit targets are highlighted.

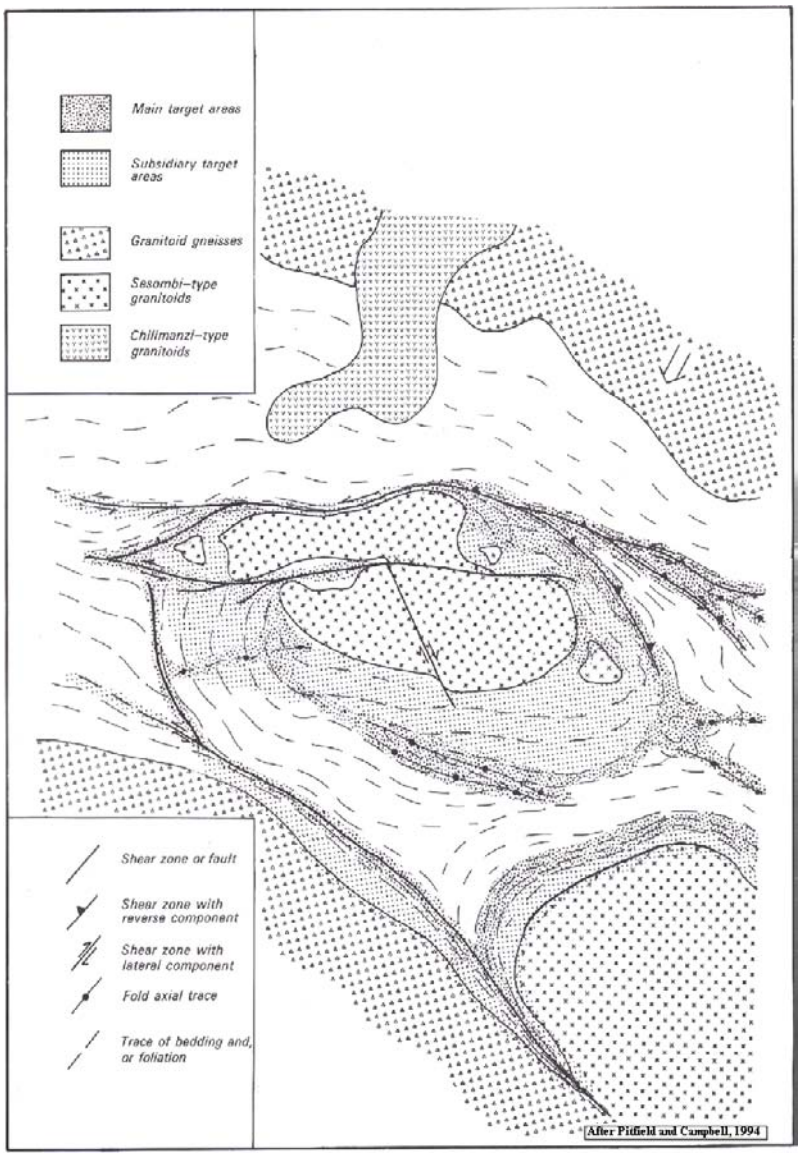

Figure 4.4: Idealized structural configuration associated with granitoids.

4.3.4 Hydrothermal alteration criterion

Hydroxyl alteration zones resulting from hydrothermal activity during emplacement of mineralization and iron oxide enrichment associated with the weathering of sulphides indicate potentially mineralized sites. On a regional scale, the zones of alteration can be extracted from appropriately processed satellite images.

4.3.5 Conclusions

From the above account, the major features of Archean lode gold deposits important for mapping potentially gold bearing areas are their proximity to lithological contacts, shear and fold structures, diapiric granitoids and hydrothermal alteration zones. The spatial associations of potential gold deposit targets with shear zones, fold structures and diapiric granitoids in an idealized greenstone belt are shown on Figure 4.5. Potential gold deposit targets are highlighted. Extraction of these features from the data set of the study area in order to generate predictive models for Archean lode gold deposits is described in chapter 5.

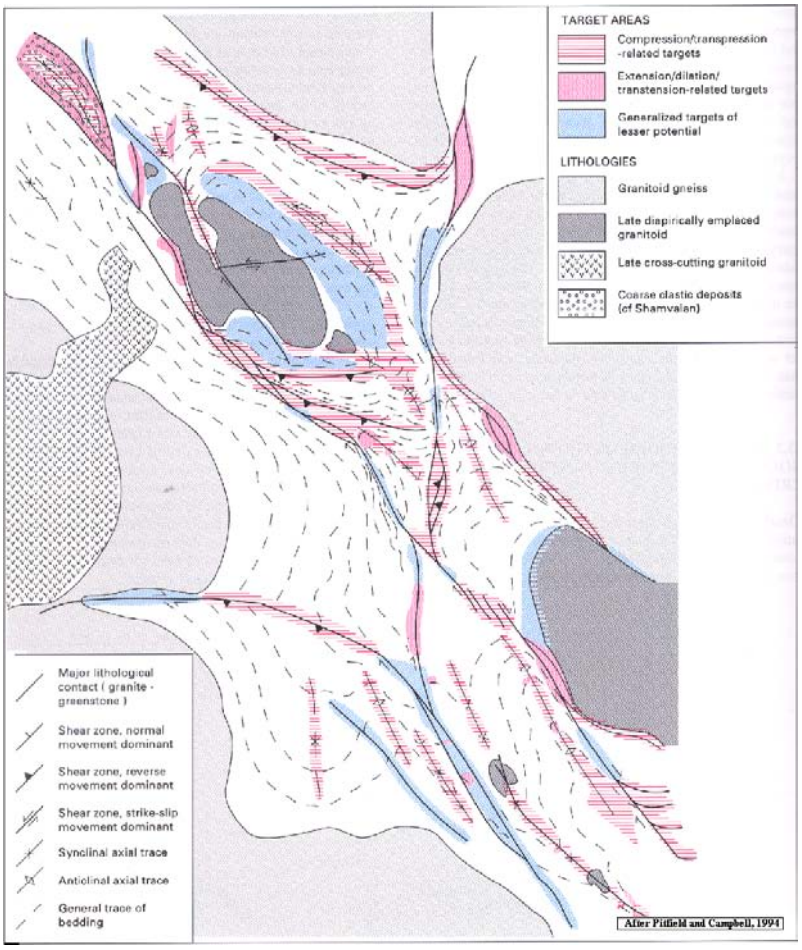

Figure 4.5: Idealized structural configuration of a greenstone belt.

Chapter 5

Extraction of geological features indicative of Archean lode gold potential

5.1 Introduction

This chapter describes the extraction, from geoexploration datasets, the geological features indicative of Archean lode gold mineralization according to the conceptual Archean lode gold deposit model discussed in the previous chapter. Qualitative knowledge on the spatial associations of mineral occurrences with the different geological features is the basis of most exploration programmes [10]. In this study, the qualitative and quantitative knowledge of the spatial associations between geological features and gold deposits is used to judge the importance of the different geological features for gold mineralization in the study area. The geological features examined are lithology, granitoids, structure and alteration zones.

5.2 Gold deposits

Records of gold production show that individual gold deposits range in size from less than 1 tonne to 35 tonnes (Lonely Mine) cumulative production, but there are no appreciable regional differences in gold output within the greenstone belt. The fractal (scale invariance) distribution of known gold deposits indicates that the 1 to 10 tonne category of gold deposits is under-represented in the Bubi greenstone belt [28]. Due to the similarities in Archean lode gold mineralization processes in the Zimbabwe Archean craton, this category of gold deposits therefore has a higher probability of being discovered within the study area in future.

Two hundred and one gold deposits occur in the study area. The gold deposits were grouped into two classes according to recorded gold production, small deposits (<10-100 kg gold) and large deposits (>100 kg gold). In chapter six, the 149 small deposits (Figure 5.1) are used for modelling gold potential. The 51 large deposits (Figure 5.2) are used for validating

the predictive models. A scanned hard copy map of gold deposit locations was georeferenced and the locations of the gold deposits were digitized on-screen.

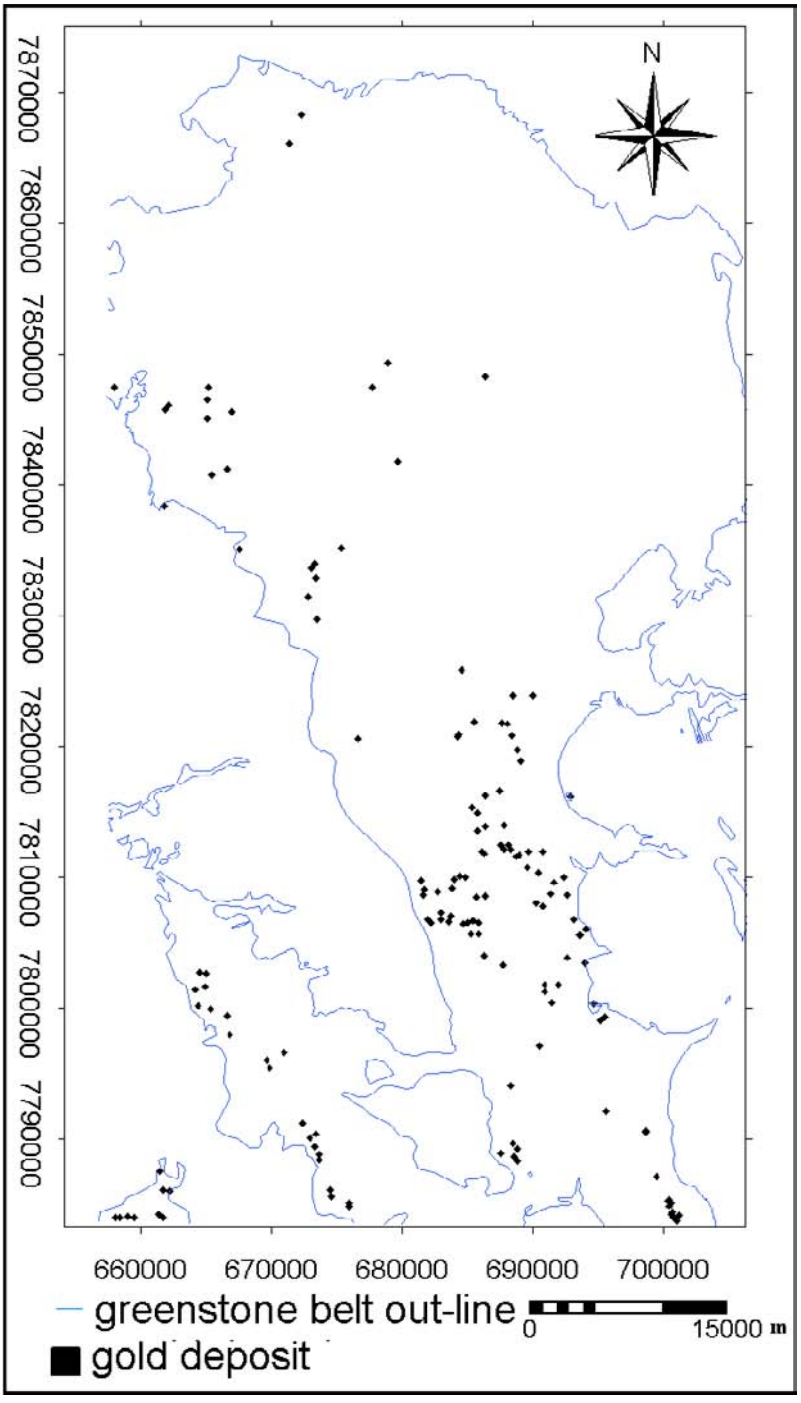

Figure 5.1: Gold deposits used for generation of predictive gold potential models.

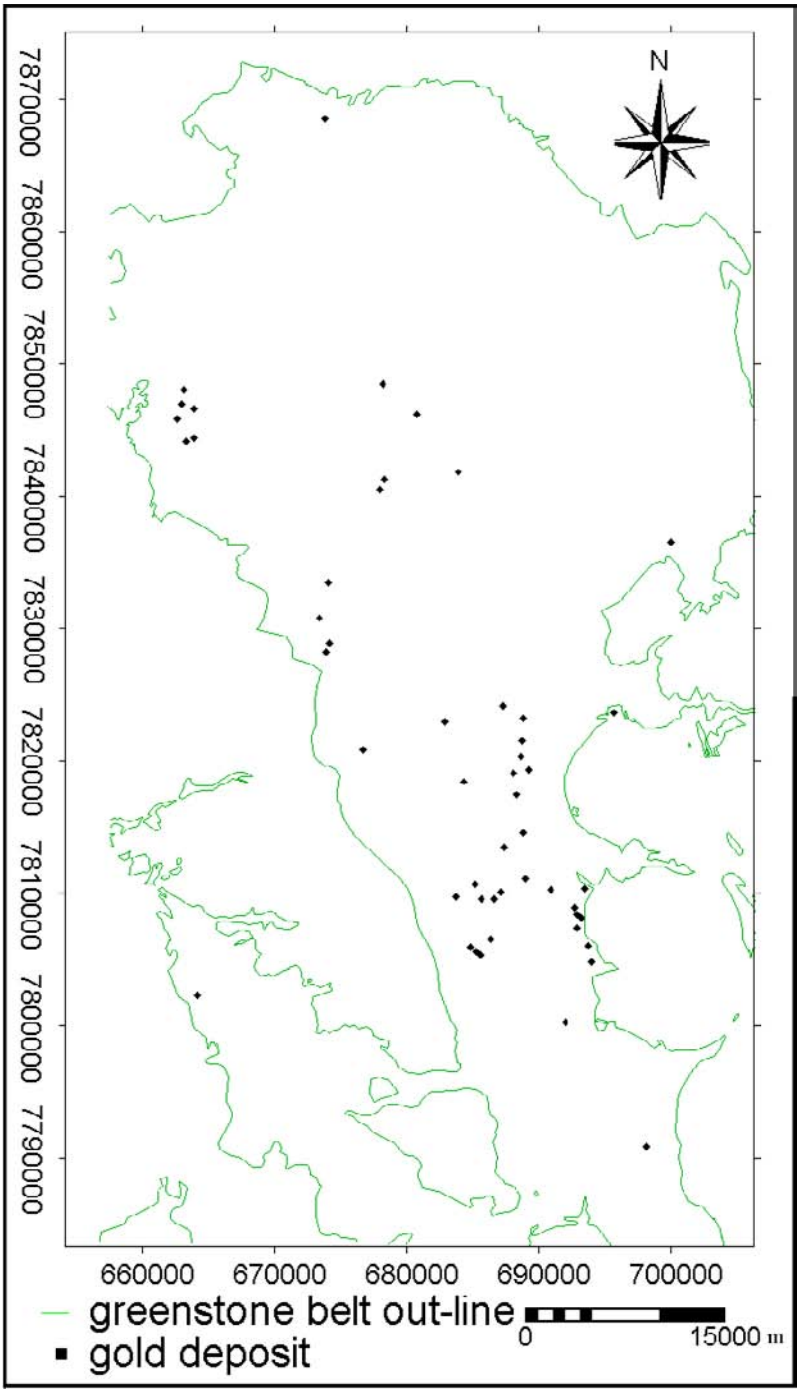

Figure 5.2: Gold deposits used for validation of predictive gold potential models.

5.3 Lithology

The Bubi greenstone belt is covered by 4 ZGS geological map sheets of variable quality (Figure 5.3). These are as follows; Bulawayo area (scale 1:100, 000, [8]), Gwampa Valley area

(scale 1:100, 000, [18]), Lonely Mine area (scale 1:119,000, [17]) and Queens Mine area scale 1:100 000, [18].

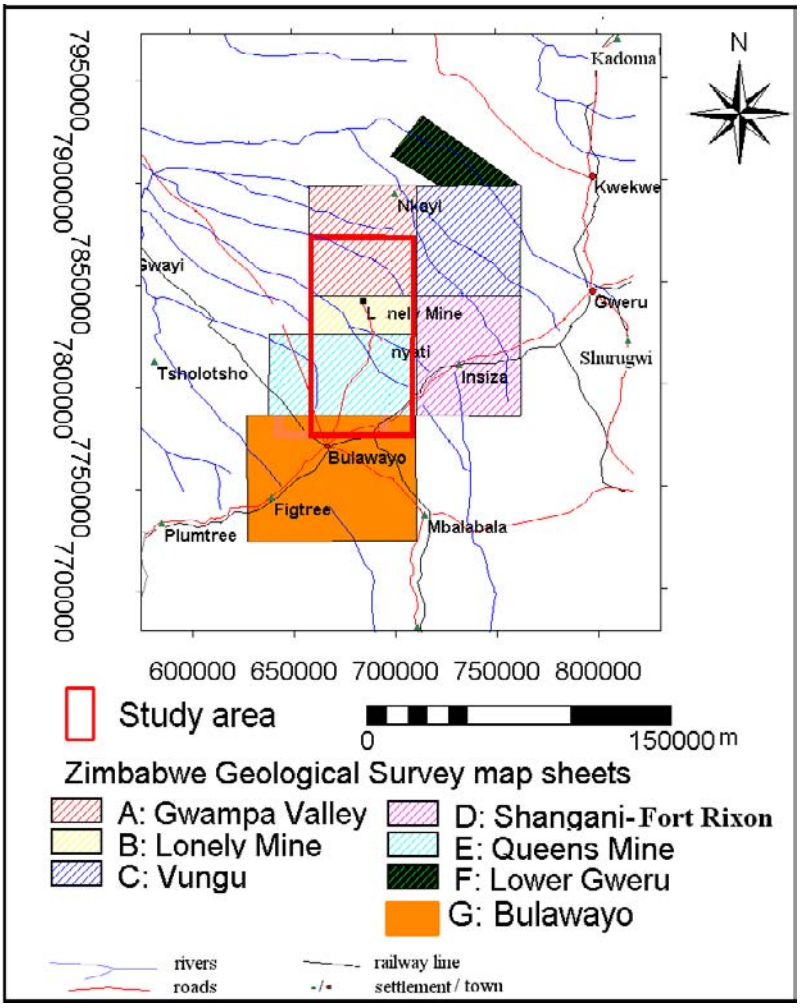

Figure 5.3: Map showing Zimbabwe Geological Survey map sheets in the vicinity of the Bubi greenstone belt.

The Gwampa Valley geological map sheet, covering the northern half of the study area, is the most detailed and has a comprehensive legend (Figure 5.4). This map was used as the reference map during map compilation. The scanned geological maps were georeferenced and digitized on screen as segment maps which were subsequently glued together and polygonized. The resultant geological map was overlaid on the processed aeromagnetic image of the study area and geological contacts were slightly adjusted according to the aeromagnetic intensity variations on the image.

Known gold deposits are spatially associated with some lithological units and not with others. The spatial distribution of gold deposits in relation to lithology is shown on Figure 5.5.

Lithologic formations favorable for gold mineralization, in descending order, according to density of known gold deposits hosted are; Mbembesi River Volcanic member (y7), Dollar Block Formation (y12), Zwangendaba Formation (y6), Dagmar Formation (y14), Lonely Mine Volcanic Formation (y10), Ventor Formation (y8) and Ndutshana Formation.

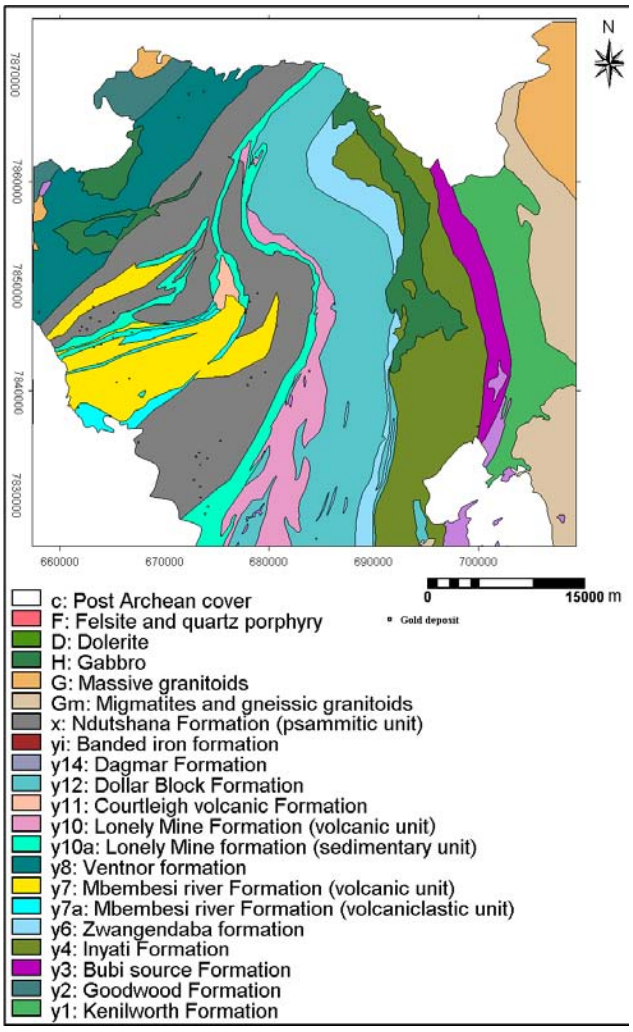

Figure 5.4: Simplified lithological map of the Gwampa Valley area.

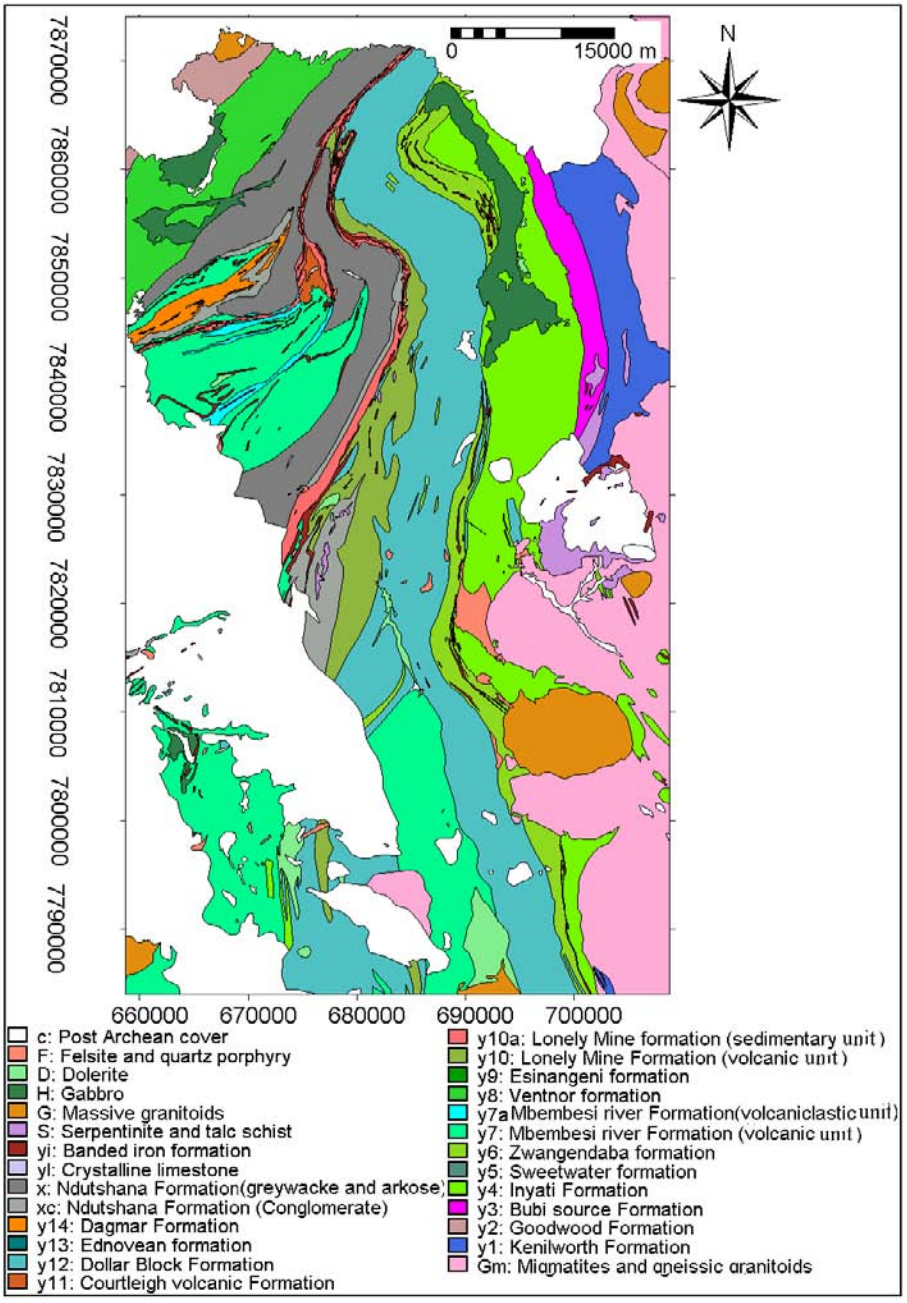

Figure 5.5: Lithological map of the study area: compiled from 4 ZGS geological map sheets.

5.4 The granite-greenstone contact

Sm-Nd age dating of scheelites from gold deposits in the Midlands greenstone belt indicates that one of the two gold mineralization phases was broadly coeval with the diapiric emplacement of the Sesombi suite of granitoids (c. 2.65 Ga) [27]. The exact role played by the granitoids in gold mineralization (source of gold bearing fluid and/or heat source driving hydrothermal circulation of fluids in adjacent discontinuities) is uncertain. Forceful granitoid diapirism influenced the local and regional structure of the Bubi greenstone belt. At the margins of the greenstone belt, gold-hosting structures with mainly reverse dominated movement and dipping away from the granitoid contacts are common [28]. This is evidence for a genetic link between the granitoids and gold mineralization.

The granite-greenstone contacts were digitized from the geological maps covering the Bubi greenstone belt, glued together and polygonized. Gold deposits tend to occur close to the granite-greenstone contacts (Figure 5.6).

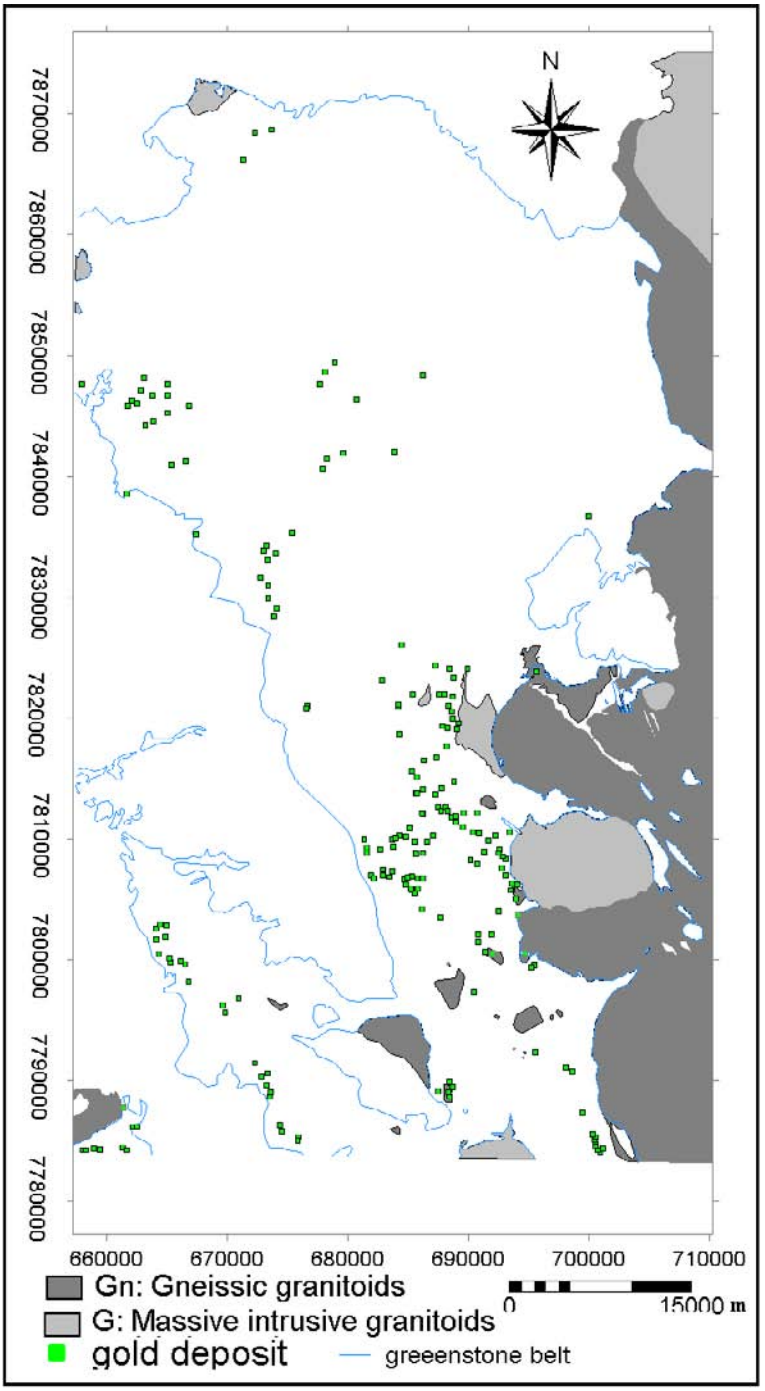

Figure 5.6: Granitoids extracted from geological maps.

5.5 Structural features

Structure is the single most important control factor on the spatial location of the dominantly epigenetic Archean lode gold deposits [12]. Structural features are therefore valuable evidence for predictive modelling of gold potential. In the Bubi greenstone belt, most gold deposits exhibit clear structural controls. The deposits typically occur in or close to deformation and shear zones, fold axial traces, faults and fractures and zones with high foliation/shear fabric density. An important aspect of using structural analysis during area selection in gold exploration is the scale invariance or fractal nature of the structural patterns produced during deformation which implies that the same geometries are identifiable at all scales from local (deposit) scale to regional scale [4].

Most of the gold-only mineralization in Archean greenstone belts was formed during the main deformation, metamorphism and syn-to late-kinematic emplacement of granitoids [26]. Archean lode gold deposits in the study area are hosted by shear and deformation zones. These are typically linear to curvilinear features in plan. Zones of strain contrast during deformation are important sites of gold mineralization [12]. Foliations and shear fabrics are useful measures of strain suffered by the different rock units.

Shear and deformation zones, foliation and shear fabrics occur as lineaments on remotely-sensed images. A lineament is a mappable, simple or composite linear feature of a surface whose parts are aligned in a straight or slightly curving relationship and which differs distinctively from the patterns of adjacent features and presumably reflects a sub-surface phenomenon [31].

The Bubi greenstone belt is predominantly of low deformation strain, with dominantly northerly trending structural features (NNW to NE), similar to greenstone belts in the central parts of the Zimbabwe Archean craton. The first-order high-strain zones in the study area follow the boundaries of the calc-alkaline formation and subdivide the greenstone belt longitudinally into periclinal synclinoria with an intervening upright, doubly- plunging anticline which is cored by the Ncema granitic complex [27]. The gold-bearing shear and deformation zones are essentially second-order and third-order structures related to ductile shear zones with strike lengths of tens of kilometers and are readily detectable on suitably enhanced satellite images. The gold mineralization is generally associated with the late stage Archean deformation of the granite-greenstone terrain [26].

Archean lode gold deposits occur in similar geological environments world wide [3]. An example of a particulary well studied greenstone belt in Zimbabwe, with similar geological characteristics to the Bubi greenstone belt is the Midlands greenstone belt [27] (Figure 1.1). On a local scale, gold-bearing shear zones in the Midlands greenstone belt are up to three kilometers in strike and rarely exceed 6 m in width. They extend to depths of up to 2 km below surface. However, most gold mines have maximum depths of 300m [27]. There are three main orientations of gold-hosting shear zones within the Midlands greenstone belt [28]. The most common gold-bearing shear zones strike parallel to S1, have typically shallower dip angles than the foliation and are often reverse-dominated shears related to D1-deformation.

Mineralized shear zones that strike acutely to and dipping shallower than S1 are associated with oblique reverse kinematics related to D1-deformation. Shear zones that strike approximately oblique to S1 but parallel to S2, with generally shallower dip than S2 are associated with a wide range of kinematics and are related to more than one phase of deformation (D1 and D2) [27].

5.5.1 Structural features from aeromagnetic imagery

Magnetic properties of rocks are mostly a direct result of the presence or absence of magnetite in the rocks. Aeromagnetic imagery is therefore a useful tool for mapping subsurface geological and structural differences made visible by the variations in magnetic susceptibility. Structural discontinuities can be detected from aeromagnetic images because of sharp gradients in magnetic intensity between the structural discontinuities and their surroundings. Oxidation in fractures, faults and shear zones during weathering destroys magnetite. This results in narrow zones with markedly less magnetic variations than the surrounding rocks in which they occur [20]. Structures can therefore be delineated in suitably enhanced aeromagnetic images.

In this study, aeromagnetic imagery is used to extract deep-seated planar structures which are probably conduits for mineralizing fluids. Airborne magnetic data covering the Bubi greenstone belt were windowed in from a larger data-set obtained from the Zimbabwe Geological Survey (Appendix 1). The grid cell size is 325m X 325m.

The average magnetic field inclination and declination in the study area is -60^o and 6.5^oW respectively. In Zimbabwe, magnetic anomalies over typical magnetic bodies have shapes that display negative anomalies to the south of the sources causing them [30]. These bipolar anomalies complicate the delineation of linear structures. A shaded-relief aeromagnetic image of the study area was generated (see Appendix 1). The shaded-relief image is an effective representation of complex textural and linear features [20]. The shaded-relief image was reduced to the pole (a procedure that produces profiles as they would appear at a magnetic inclination of 90^o) in order to give simpler shapes to the anomalies in the shaded relief image (Appendix 1).

Grey scale shaded-relief images were created from which lineaments were interpreted. Successful representation of lineaments in shaded-relief images depends on the illumination azimuth, illumination angle above the horizon and vertical scale exaggeration. General structural trends in the area are variable, therefore a series of grey scale shaded relief images of reduced to the pole data were generated. Three images with illumination angle above the horizon of 0^o and illumination azimuths of 090^o, 152^o, and 170^o respectively exhibited the best lineament definition. These were used for structural interpretation. The lineaments were digitized as segments and labelled by orientation (N-S, NE-SW, and NW-SE). Figure 5.7 shows one of the grey scale shaded-relief images. The image has Artificial illumination angle above the horizon of 5^o , illumination azimuth of 090^o and a vertical scale of 0.08. The gold deposits and interpreted lineaments are shown on the figure.

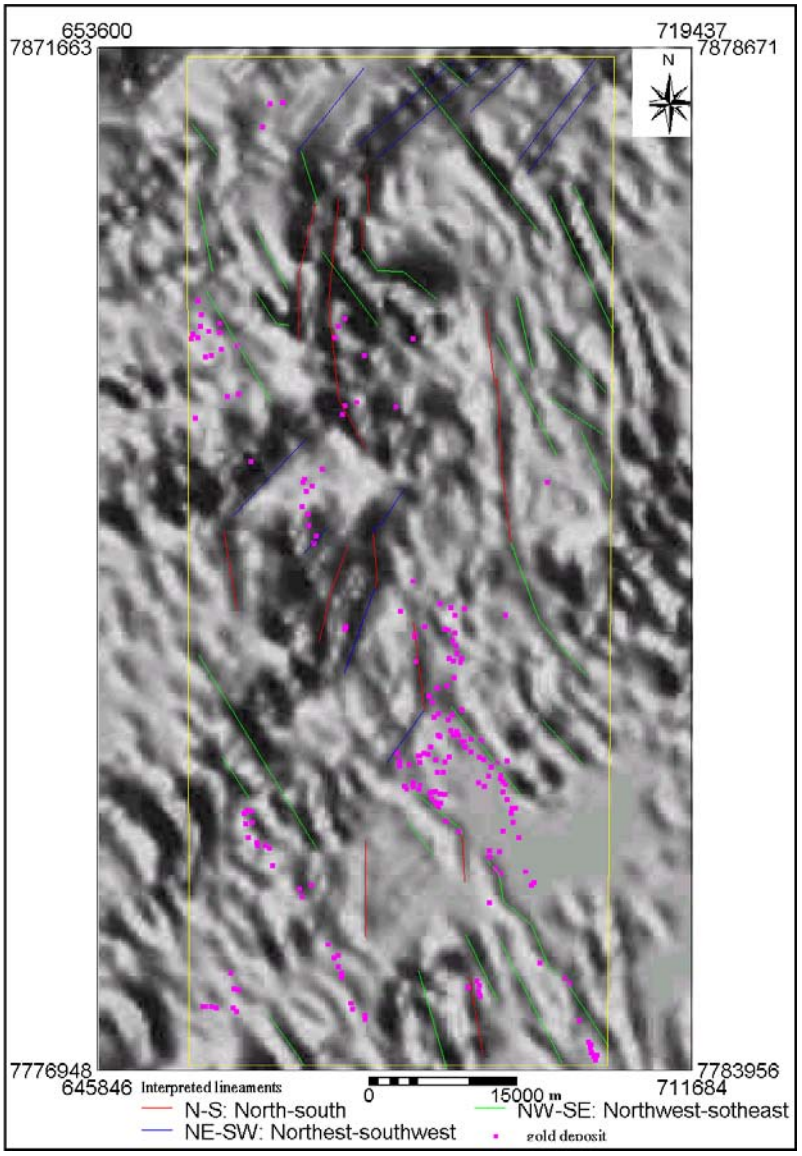

Figure 5.7: Grey scale shaded relief image of the air-borne magnetics data with interpreted lineaments.

There is spatial association between the gold deposits and the interpreted lineaments, suggesting a genetic link between the two. The Lineaments from airborne magnetic data are probably expressions of deep-seated first-order deformation and shear zones exploited by mineralizing fluids.

5.5.2 Structural features from Landsat TM imagery and geological plans

The structural framework of the Bulawayo-Bubi greenstone belt based on analysis of Landsat TM with limited ground reconnaissance data was established during the Midlands Goldfield Project [27]. Landsat TM scenes 171-073 and 171-074 were used to produce edge-enhanced and contrast-stretched false color composites comprising bands 4-1-7 (R-G-B) at a scale of 1:100,000. Single band 5 composite and false color de-correlation stretch (components 4, 5, 6) imagery was also used in the Bubi area due to difficulties in interpretation related to poor definition and color balance in the 4-1-7 color composite covering this area [27].

A hard-copy map of the interpreted structures at a scale of 1:85 000 was obtained from a publication summarizing the results of the Midlands Goldfield Project.The map was digitized and georeferenced. Deformation/shear zones and foliation/s fabric were digitized as separate layers and stored as segment files. The deformation/shear zones were labelled by type while the foliation/s fabric layer was edited to remove post Archean deformation fabrics which cut earlier structures. Deformation/shear zones are anostomosing with general NE-SW trends in the northwest part of the greenstone belt and NNE- SSW in the southeastern part of the greenstone belt (Figure 5.8). Foliation/s fabric trend sub-parallel to the deformation/shear zones (Figure 5.9). Dips are generally steep, $> 70^o$. Both deformation/shear zones and foliation/s fabric are spatially related to gold mineralization (Figures 5.8 and 5.9).

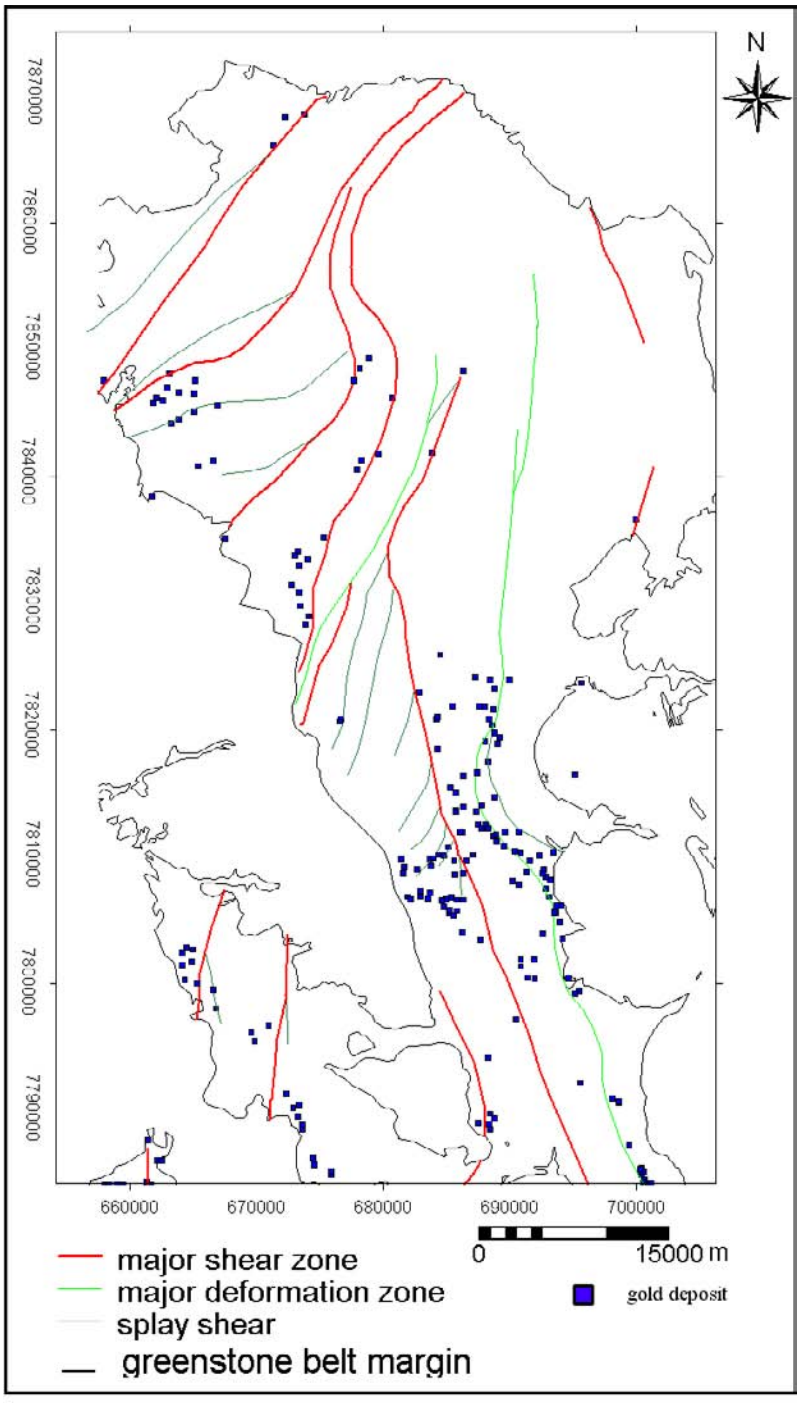

Figure 5.8: Deformation/shear zones extracted from Landsat TM imagery.

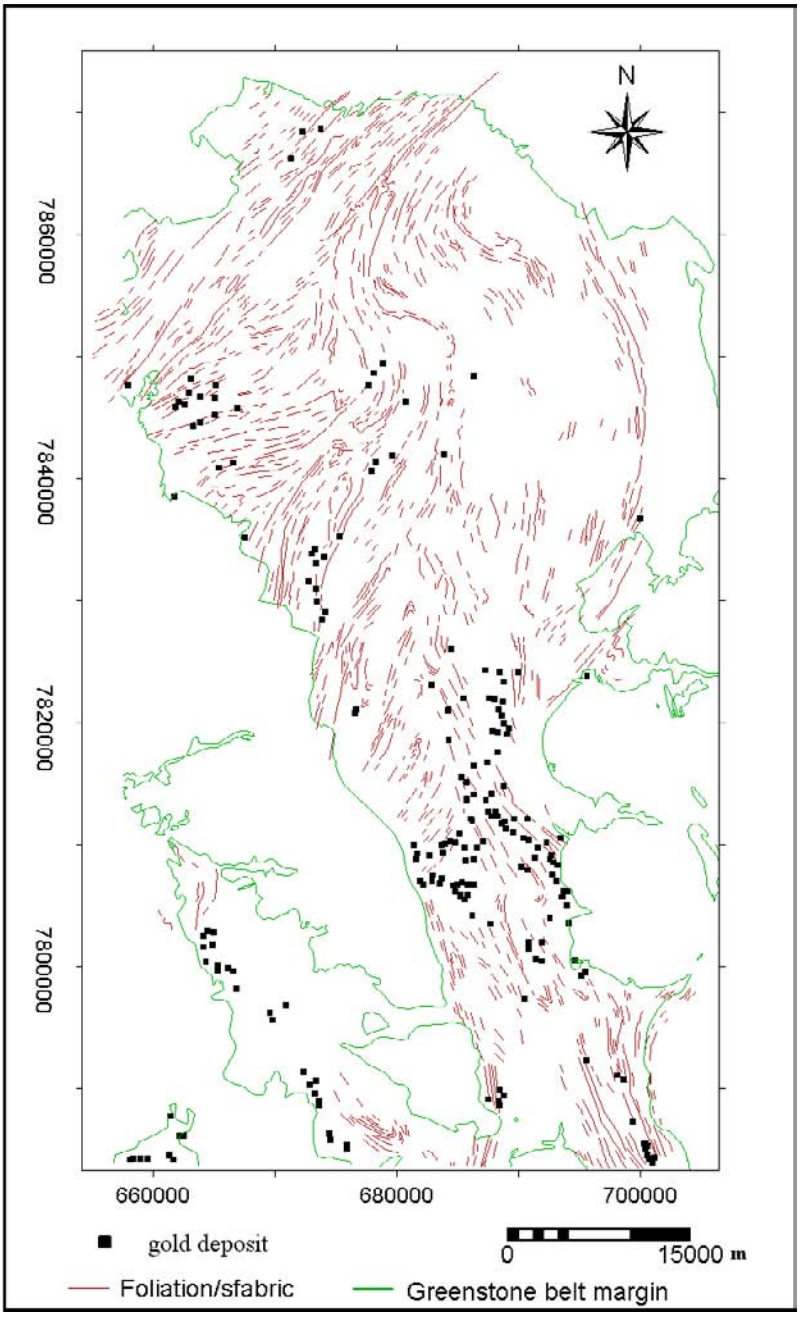

Figure 5.9: Foliation/s-fabric extracted from Landsat TM imagery.

Fold axial-traces were interpreted from orientation and shape of foliation/s fabric and geological contacts, as well as from strike and dip information on geological maps and stratigraphic descriptions in geological literature. The folds axial traces were digitized as segments. The spatial associations of fold axial traces with gold deposits are shown on Figure 5.10.

The dominant fold structure in the northern part of the Bubi greenstone belt is an as-

symetric, southward-plunging synclinorium which is refolded by the Inunwa inflection, a z-shaped D2-warp. The folds in the study area are dominantly, upright, tight to isoclinal and are parallel to the major deformation zones which, together with the shear fabric, are deflected around the Ncema granitic complex in the southern part of the study area.

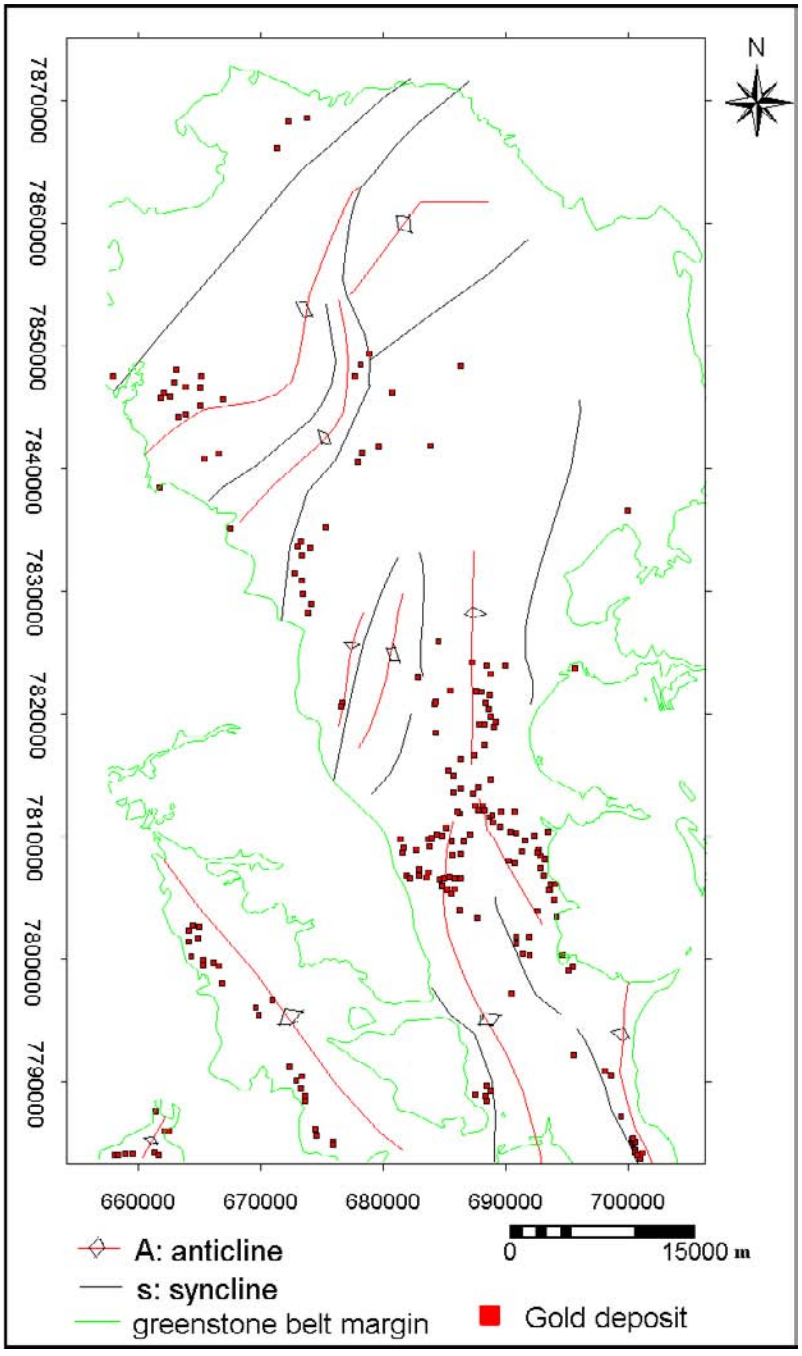

Figure 5.10: Fold axes interpreted from structural and geological maps.

The Gwampa Valley geological map sheet, covering the extreme northern part of the study area has detailed structural information. The rest of the map sheets have scant structural information. The faults and fractures on the Gwampa Valley map sheet were digitized as segments. These were then classified into 4 groups with N-S, E-W, NE-SW and NW-SE. Figure 5.11 shows the spatial association of faults and fractures with gold mineralization in the area covered by the Gwampa Valley map sheet.

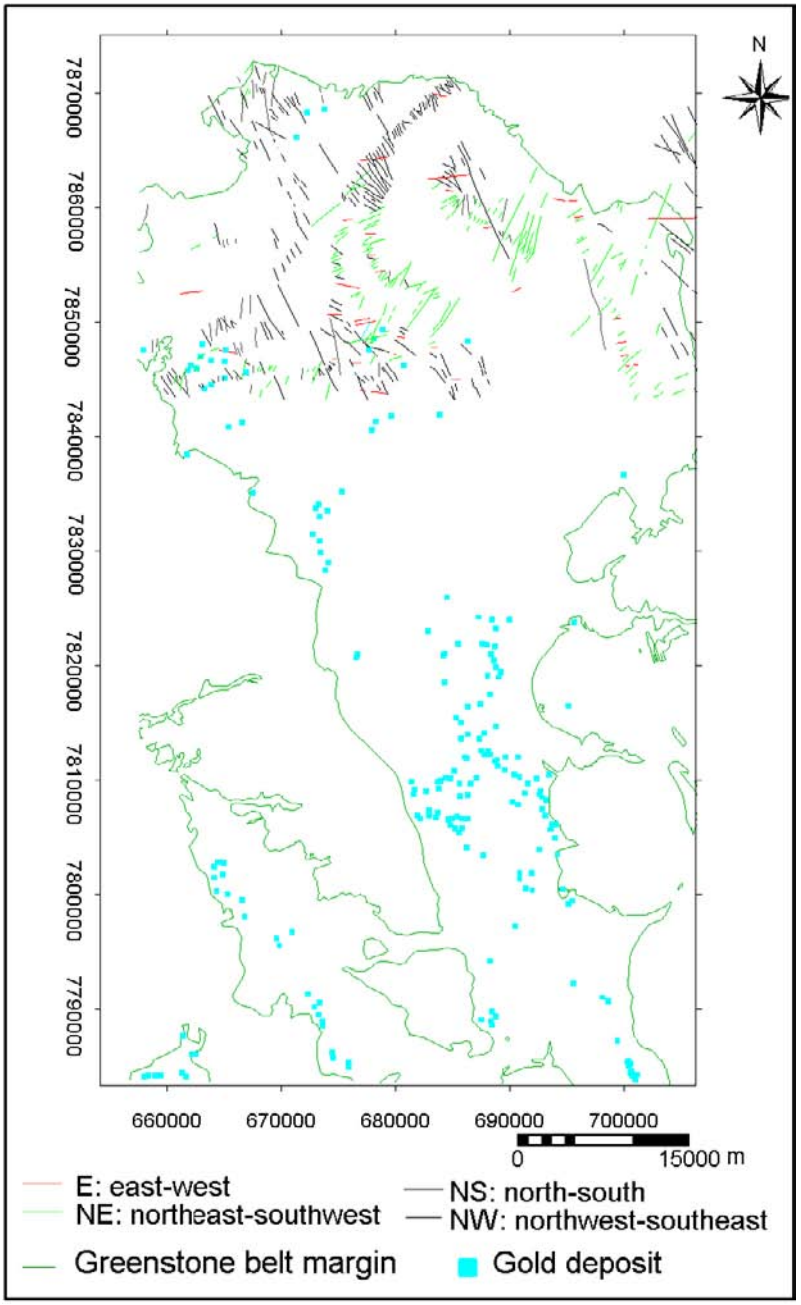

Figure 5.11: Faults and fractures extracted from the Gwampa Valley geological map.

5.6 Alteration zones

5.6.1 Introduction

Principal component analysis (PCA) was applied to ASTER imagery data in order to map zones of hydrothermal alteration. Kaolinite and silica are formed during hydrothermal alteration of the host rocks of many classes of mineral deposits, including Archean lode gold deposits. Secondary iron oxide minerals, mainly limonite can indicate hydrothermally altered rocks. In most cases, Archean lode gold deposits are associated with sulphides, which are oxidized to iron oxides, resulting in gossans. Zones of kaolinite, silica and limonite enrichment are useful indications of hydrothermal alteration [16].

PCA is a multi-variate statistical technique, which selects uncorrelated linear combinations (eigen-vector loadings) in such a way that each successively extracted linear combination or principal component (PC) has a smaller variance [5, 21]. The statistical variance in multispectral images is related to the spectral response of the various surface materials. The spectral response of limonite is characterized by absorption in ASTER band 1 and reflectance in band 2. Kaolinite absorbs in ASTER bands 5 and 6 and reflects in band 4 (Appendix 2).

In PCA the chance of defining a unique PC, which maps a specific mineral class can be increased if the number of input bands is reduced to avoid a particular spectral contrast [5]. Due to difficulties of discriminating kaolinite and limonite using the standard PCA on six bands, selective use of four input bands (Crosta technique) is used for mapping the two minerals separately [5]. The subtle spectral information related to limonite and kaolinite enrichment can be detected by using appropriate bands selected on the basis of reflection and absorption regions on spectral reflectance curves of the two minerals. The Crosta technique relies on the principal component transformation to map overall scene brightness into PC1 and specific spectral contrasts into successive PCs. In the Crosta technique, the PC eigen-vector loadings are examined to determine which of the PC images will concentrate information related to the spectral signatures of particular materials [5]. The technique is capable of predicting whether the target mineral will be represented by bright or dark pixels in the PC images according to the magnitude and sign of the eigen-vectors. In this study, the Crosta technique is applied to ASTER imagery data. This technique has been tried and tested on TM and ATM images from various parts of Nevada and Oregon, and on TM images from southern Spain, the eastern Mediterranean, the Middle East and the Andes [5].

5.6.2 Image pre-processing and georeferencing

The ASTER images were acquired on 01-09-2001 at approximately 08:24 Hrs and 04-11-2001 at approximately 08:22 Hrs respectively. Each data set comprises three scenes.

The ASTER images were geometrically corrected. Topographic features (mainly river and road junctions) were used as ground control points to georeference the images. UTM coordinates from topographic maps were entered for the corresponding features on the image. The

individual bands were resampled to the same georeference and glued together. Un-stretched data did not give satisfactory results. Linearly stretched images, prior to PC transformation were used.

5.6.3 Extraction of iron oxide enriched zones

Limonite is characterized by absorption in ASTER band 1 and reflectance in bands 2 (Appendix 2). A PC image with strong eigen-vector loadings of opposite sign in band 1 and band 2 will map limonite enriched zones.

PCA (Crosta technique) was applied on linearly stretched ASTER image bands 1, 2, 3, 4. The matrices from the two data-sets are very similar. The PC 4 has the highest eigen-vector loadings in both bands 1 and 2 (in bold, Table 5.1) with positive and negative signs respectively. The strong eigen-vector loadings in PC 4 highlight limonite-enriched zones as dark pixels. This is because limonite has strong absorption and reflection in bands 1 and 2 respectively. If the eigen-vector loadings are positive for band 2 and negative for band 1, limonite-rich pixels will be displayed as bright pixels. The PC 4 image was negated in order to enhance the limonite rich zones as bright pixels (see appendix 2).

Table 5.1: Principal component analysis for limonite mapping.

Dataset 1	Band 1	Band 2	Band 3	Band 4	Eigen-value(%)
PC1	0.440	0.480	0.531	0.542	90.67
PC2	0.398	0.335	0.212	-0.827	6.59
PC3	0.463	0.317	-0.815	0.142	2.19
PC4	**0.659**	**-0.746**	0.090	0.038	0.55
Dataset 2	Band 1	Band 2	Band 3	Band 4	Eigen-value(%)
PC1	0.464	0.480	0.539	0.514	85.88
PC2	-0.047	0.070	-0.699	0.710	6.92
PC3	-0.494	-0.558	0.464	0.480	6.42
PC4	**0.734**	**-0.674**	-0.073	0.043	0.79

5.6.4 Extraction of kaolinite enriched zones

Kaolinite is characterized by absorption in ASTER bands 5 and 6, and reflection in band 4 (Appendix 2). A PC image with strong eigen-vector loadings of opposite sign in band 4 and in band 5 or 6 will map kaolinite enriched zones. The best results were obtained using ASTER band 6.

The Crosta technique was applied to ASTER bands 1, 3, 4 and 6. As in the case of limonite, the matrices from the two data-sets are very similar. PC 4 (in bold, Table 5.2) has the highest

eigen-vector loadings in bands 4 and 6 with positive and negative signs respectively. This means that the kaolinite enriched zones will show as dark pixels in the PC 4 image. The PC 4 image was negated in order to enhance the kaolinite rich areas as bright pixels (see appendix 2).

Table 5.2: Principal component analysis for kaolinite mapping.

Dataset 1	Band 1	Band 3	Band 4	Band 6	Eigen value(%)
PC1	0.423	0.517	0.564	0.486	89.80
PC2	0.507	0.546	-0.501	-0.440	7.26
PC3	0.686	-0.600	-0.248	0.328	2.19
PC4	-0.306	0.274	**-0.609**	**0.680**	0.75
Dataset 2	Band 1	Band 3	Band 4	Band 6	Eigen value(%)
PC1	0.435	0.512	0.537	0.510	83.73
PC2	0.262	0.699	-0.330	-0.578	11.13
PC3	0.855	-0.448	-0.261	-0.005	3.88
PC4	-0.104	0.220	**-0.731**	**0.637**	1.26

5.6.5 The F+H-image

PCA transformations on the two data sets produced similar results. Data set 1 covers a larger portion of the study ares. Subsequent analysis was carried out on data-set 1 only.

The monochrome limonite (F-image) and kaolinite (H-image) images were integrated to produce an image on which pixels with anomalous concentrations of limonite and kaolinite are brightest (F+H image). This was done through a pair-wise PCA in which the inputs are the F image and H image. The input images were suitably stretched prior to PCA transformation in order to equalize their statistics such that the eigen-vector loadings are approximately equal in the output PCs . The output matrix for the pairwise PC transformation is shown on Table 5.3

Table 5.3: Pairwise Principal component analysis for limonite and kaolinite mapping.

PC	F image	H image	Eigen value(%)
PC1	-0.316	0.949	62.09
PC2	**0.949**	**0.316**	37.91

The image with positive loadings from both input images is the F+H image (in bold, Table 5.5). This image is shown in Appendix 2.

5.6.6 The Crosta color composite

A color composite was created by combining the monochrome H-image, H+F-image and F-image in red, green and blue respectively. The color composite, with interpreted alteration zones overlain, is shown in Figure 5.12. On this color composite, white pixels within alteration zones are both iron stained and argillized, bright reddish to orange zones are more argillized than iron stained and bright cyan to bluish zones are more iron stained than argillized. In areas of intense kaolinization or silicification with heavy iron staining, the reflectance is higher in TM band 7 (ASTER band 6) than in TM band 5 (ASTER band 4). These areas will appear dark in the color composite but with identifiable alteration characteristics. This is because the presence of iron oxides destroys the argillic response in the SWIR and the presence of argillite destroys the iron oxide response in the visible spectrum [5].

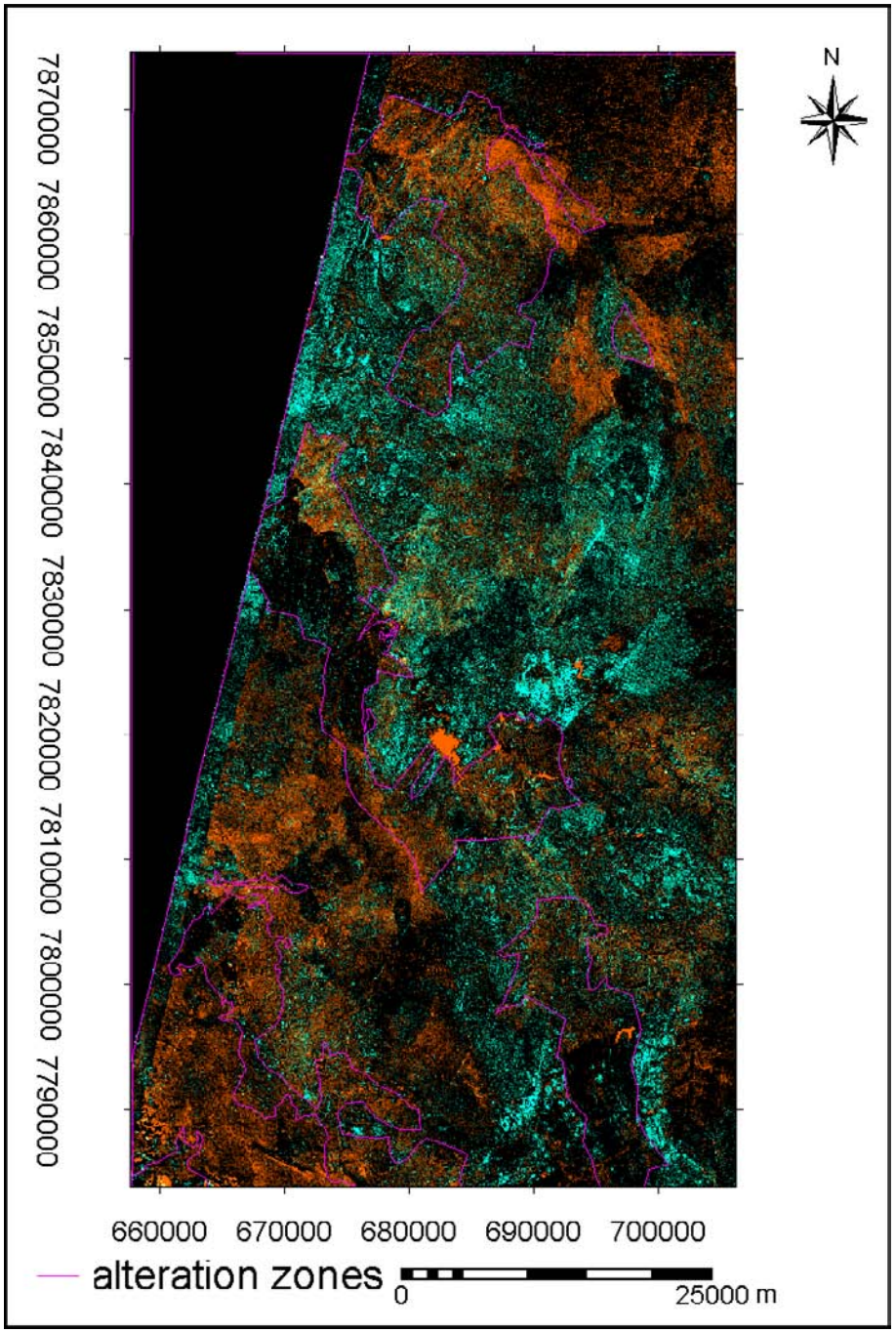

Figure 5.12: Color composite, H (R), H+F (G) and F (B).

5.6.7 Discussion

The alteration zones were interpreted from the color composite and digitized as segments,and polygonized (Figure 5.14).

The effect of vegetation cover on alteration mapping was tested by making a Normalized Difference Vegetation Index (NDVI) image which maps vegetated areas. NDVI is the ratio of the difference between the near infra red (NIR) and red (R) bands to their sum. Using ASTER data, the formula is; **NDVI =** $[\frac{band3-band2}{band3+band2}]$. The intensity variation due to illumination is removed through normalizing of the bands by dividing their difference with their total intensity (NIR+R) [33]. Chlorophyll exerts the most influence on the spectral characteristics of vegetation because it strongly absorbs the blue (0.48 μm) and the red radiation (0.68 μm) but reflects in the green wavelengths (0.56 μm) [33]. The reflectance curve of vegetation is shown on Figure 4. The NDVI image shows that vegetation cover (in reddish tones) is generally uniform but sparse within the greenstone belt. The Crosta color composite and the NDVI image do not show any correlation (Figures 5.12 and 5.13). Vegetation cover therefore did not affect the results of alteration mapping.

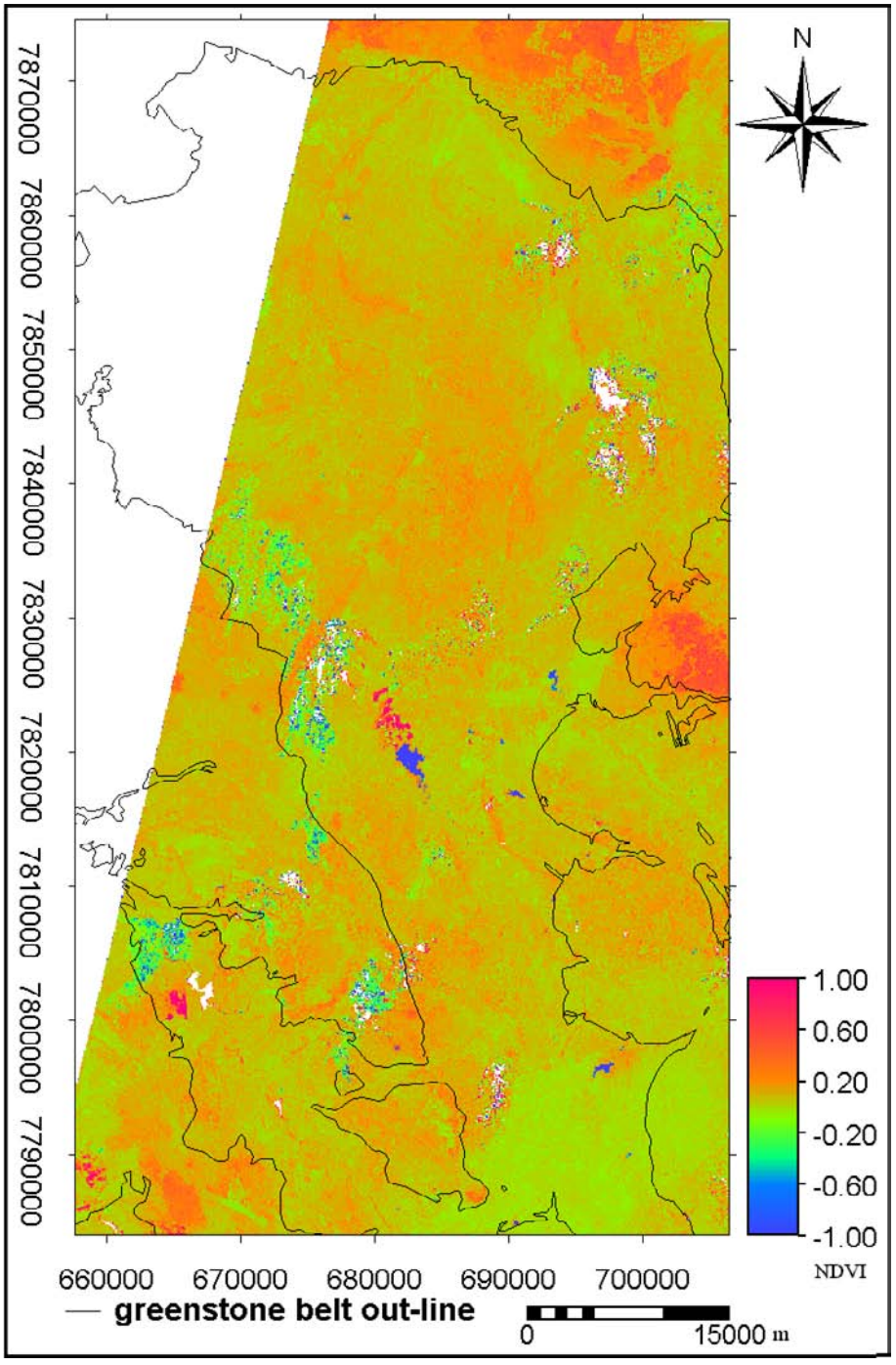

Figure 5.13: Normalized Difference Vegetation Index image.

Three types of alteration zones were distinguished, dominantly kaolinised zones with limonitization (bright reddish to orange zones), limonitized zones with kaolinization (cyan to bluish zones) and zones of intense alteration, either kaolinization or silicification with limonitization (very dark but with identifiable alteration characteristics [16]). Care was taken to leave out areas which are anomalous on the color composite for reasons other than Archean lode gold mineralization by overlying the geological map of the study area with the Crosta color composite during interpretation of alteration zones. The pseudo-anomalies occur on ultramafic rocks, some mafic intrusives and post-Archean cover rocks.

Spatial correlation between the interpreted alteration zones and known gold deposits vary with alteration type with a higher concentrations of gold deposits localized in kaolinized zones.

5.7 Conclusions

Seven different geological features indicative of Archean lode gold deposit potential in the Bubi greenstone belt were extracted from different geoexploration data sets. The indicative geological features are particular lithological units, granitoids, deep-seated discontinuities, deformation/shear zones, foliation/s-fabric, fold axial planes, and alteration zones. The indicative geological features show spatial association with the known gold deposits in the area. The feature maps will be converted to binary predictor patterns and will be used as evidential layers for predictive modelling of gold potential in the area. Quantitative analysis of the spatial associations between the gold deposits and the different geological features was carried out during generation of predictive models for Archean lode gold deposits in the next chapter.

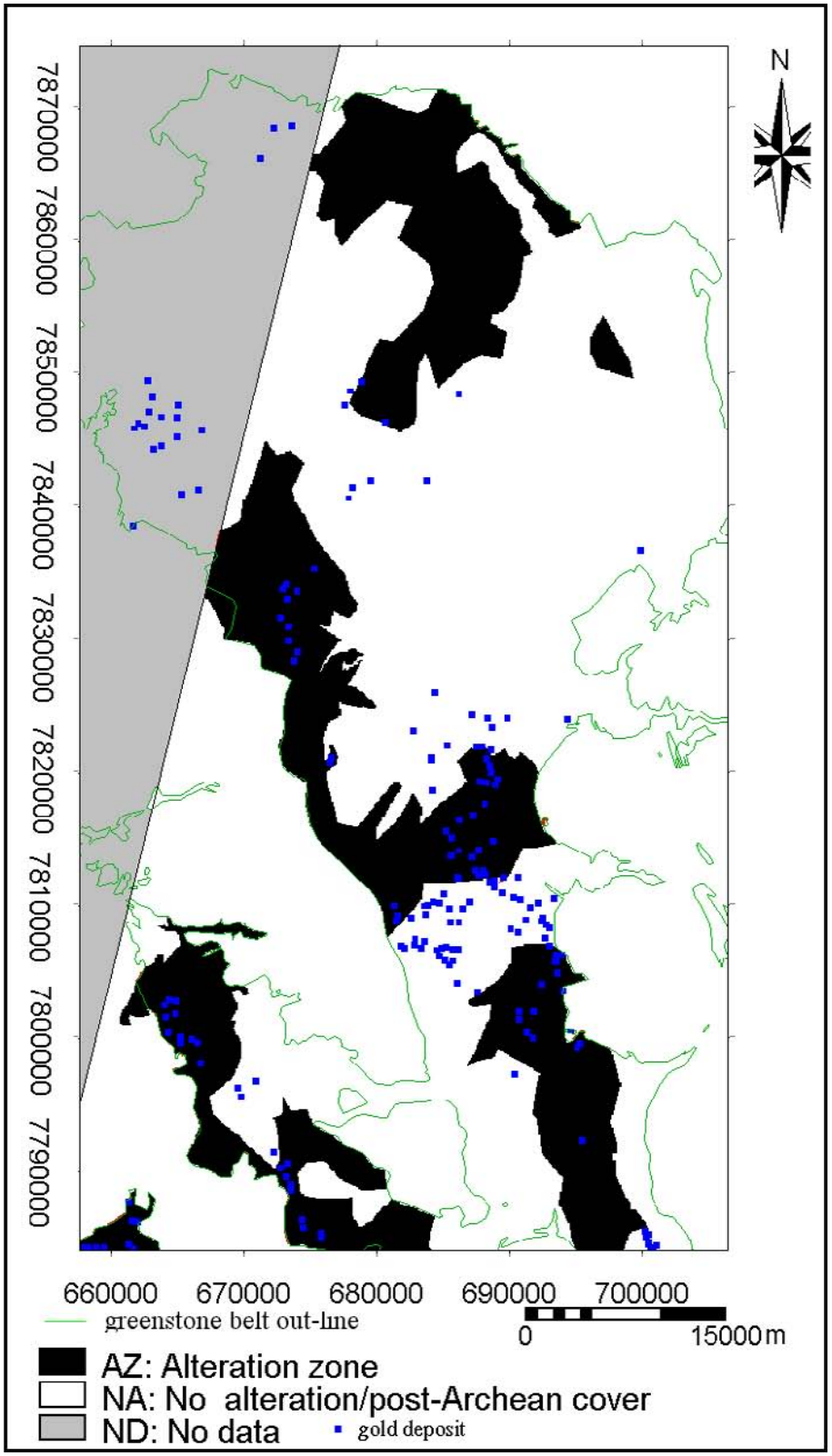

Figure 5.14: Alteration zones extracted from the crosta color composite.

Chapter 6

Spatial data analysis and integration

6.1 Introduction

In this chapter, the results of GIS based spatial data analysis and integration to produce predictive models for Archean lode gold potential in the Bubi greenstone belt are presented. The purpose of spatial data analysis and integration is to produce models which predict the location of the unknown gold deposits, based on geological features that are associated with the location of known gold deposits according to the conceptual model for Archean lode gold deposits. It is assumed that the known gold deposits used in spatial data analysis represent a sample of some population and that the sample is large enough to provide an estimate of the spatial association of the gold deposits with each geological feature. The predictive model is then validated against the gold deposits not used in predictive modelling.

6.2 The weights of evidence method

The weights of evidence method based on Bayesian probability was used to quantify the spatial association between the known small gold deposits and the geological features. Based on the quantified spatial association, binary predictor patterns were created and used as inputs to the predictive models. The output predictive maps indicate the probability of gold deposits and the uncertainties associated with them.

According to Bayes' rule [2], the probability of finding a point (eg. a gold deposit) given the presence of a predictor pattern is given by

$$P\{D/B\} = \frac{P\{D \cap B\}}{P\{B\}} = P\{D\}\frac{P\{B/D\}}{P\{B\}} \tag{6.1}$$

The favorability of finding a mineral occurrence given the absence of a predictor pattern is expressed by

$$P\{D/\overline{B}\} = \frac{P\{D \cap \overline{B}\}}{P\{\overline{B}\}} = P\{D\}\frac{P\{\overline{B}/D\}}{P\{\overline{B}\}} \tag{6.2}$$

Expressed as odds, equations 6.1 and 6.2, respectively become,

$$O\{D/B\} = O\{D\}\frac{P\left(B/D\right)}{P\left(B/\overline{D}\right)} \tag{6.3}$$

$$O\{D/\overline{B}\} = \frac{P\left(\overline{B}/D\right)}{P\left(\overline{B}/\overline{D}\right)} \tag{6.4}$$

The weights of evidence for the binary map relationships are then defined as

$$W^{+} = \ln\left[\frac{P\left(B/D\right)}{P\left(B/\overline{D}\right)}\right] \tag{6.5}$$

and

$$W^{-} = \ln\left[\frac{P\left(\overline{B}/D\right)}{P\left(\overline{B}/\overline{D}\right)}\right] \tag{6.6}$$

where W^{+} and W^{-} are the weights of evidence when a binary is present and absent respectively.
The variances of the weights can be calculated by the following expressions,

$$S^{2}\left(W^{+}\right) = \frac{1}{N\{B \cap D\}} + \frac{1}{N\{B \cap \overline{D}\}} \tag{6.7}$$

$$S^{2}\left(W^{-}\right) = \frac{1}{N\{\overline{B} \cap D\}} + \frac{1}{N\{\overline{B} \cap \overline{D}\}} \tag{6.8}$$

The contrast, C and its standard deviations, s(C), are defined respectively as,

$$C = W^{+} - W^{+} \tag{6.9}$$

$$s\left(C\right) = \sqrt{s^{2}\left(W^{+}\right) + s^{2}\left(W^{-}\right)} \tag{6.10}$$

The studentized contrast [sigC] is then defined as,

$$sigC = c/stdc \tag{6.11}$$

SigC indicates the most statistically significant contrast [10]. Values of sigC>2 are considered to be statistically significant. The contrast or the studentized C provide a useful measure of spatial association. The studentized C, is used as a guide for selecting the optimum proximity distance to a geologic feature [2].

Using the log-odds formulation of Bayes' rule, two or more binary predictive patterns can be combined to generate a predictor map using the expression

$$lnO\{D/B_{1}^{k} \cap B_{2}^{k} \cap B_{3}^{k}....B_{n}^{k}\} = \sum_{j=1}^{n} W_{j}^{k} + lnO\{D\} \tag{6.12}$$

where the superscript k is positive (+) or negative (-) if the binary predictor pattern is present or absent, respectively.

Bayes' rule requires that all input maps should be conditionally independent of one another with respect to the mineral occurrences. If this rule is violated, the resultant predictive map will be biased and under or over-estimates the undiscovered mineral deposits [2]. The following relationship is satisfied if two binary maps are conditionally independent.

$$N\{B_1 \cap B_2 \cap B_3\} = \frac{N\{B_1 \cap D\}N\{B_2 \cap D\}}{N\{D\}} \tag{6.13}$$

The left hand side of the equation is the observed number of occurrences in the overlap zone of B_1 and B_2. The right-hand side is the predicted number of deposits in this overlap zone. A contingency calculation table is used to test for conditional independence of two maps. The chi-square test defined as follows is then applied.

$$\chi^2 = \sum_{i=1}^{4} \frac{(observed_i - predicted_i)^2}{predicted_i} \tag{6.14}$$

An overall test of conditional independence is finally applied to the predictive maps. The predicted number of mineral occurrences $N\{D\}_{pred}$ is calculated as the sum of the products of the number of pixels and their posterior probabilities for all the pixels on the map ie.

$$N\{D\}_{pred} = \sum_{k=1}^{m} P_k * N\{A\}_k \tag{6.15}$$

6.3 Data inputs

The geological features associated with Archean lode gold deposits in the study area include certain lithologic units, granitoids, alteration zones, shear and deformation zones, foliation and s-fabric, fold axial traces and deep seated discontinuities. The different maps of the geological features which characterize the location of the known gold deposits were rasterized using a pixel size of 100mX100m for use as evidential layers for predictive model generation. This pixel size was chosen to ensure that there is only one deposit per unit cell. Each gold deposit is associated with a small unit area such that the point density, which is a reasonable approximation to the known gold deposits, is expressed as the number of gold deposits per unit area. The feature maps were converted to binary format prior to integration.

6.4 Generation of binary predictor patterns

A pair of weights (W^+ for pattern presence and W^- for pattern absence) was calculated for each binary pattern, according to equations 6.5 and 6.6 respectively. If more points (e.g. gold deposits) occur on a map pattern indicating presence of a geological feature than would be expected due to chance, W^+ is positive and W^- is negative. If less gold deposits occur on a map pattern indicating presence of a geological feature than would be expected due to chance,

W^+ is negative and W^- is positive. Where W^+ and W^- are both zero,there is no spatial association between the map pattern indicating presence of a geological feature and the points.

For rock units, the lithological formations were reclassified into two classes, favorable (hosting known gold deposits) and unfavorable (very few or no known gold deposits). The positive weights of the favorable units were calculated according to equation 6.5. The negative weights of the unfavorable units were calculated according to equation 6.6. For linear geological features, the optimum distance within which the spatial association of the features with the gold deposits is optimal was determined by calculating the weights according to equations 6.5 and 6.6, and contrast (equation 6.9) for successive distances away from the geological features, and examining variations in C or sigC [equation 6.11]. Different buffer zone intervals were experimented with in order to determine the optimum buffer intervals. Table 6.1 shows the weights and contrasts of the binary predictor patterns of the various geological features with respect to the small gold deposits (recorded production > 100kg). The optimum cut off distances are indicated in the buffer zone column (see also Appendix 3).

Table 6.1: Weights and contrasts of the binary predictor patterns of the various geological features with respect to the small gold deposits.

	Optimum Distance (m)	npixb	npixbd	Wp	stdWp	Wn	stdWn	C	stdC	sigC
Fold axes	3000	130840	118	1.0027	0.0921	-1.2743	0.1857	2.2770	0.2070	10.9849
shear zones	1500	142125	110	0.8496	0.0954	-0.9939	0.1644	1.8435	0.1900	9.6988
Alteration zones	500	103443	80	0.8487	0.1118	-0.5206	0.1222	1.3693	0.1660	8.2674
Foliation and s-fabric	2000	259712	120	0.2766	0.0913	-0.8191	0.1925	1.1458	0.2130	5.3782
Granite-greenstone contact	2000	74555	42	0.5318	0.1543	-0.1527	0.0976	0.6845	0.1830	3.7491
Magnetic lineaments	3000	322823	127	0.1726	0.0888	-0.6964	0.2236	0.8689	0.2410	3.6116
npixb = No. of pixels where pattern is present										
npixbd = No. of gold deposits in pattern										

The geological map was generalized to a smaller number of units by combining rock units with similar characteristics. The density of gold deposits together with positive and negative weights were calculated for each unit. The lithologic map was reclassified into a binary predictor pattern with favorable and unfavorable classes based on the calculated densities. Weights (W^+ and W^-) were assigned to the binary pattern, Figure 6.1.

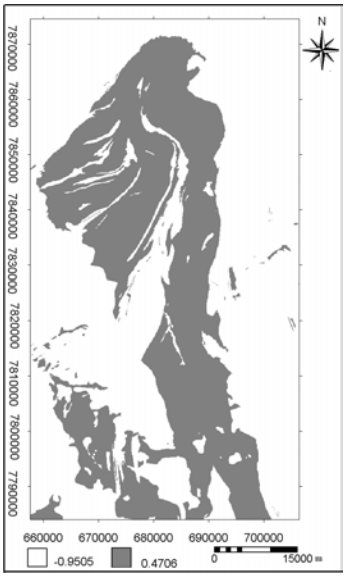

Figure 6.1: Binary predictor pattern of favorable lithology.

For alteration zones, buffer zones were created at 500 m intervals. Weights and sigC for cumulative distances from the alteration zones were calculated [Figure 6.2]. The alteration map does not cover the whole study area. Areas lying outside the ASTER images were assigned a weight of zero. Results of the analysis are shown on Figure 6.3.

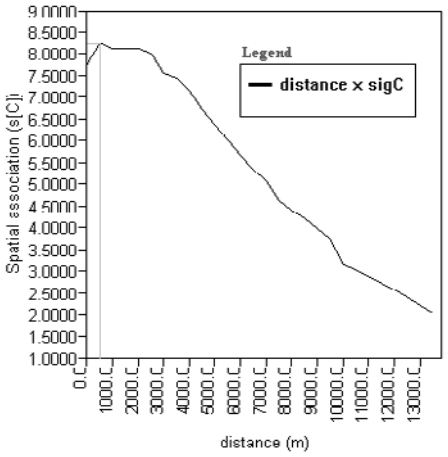

Figure 6.2: Variation of spatial association (sigC) with cumulative distances from alteration zones.

Buffer zones were created around the granite greenstone contact at 1000 m intervals. Weights and sigC [Figure 6.4] for binary patterns of cumulative distances from the granite greenstone contact were calculated in order to determine spatial association (i.e., distance at which either C or sigC is maximum. Figure 6.5 shows the binary predictor pattern of favor-

Figure 6.3: Binary predictor pattern of proximity to alteration zones.

able proximity to the granite-greenstone contact. There are two peaks of sig C on Figure 6.4. The lower peak was chosen because the main peak at 10000m is unrealistic the observed influence of the granite greenstone contact on Archean gold mineralization.

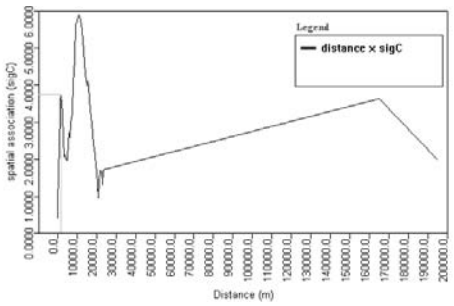

Figure 6.4: Graph showing variation of spatial association (sigC) with cumulative distances from the granite-greenstone contact.

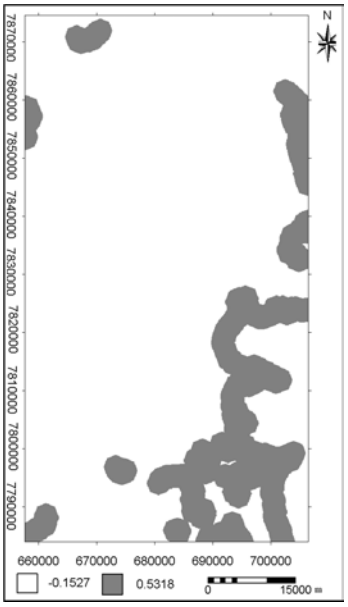

Figure 6.5: Binary predictor pattern of proximity to the granite-greenstone contact.

Buffer zones were created around the shear zones at 500 m intervals. Weights and sigC were calculated [Figure 6.6]. Results of the analysis are shown on Figures 6.7.

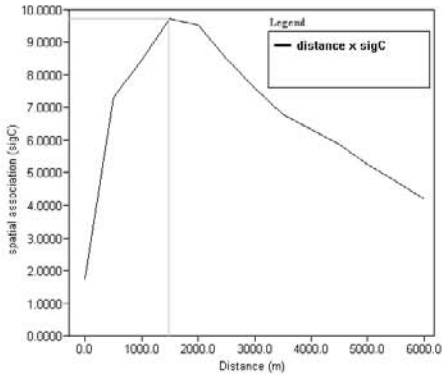

Figure 6.6: Graph showing variation of spatial association (sigC) with cumulative distances from shear zones.

Figure 6.7: Binary predictor pattern of proximity to shear zones.

Buffer zones were created around the foliations/s-fabric at 1000 m intervals. Weights and sigC [Figure 6.8] were then calculated. Results of the analysis are shown on Figure 6.9.

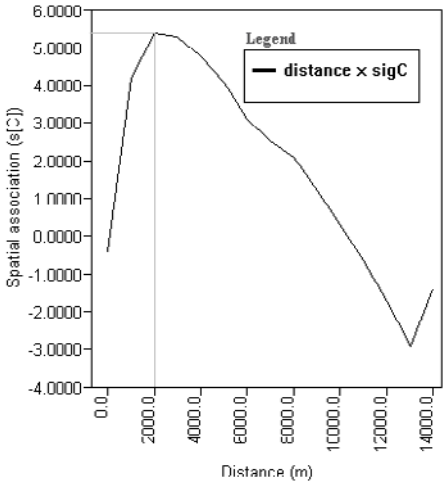

Figure 6.8: Graph showing variation of spatial association (sigC) with cumulative distances from foliation/s-fabric.

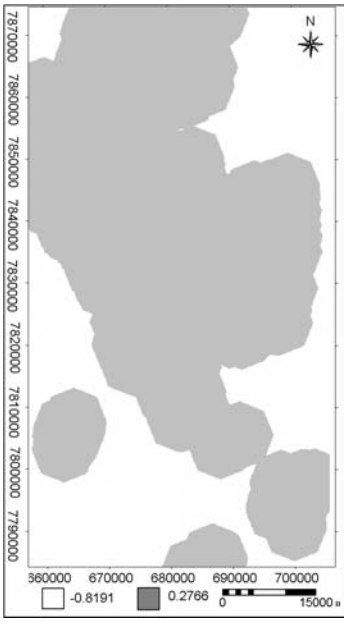

Figure 6.9: Binary predictor pattern of proximity to foliations.

Buffer zones were created around fold axial traces at 500 m intervals. Weights and sigC [Figure 6.10] for cumulative distances from the fold axial traces were calculated. Results of the analysis are shown on Figure 6.11.

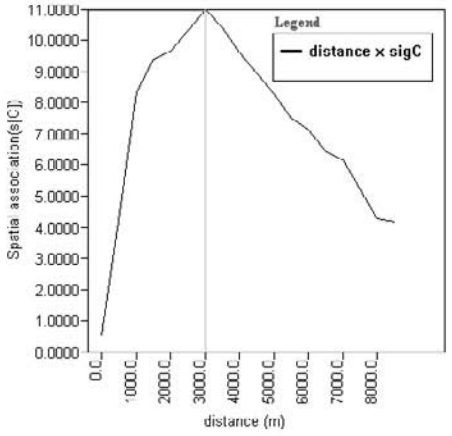

Figure 6.10: Graph showing variation of spatial association (sigC) with cumulative distances from fold axial traces.

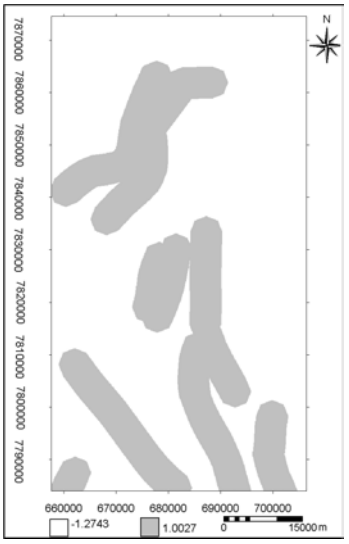

Figure 6.11: Binary predictor pattern of proximity to fold axes.

Aeromagnetic Lineaments were interpreted as indications of deep seated discontinuities. The lineaments were buffered at 500 m intervals. Weights and sigC [Figure 6.12] for the cumulative distances were calculated. Results of the analysis are shown on Figure 6.13.

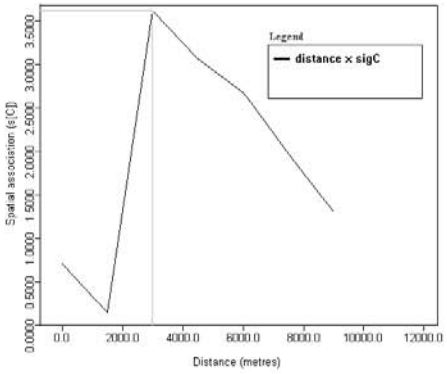

Figure 6.12: Graph showing variation of spatial association (sigC) with cumulative distances from magnetic lineaments.

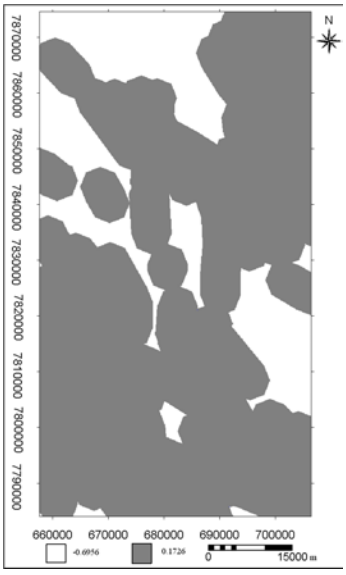

Figure 6.13: Binary predictor pattern of proximity to magnetic lineaments.

6.5 Pairwise test for conditional independence

Bayes' rule requires that all input maps should be conditionally independent of one another with respect to the mineral occurrences. This can be tested using equation 6.13. A contingency calculation table was used to test conditional independence of the various input predictor patterns. The chi-square test (equation 6.14) was applied to all possible map pairs. The results are shown on Table 6.2. The values in bold indicate conditionally independent map pairs (critical chi squared value is 3.84 at a confidence limit of 90% [5]).

Conditional dependence exists between some map pairs eg. the shear zones and foliation maps. If such maps are combined during the generation of the models, this will result in a model which over-predicts or under-predicts the undiscovered deposits [5]. Creating mineral potential maps using conditionally dependent binary predictor patterns was avoided.

Table 6.2: Calculated Chi square values for testing for conditional independence between all pairs of binary maps with respect to small scale gold deposits used to generate predictive models.

	Lithologial units	Anticlinal fold axes	Alteration zones	Foliations	Granite-greenstone contact	Aeromagnetics lineaments
fold axes	2.6					
Alteration zones	0.87	8.88				
Foliations	0.001	5.2	1.8			
Granite-greenstone contact	2.08	1.78	1.3	3.4		
Aeromagnetics lineaments	0.7	6.61	4.14	2.47	0.58	
Shear zones	0.31	4.2	1.02	10.9	0.79	4.28

6.6 Data integration

Seven binary predictor patterns were created and integrated in combinations of 3 in order to avoid combining conditionally dependent maps. The binary predictor patterns, with assigned positive and negative weights were integrated according to equation 6.12.

The prior probability P[D] for the known gold deposits was calculated as: number of deposits/total area=$147/444011$=0.000331. Prior odds of deposits O[D]=($prior probability/(1-prior probability)$=0.000379. $\text{Log}_e Prior odds(\text{log}_e O\{D\})$=-8.0128.

The magnitude of the ratio of posterior probability to prior probability represents mineral potential [10]. Areas where this ratio is less than 1 were classified as unfavorable. The favorable areas were grouped into three classes, low potential, moderate potential, and high potential.

Five mineral potential maps were generated using different combinations of the binary predictor patterns (Figures 6.14, 6.15, 6.16, 6.17, and 6.18).

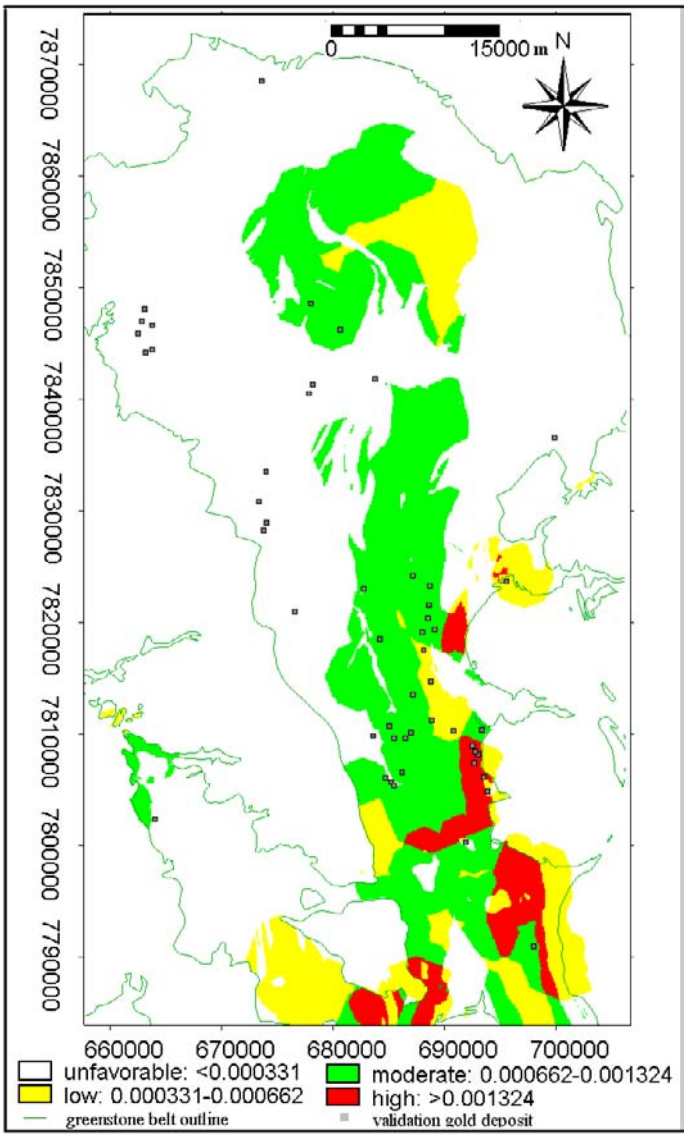

Figure 6.14: Predictive gold potential map (granite-greenstone contact, lithology and foliation binary predictor patterns).

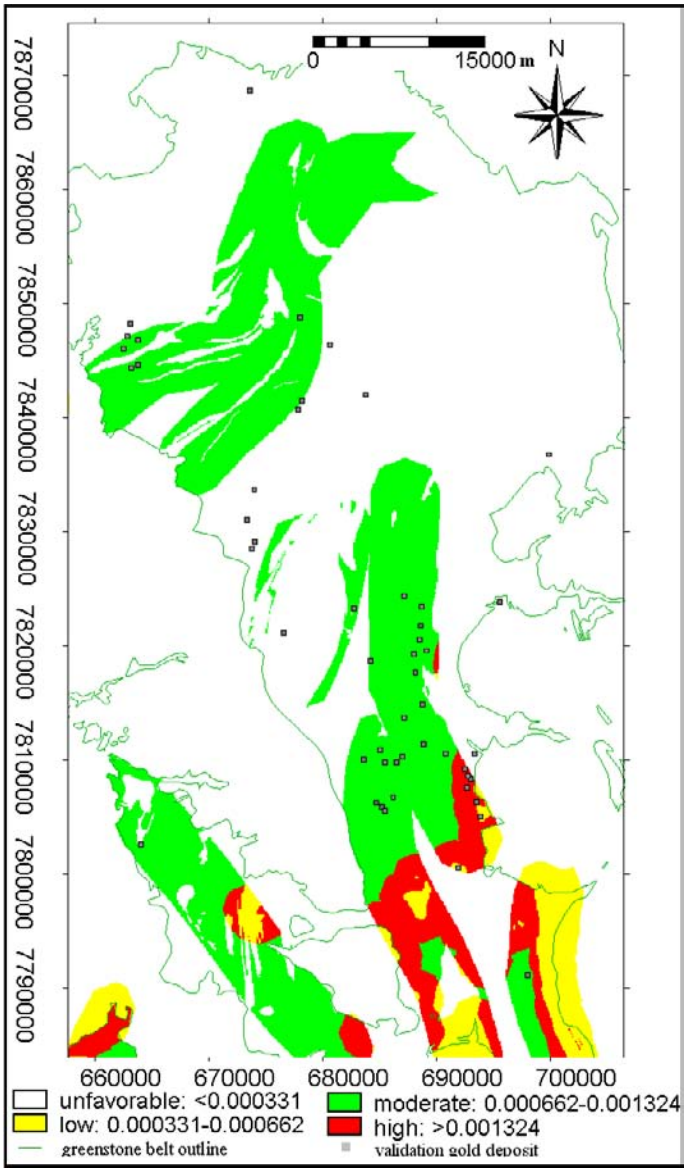

Figure 6.15: Predictive gold potential map (granite-greenstone contact, lithology and fold axes binary predictor patterns).

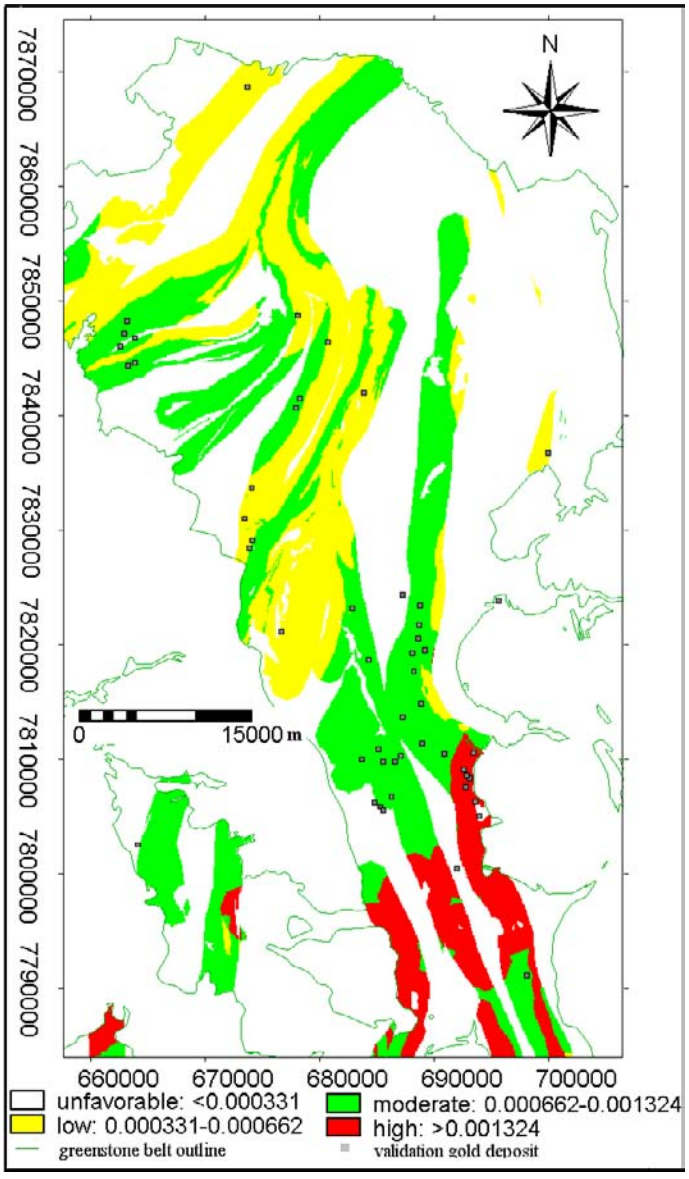

Figure 6.16: Predictive gold potential map (granite-greenstone contact, lithology and shear zones binary predictor patterns).

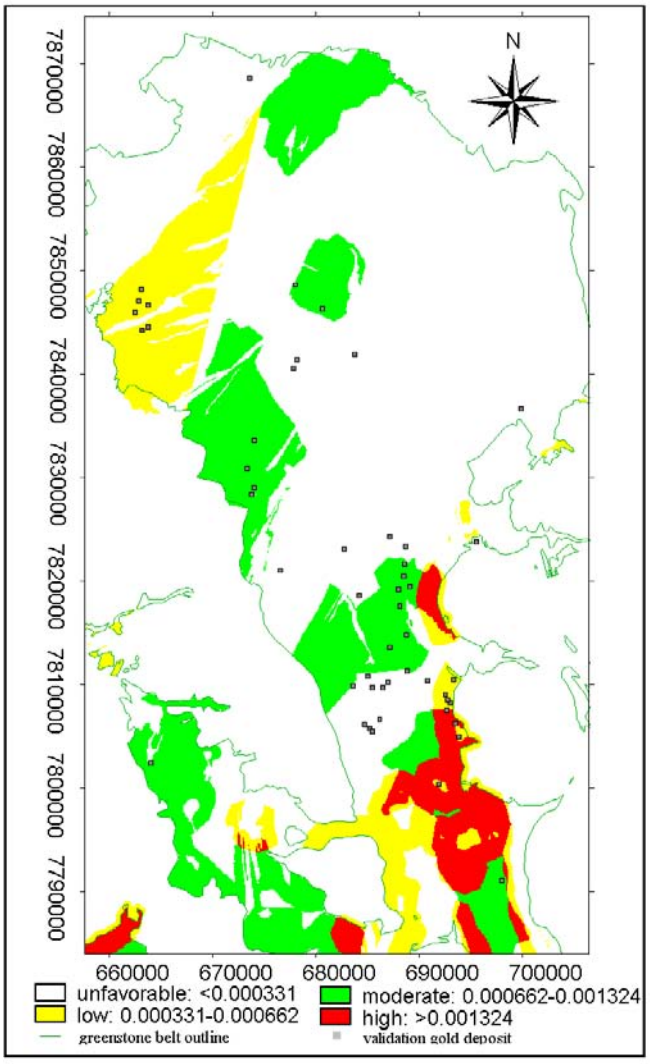

Figure 6.17: Predictive gold potential map (granite-greenstone contact, lithology and alteration zones binary predictor patterns).

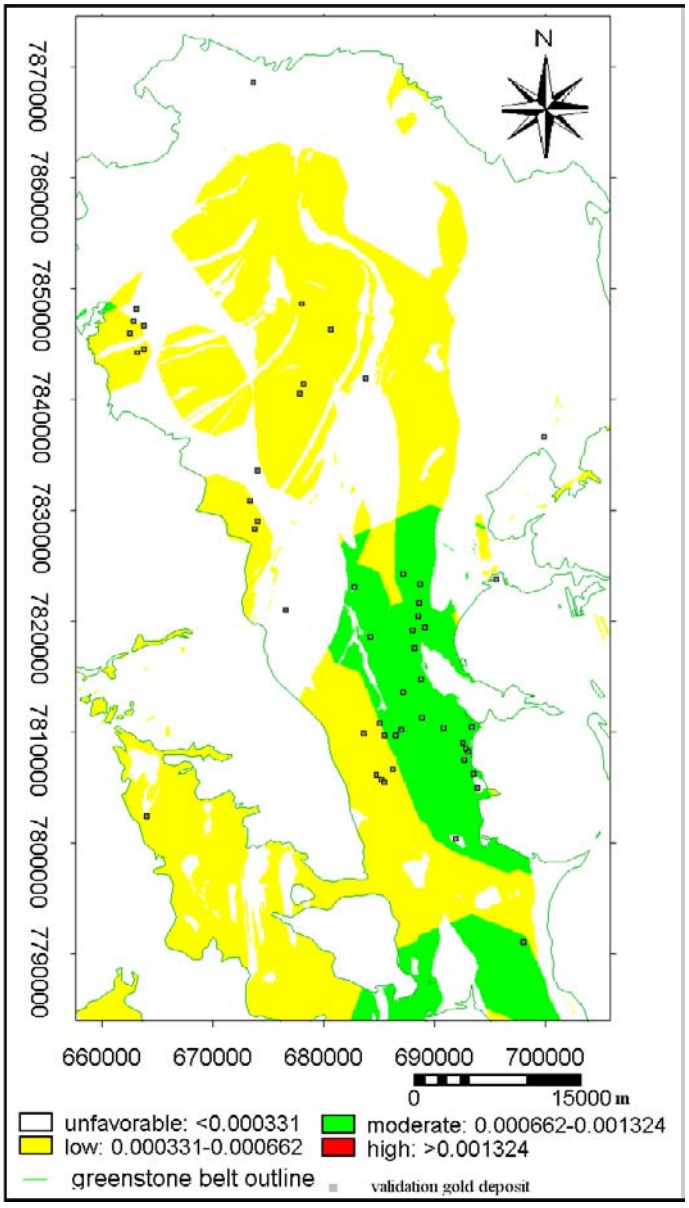

Figure 6.18: Predictive gold potential map (granite-greenstone contact, lithology and magnetic lineaments binary predictor patterns).

6.7 Overall test for conditional independence

The statistical validity of the generated mineral potential maps was examined by applying an overall test for conditional independence [2] using equation 6.15. If the predicted number of deposits is larger than 10-15% of the observed deposits then the assumption of conditional independence is seriously violated [5].

Integration of all the binary input maps was found to over estimate the number of predicted gold deposits in the study area due to conditional dependence of some of the input maps. Several combinations of the input maps were tried out. The combination of the granite-greenstone contact and the lithology binary predictor patterns with either foliation, fold axes, alteration or deep seated discontinuities binary predictor patterns are within the acceptable prediction limits. Results of the overall test for conditional independence are: granite-greenstone contact; lithology and shear zones (+8%); granite-greenstone contact, lithology and foliation (-7%); granite-greenstone contact, lithology and fold axes (+5%); granite-greenstone contact, lithology and alteration (-11%); and granite-greenstone contact, lithology and deep seated discontinuities (-15.6%).

6.8 Validation

The five predictive gold potential maps were each crossed with the large scale gold deposits (validation deposits) occurring in the study area and the number of deposits falling within favorable areas noted.

The gold potential map generated from the granite-greenstone contact, lithology and fold axes binary predictor patterns indicates that about 28% of the study area is favorable with 76% of the validation deposits within favorable areas and 24% in unfavorable areas (Figure 6.15).

The gold potential map generated from the granite-greenstone contact, lithology and shear zones binary predictor patterns indicates that about 53% of the study area is favorable, with 86% of the large gold deposits used for validation within favorable areas and 14% in unfavorable areas (Figure 6.16).

The gold potential map generated using the granite-greenstone contact, lithology and foliation binary predictor patterns indicates that about 42% of the study area is favorable, with 62% of the validation gold deposits within favorable areas and 38% in unfavorable areas (Figure 6.14).

The gold potential map shown on Figure 6.18, was generated using the granite-greenstone contact, lithology and deep seated discontinuities binary predictor patterns. This map indicates that about 53% of the study area is favorable, with 60% of the large gold deposits used for validation within favorable areas and 40% in unfavorable areas. The map does not indicate any highly favorable zones. This is due to the effect of combining the very low weights of the magnetic lineaments binary pattern with the higher weights of the lithology and granite-greenstone contact patterns.

The gold potential map shown on Figure 6.17, was generated using the granite-greenstone contact, lithology and alteration zones binary predictor patterns. This probabilistic map indicates that about 50% of the study area is favorable, with 73% of the large gold deposits used

for validation within favorable areas and 27% are in unfavorable areas.

6.9 Discussion

The variation of the studentized contrast sigC for cumulative distances from the different geological features with respect to gold deposits are shown on Appendix 3. The magnitude of sigC indicates the degree of spatial association of the geological features and the gold deposits. It can be seen from Table 6.1 that the fold axial traces and the shear zones have the strongest spatial associations with the known gold deposits (very high values of sigC of 10.9849, and 9.6988 respectively). Hydrothermal alteration zones have the third highest value of sigC (8.2674). The foliation/s-fabric pattern has a moderately high value of sigC (5.3782). The granite-greenstone contact and magnetic lineaments have relatively weak spatial association (sigC is 3.7491 and 3.6116 respectively). There is a positive correlation between the magnitude of sigC of the input patterns and the percentage of validation deposits correctly predicted. Generally, the higher the sigC value of the input patterns, the better the predictive power of the resultant predictive model eg. the predictive model including the shear zones sigC=9.6 correctly predicts 86% of the validation deposits while the predictive model including the magnetic lineaments (sigC=3.6) correctly predicts only 60% of the validation deposits. The geological features useful for modelling Archean lode gold potential in the Bubi greenstone belt, in descending order of importance are: fold axial traces, shear zones, alteration zones, foliation/s-fabric, the granite-greenstone contact and magnetic lineaments.

Shear zones, fold axes and alteration zones exhibit the highest sigC values. This is as expected from the conceptual model for Archean lode gold deposits and field observations in the study area. The conceptual model for Archean lode gold deposits states that the gold deposits are primarily controlled by structural features which acted as depositional sites during mineralization (shear zones and fold axes) and that the host rocks of the gold deposits have under-gone hydrothermal alteration. Foliation/s-fabric is a measure of the strain suffered by the rocks. The relatively low value of sigC for foliations/s-fabric is probably due to the existence of some post Archean foliations that are not related to mineralization. The granite-greenstone contact indirectly affects the development of the host structures due to competence contrasts between the granitic rocks and the greenstone belt lithologies and forceful intrusion of diapirically emplaced granitoids. Late diapirically emplaced granitoids probably supplied the heat source driving the mineralizing hydrothermal systems and/or the gold bearing fluids. The magnetic lineaments are interpreted as deep-seated discontinuities through which mineralizing fluids ascended.

From the validation results of the different gold potential maps it can be seen that the highest prediction rates are achieved by a combination of the granite-greenstone contact and lithology binary predictor patterns with the shear zones binary predictor pattern (86% of the deposits are within favorable areas). The combinations of granite-greenstone ,lithology and fold axes has the second highest rate of success (76% of the validation deposits are within the favorable areas). The combination of the granite greenstone contact, lithology and folia-

tion patterns correctly predicts 62% of the validation gold deposits. The combination of the granite-greenstone contact and lithology binary predictor patterns with the deep seated lineaments and alteration zones correctly predicts 60% of the validation deposits. These results reflect the greater reliability of shear zones, fold axes and alteration zones as predictors for the structurally controlled, dominantly shear zone hosted Archean lode gold deposits. The lowest prediction rate (53%) was achieved by the model that includes magnetic lineaments. Some of the magnetic lineaments are probably related to post Archean structural features that are not related to gold mineralization in the study area, such as later dyke intrusions, hence the low success rate of this model. This model also fails the overall test for conditional independence (under predicts by 15.6%)

An integration of all the binary predictor patterns into a single mineral potential map would be the ideal situation because the resultant predictive map would be based on all the geological features which are spatially associated with the gold deposits. This was ruled out by conditional dependence between some of the binary predictor patterns. Favorable areas on the five mineral potential maps cover the same broad areas.

Chapter 7

Conclusions and recommendations

7.1 Conclusions

1. A review of the conceptual model for Archean lode gold deposits and previous geological work in the study area and other Zimbabwe greenstone belts, particularly the Midlands greenstone belt, provided criteria for selecting geological features that are spatially associated with Archean lode gold deposits.

2. The geological features useful for modelling Archean lode gold potential in the Bubi greenstone belt, in descending order of importance include: a) proximity to fold axial traces; b)proximity to shear zones; c) proximity to alteration zones; d) proximity to foliation/s-fabric; e) proximity to the granite-greenstone contact; and f) proximity to magnetic lineaments. The density of the gold deposits on different lithological units are useful as a guide to Archean gold mineralization.

3. Grey scale, reduced to the pole aeromagnetic images successfully mapped magnetic lineaments. verifying the origin of the different magnetic lineaments would require field validation.

4. The Crosta technique, applied to ASTER data, successfully mapped zones of kaolonization and/or silicification. verifying the origin of the exact nature of the alteration would require field validation. For limonitic alteration mapping, the method did not give satisfactory results. This is probably due to widespread limonitic alteration which is associated with both mineralization and the normal weathering of iron rich rocks.

5. Shear zones and fold axial traces have the strongest spatial associations with the known gold deposits. Hydrothermal alteration zones have the third strongest spatial association with the gold deposits. The foliation/s-fabric pattern has moderate spatial association while the granite-greenstone contact and magnetic lineaments have relatively weak spatial association with the gold deposits.All the spatial associations are significantly positive (sig$C > 2$).

6. GIS-based weights of evidence probabilistic modelling provided a quantitative method for delineating areas with potential to host Archean lode gold deposits in the study area. Seven binary predictor patterns were generated some of which were found to be conditionally dependent. The magnitude of both the contrast and the studentized C was useful for determining the optimum distance of spatial association between the gold deposits and the geological features.

7. An overall test for conditional independence was carried out on the five mineral potential maps produced. The maps were within the recommended limit of 15% over or under prediction rate except the map including the aeromagnetic lineaments pattern which under-predicted slightly (-15.6%).

8. Successful validation of the predictive model generated using the spatial association of the small scale gold deposits and the geological features shows that the small scale gold deposits that are more numerous than the large scale gold deposits are useful for predictive modelling of gold potential in the study area.

9. The five mineral potential maps created using different map sets define broadly coincident favorable areas, boosting confidence in the predictive maps. The predictive models generated new target areas without known gold deposits, especially in the northern parts of the study area.

10. All the generated predictive models can be used to guide further exploration work in the study area. However, due to conditional dependence and a low success rate in predicting validation deposits, the model involving magnetic lineaments should be used with caution.

11. The most reliable predictive models are those with high predictive strengths and high success rates of predicting validation deposits. These are the models including the shear zones, fold axes and alteration zones binary patterns.

7.2 Recommendations

The following recommendations are made:

1. Carry out stream sediment geochemical sampling over the study area and incorporate the results in the predictive model.

2. Carry out predictive modelling on other Zimbabwe greenstone belts and compare the results with the results of this study. The Midlands greenstone belt would be ideal for such a study because it has abundant known gold deposits and an extensive data set, including stream sediment geochemical data.

3. Carry out the Crosta technique for alteration mapping using Landsat TM data and compare the results with the results presented in this study in order to validate the results of alteration mapping. The Crosta technique was originally developed using Landsat TM data which has different band coverage compared to ASTER data.

4. Carry out field checks and follow up work in the favorable areas delineated in this study. This work could involve detailed structural and lithological mapping, stream sediment geochemistry and ground geophysics.

References

[1] J. D. Bliss, editor. *Developments in ore deposit modeling*. Number 2004 in bulletin. U.S Geological Survey, USGS, Denver, 1992. 168 pp.

[2] G. F. Bonham-Cater. *Geographic information systems for earth scientists: Modelling with GIS*, volume 13. Pergamon (Elsevier Science Ltd), 1998. 398pp.

[3] R. W. Boyle. Auriferous archean greenstone sedimentary belts. In R.W. Hutchinson and I.R. Graunch, editors, *Historical Perspectives Of Genetic Concepts And Case Histories Of Famous Discoveries*, pages 164–191. The Economic Geology Publishing Company, 1998. Papers arising from SEG symposia.

[4] S. D. G. Campbell and T. G. Blankensop. A simple size frequency basis for assessing the exploration potential of an area-the fractal dimension. *Transactions of the institution of mining and metallurgy*, 1995.

[5] E. J. M. Carranza and M. Hale. Geologically contrained probabilistic mapping of gold potential, baguio district, philippines. *Natural Resources research*, 9, 2000.

[6] A. C. Colvine, J. A. Fyon, K. B. Heather, S. Marmont, P. M. Smith, and D. G. Troop. Archean lode deposits in ontario. Ontario Geological Survey Miscellaneous paper, 1988.

[7] M. C. Crawford. Archean lode gold deposits. In R. P Foster, editor, *Gold metallogeny and exploration*, chapter 3, pages 139–176. Blackie and son Ltd, London, 1991. 432pp.

[8] M. S. Garson. The geology of the Bulawayo greenstone belt and the surrounding granitic terrain. Bulletin 93, Zimbabwe Geological Survey, 1995. 294pp.

[9] D. I. Grooves and R. P. Foster. Archean lode gold deposits. In R. P Foster, editor, *Gold metallogeny and exploration*, chapter 3, pages 63–96. Blackie and son Ltd, London, 1991. 432pp.

[10] D. I. Grove and R. P. Foster. Archean gold deposits. In R.P. In Foster, editor, *Gold metallogeny and exploration*, pages 63–103pp. Blackie, Glasgow and London, UK, 1991.

[11] H. Harley and E. G. Charlesworth. Structural controls in the distribution of gold at the How mine, Bulawayo, Zimbabwe. *Journal of Economic Geology*, pages 1697–1710, 1990.

[12] S. E. Ho, D. I. Groves, and J. M. Bennet, editors. *Gold deposits of the Archean Yilgarn Block, Western Australia;Nature genesis and exploration Guides*, volume 20. University of Westerm Australia, 1990.

[13] D. Holloway. Archean lode gold deposits. In R. P Foster, editor, *Gold metallogeny and exploration*, chapter 4, pages 99–138. Blackie and son Ltd, London, 1991. 432pp.

[14] R. Kerrich. Geochemistry of gold deposits in the abitibi greenstone belt. In *Gold metallogeny and exploration, Archean lode gold deposits*, volume 27, pages 48–71. Blackie and son, London, 1988.

[15] T. L. Klein and W. C. Day. Descriptive and grade-tonnage models of Archean low-sulfide Au-quartz veins and a revised grade-tonnage model of Homestake au (model 36b.2). Technical report, United States department of the interior, Geological survey open-file report 94-250, 1994.

[16] W. P. Loughlin. Principal component analysis for alteration mapping. *Photogrammetric mapping and remote sensing*, 57(9):1163 to 1169, September 1991.

[17] A. M. Macgregor. The geology of the country around Turk mine, Zimbabwe. Technical report, Zimbabwe Geological Survey, 1928.

[18] H. B. Maufe, B. Lightfoot, A. M. Mcgregor, and F. L. Amm. Geological map of the country aroundQueens mine, Bubi District Zimbabwe. geological map, Zimbabwe geological Survey, 1935. scale 1:100,000.

[19] R. H. McMillan. Iron formation-hosted au. In *Selected British Columbia mineral deposit profiles*, volume 2-Metallic Deposits. Geological society of British Columbia, 1996.

[20] E. J. Mikucki. hydrothermal transport and depositional processes in archean lode-gold systems: A review. *Ore geology reviews*, 13:307–321, 1998.

[21] J. M. Moore and L. J. Guo. Image enhancement of epithermal gold deposit alteration zones in southeast spain. In *Remote sensing, an operational technology for the mining and petroleum industry*, pages 49–57, London, 1990. The Institution of and Metallurgy.

[22] J. D. G. Muirhead. The geology of the gwampa valley area, Zimbabwe. geological map, Zimbabwe geological Survey, 1972. scale 1:119,000.

[23] N. Phillips. Geodynamics and gold exploration in the yilgarn craton. Technical report, Great Central Mines Limited and Centaur Mining and Exploration Ltd, 2001.

[24] P. E. J. Pitfield and S. D. G. Campbell. The structural evolution and gold mineralization of the midlands greenstone belt, Zimbabwe. Open file report, Zimbabwe Geological Survey, 1993.

[25] P. E. J. Pitfield and S. D. G. Campbell. The use of structural controls techniques for gold exploration in Zimbabwe. Open file report, Zimbabwe Geological Survey, 1993.

[26] P. E. J. Pitfield and S. D. G. Campbell. Structural controls of gold mineralization and regional structure in the Bulawayo-Bubi greenstone belt, Zimbabwe. 75pp, 1994.

[27] P. E. J. Pitfield and S. D. G. Campbell. Structural controls of gold mineralization in the Zimbabwe craton. Bulletin 101, Zimbabwe Geological Survey, 1994.

[28] P. E. J. Pitfield and S. D. G. Campbell. Significance for gold exploration of structural styles of auriferous deposits in the Archean Bulawayo-Bubi greenstone belt of Zimbabwe. *Transactions of the Institution of Mining and Metallurgy, section B, Applied earth science*, 105(5):B41–B52, Jan to Apr 1996.

[29] G. M. Pulz. Maria lazara gold deposit (goias state brazil); an example of intense fluid/rock interaction associated with a triple point structure. In M Pagel and J. L Leroy, editors, *Source transport and deposition of metals*. Balkema, Rotterdam, 1991.

[30] C. V. Reeves. Aeromagnetic surveys, principles, practice and interpretation. Course unit i.50., Departments of Earth Resources Surveys ITC, 1990.

[31] J. P. Richards. Lineaments revisited, July 2000.

[32] R. G. Roberts. Archean lode gold deposits. In *Ore deposit models*, monograph 1. Geoscience Canada, 1990.

[33] F. F. Sabins. *Remote sensing, Principles and interpretation*. W.H. Freeman and company, 1997. 494pp.

[34] G. Tourigny, A.C. Brown, C. Hubert, and R. Crepeau. Synvolcanic and syntectonic gold mineralization at the bousquet mine, abitibi greenstone belt,quebec. *Journal of Economic Geology*, pages 1875–1890, 1989.

[35] J. M. Tsomondo. Annual ore reserves statement. Technical report, Reedbuck Investments Pvt Ltd, June 1998.

[36] A. B. Westerhof. Area selection, terrain analysis and ore deposit modelling. Workshop abstract, 1996.

[37] J. F. Wilson. The granite-gneiss greenstone shield, Zimbabwe. In Hunter D.H, editor, *Precambrian of the Southern Hemisphere*, pages 454–488. Elsevier, Amsterdam, 1981.

Appendix 1

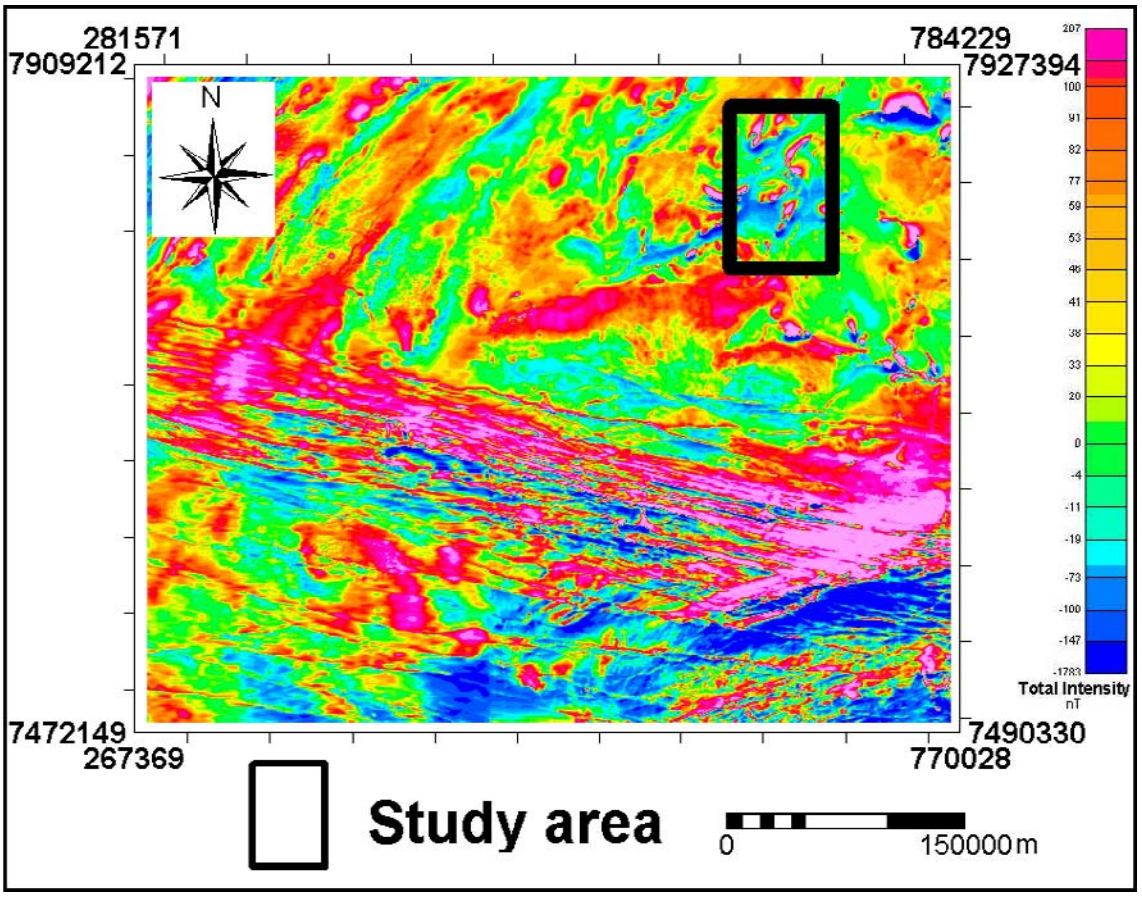

Figure 1: Airborne magnetic data as acquired.

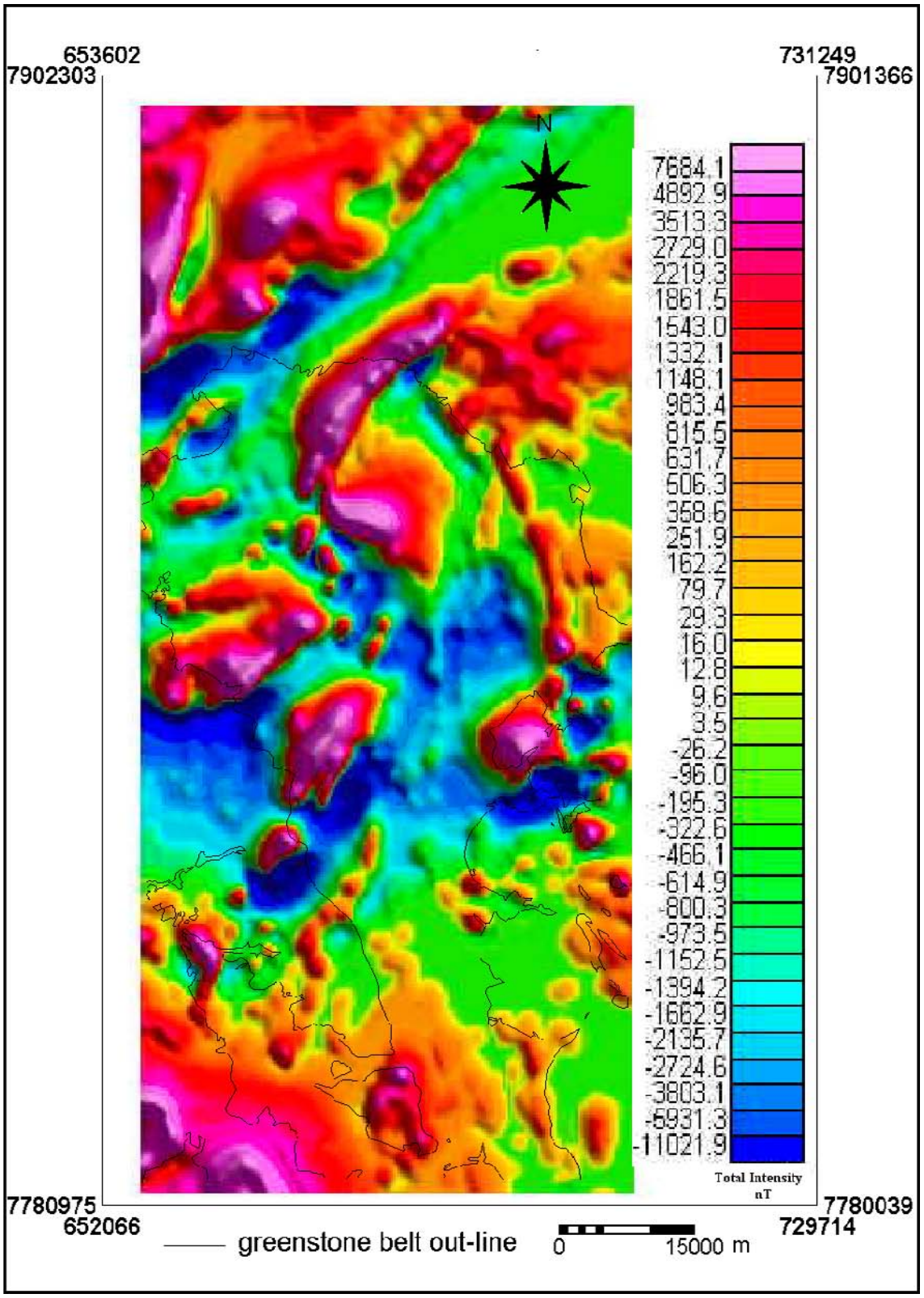

Figure 2: Color shaded relief image of the total magnetic intensity data before reduction to the pole. Magnetic declination= 6.5^o W, Magnetic inclination= -60^o.

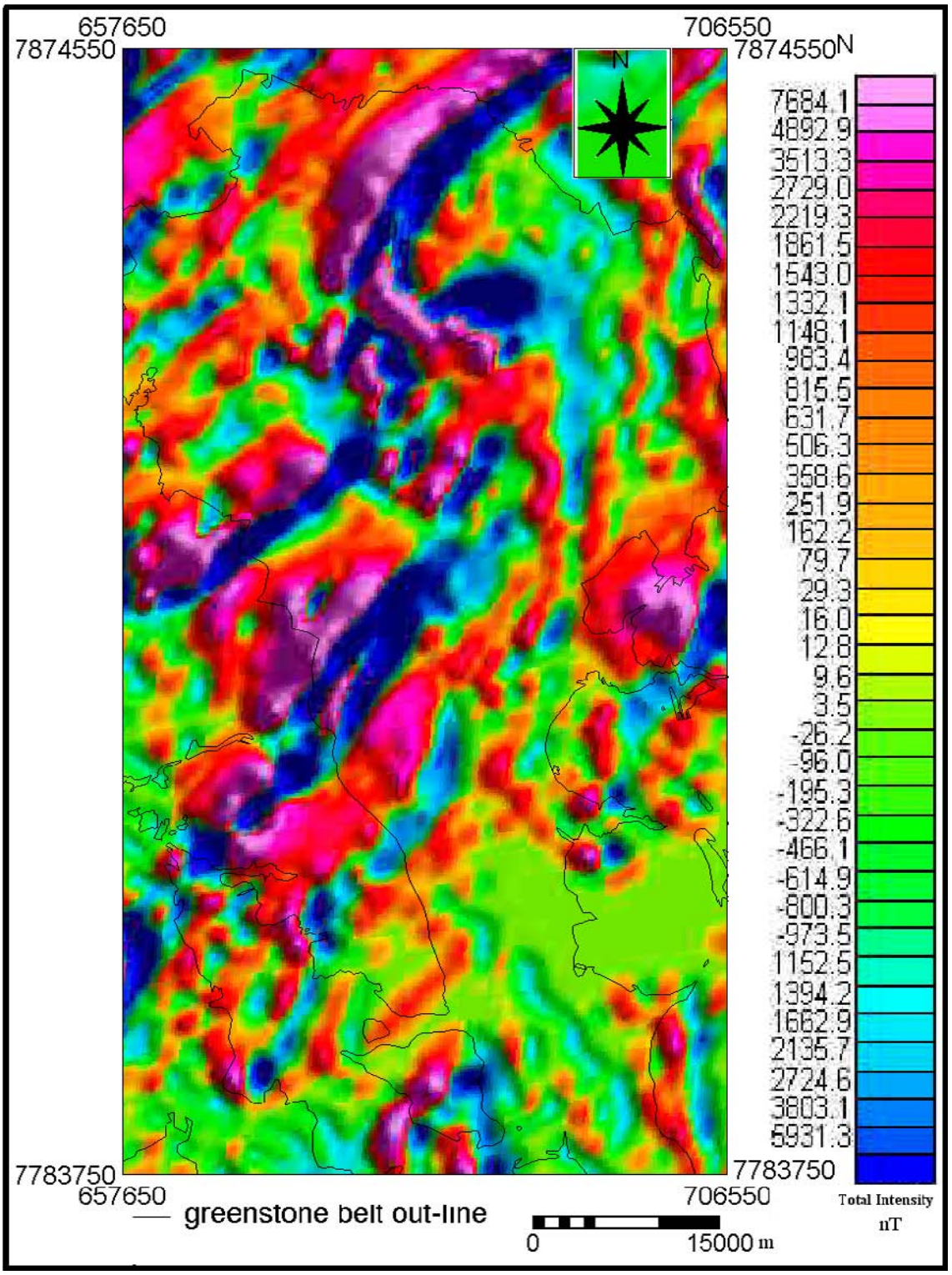

Figure 3: Color shaded relief image of the total magnetic intensity data after reduction to the pole.

Appendix 2

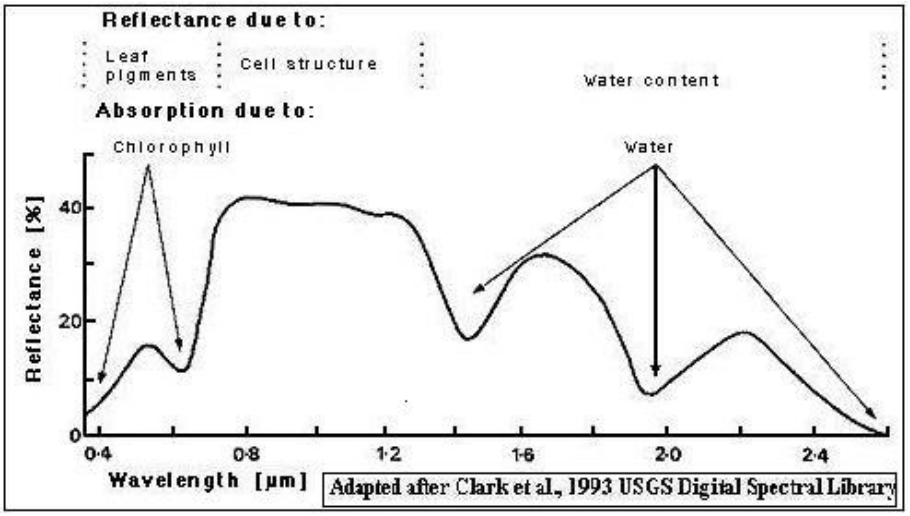

Figure 4: Typical reflection spectral curve for mature green vegetation

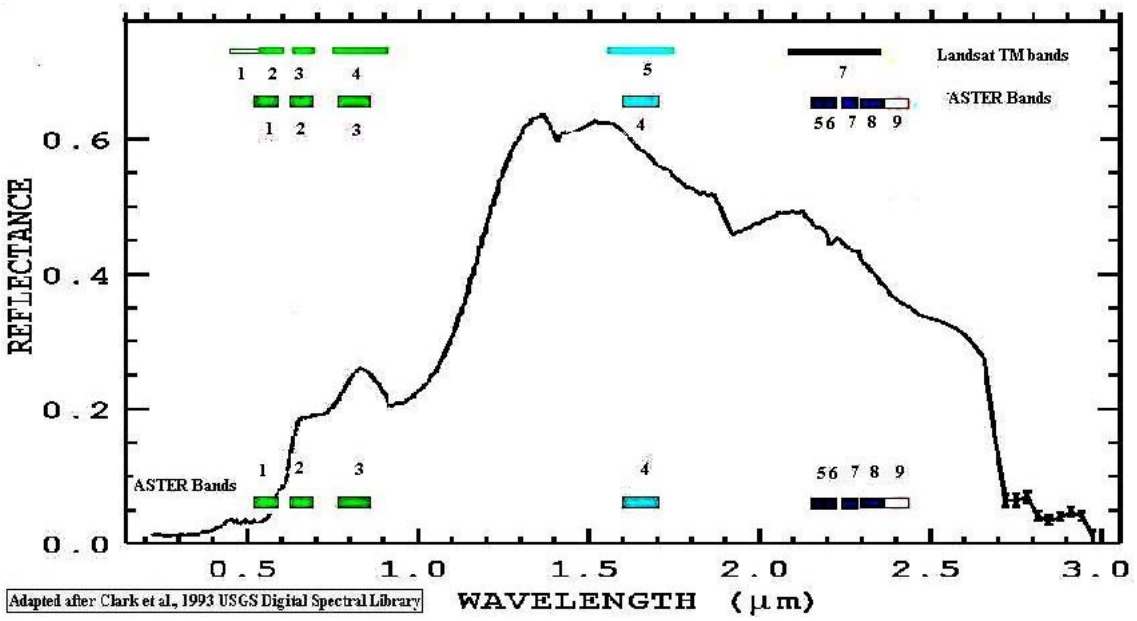

Figure 5: Typical reflection spectral curve for limonite

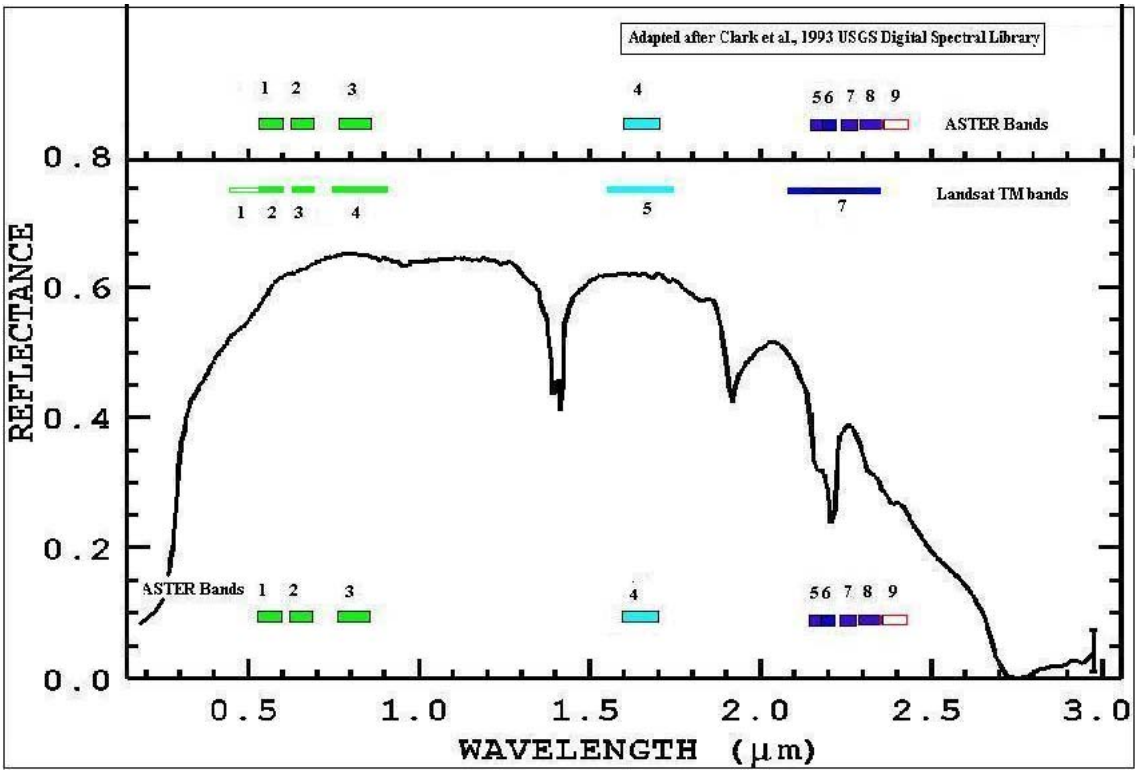

Figure 6: Typical reflection spectral curve for kaolinite

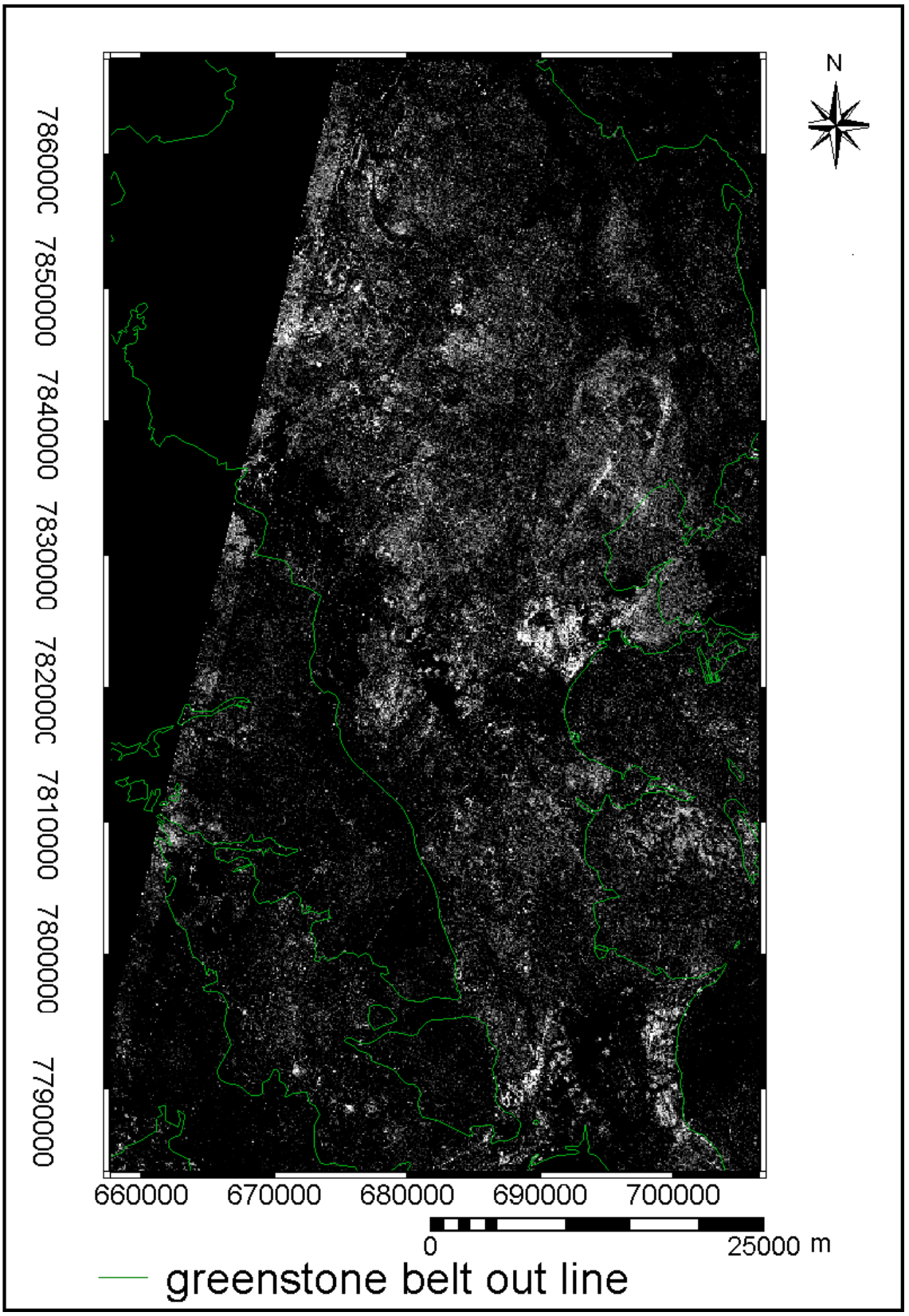

Figure 7: Negated PC 4 image (F image) displaying limonitic areas as bright pixels

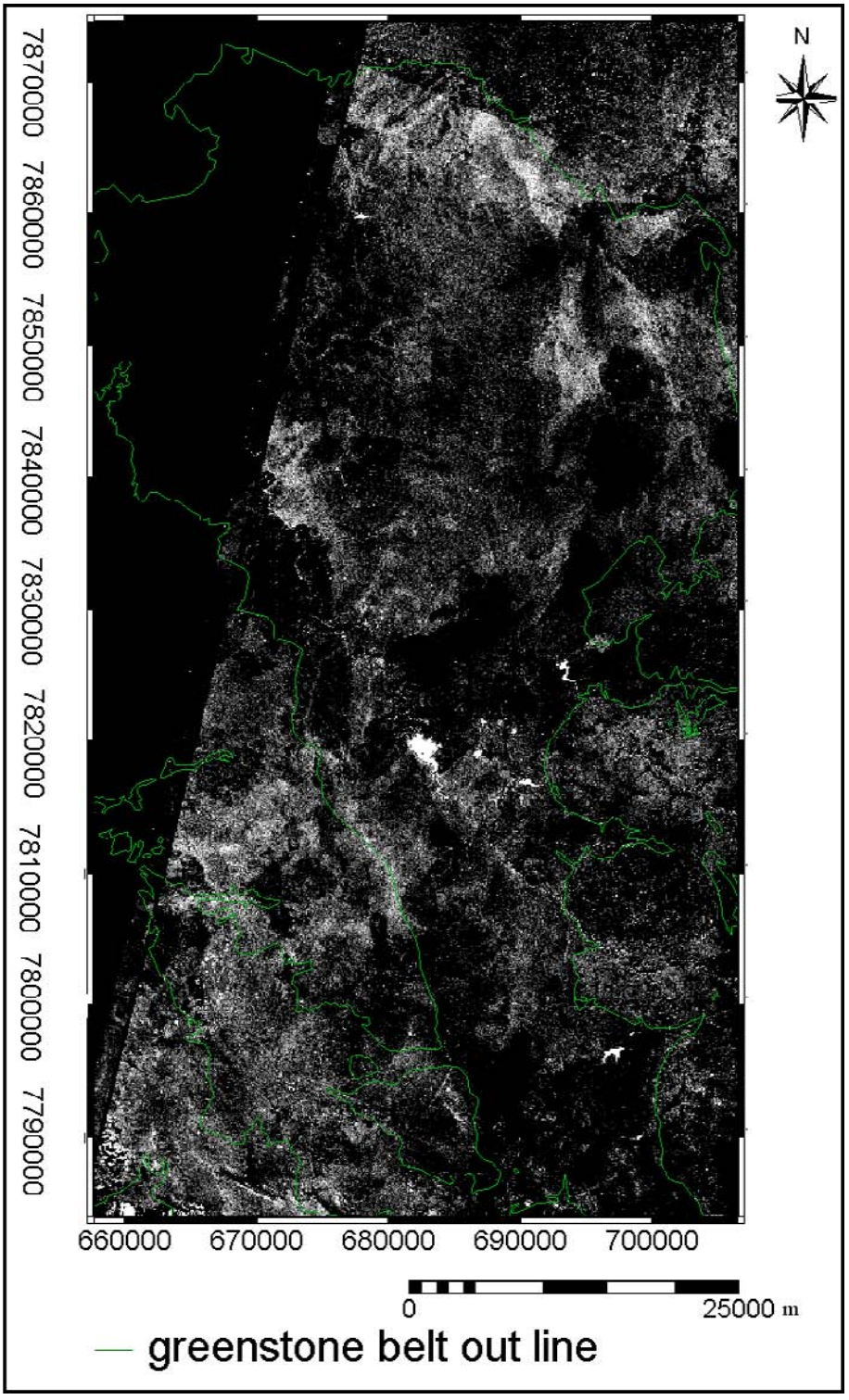

Figure 8: Negated PC 4 image (H image) displaying kaolinized areas as bright pixels

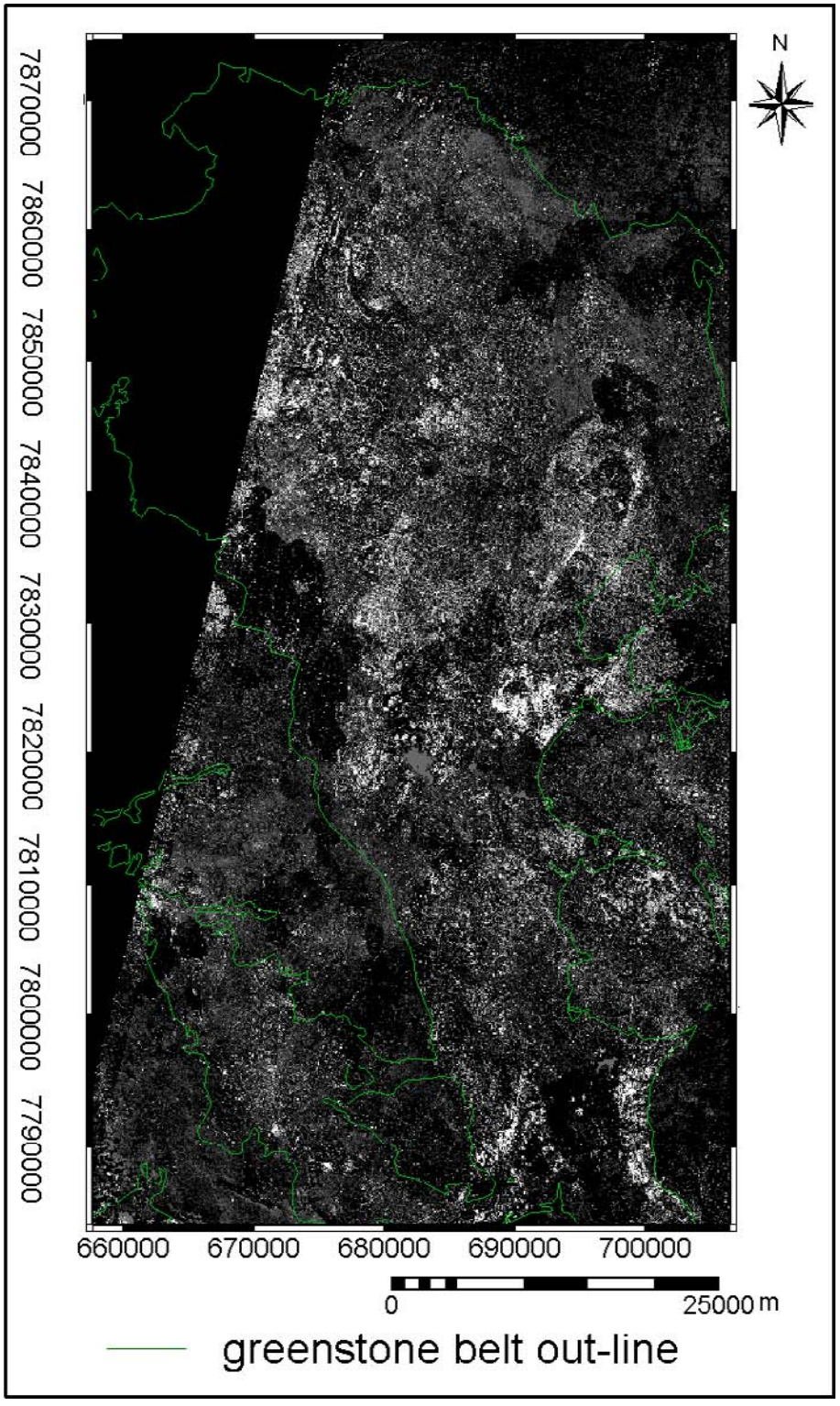

Figure 9: PC 2 image of pairwise principal component transformation of F and H images, showing areas enriched in both limonite and kaolinite as bright pixels

Appendix 3

Table 1: Spatial association of gold deposits with geological features.

Variation of weights and contrasts for cumulative distances from the geological features with respect to model gold deposits

Fold axes									
Distance buffer(m)	npixb	npixbd	Wp	stdWp	Wn	stdWn	C	stdC	sigC
0	1799	1	0.5184	1.0003	-0.0028	0.0828	0.5212	1.0040	0.5193
500	20968	19	1.0074	0.2295	-0.0901	0.0884	1.0975	0.2460	4.4625
1000	43135	47	1.1920	0.1459	-0.2831	0.1000	1.4751	0.1770	8.3395
1500	66757	67	1.1097	0.1222	-0.4456	0.1118	1.5553	0.1660	9.3904
2000	88200	81	1.0208	0.1112	-0.5795	0.1231	1.6003	0.1660	9.6468
2500	109625	98	0.9939	0.1011	-0.8152	0.1429	1.8091	0.1750	10.3349
3000	**130840**	**118**	**1.0027**	**0.0921**	**-1.2743**	**0.1857**	**2.2770**	**0.2070**	**10.9849**
4000	171774	134	0.8575	0.0864	-1.9366	0.2774	2.7941	0.2910	9.6168
5000	208793	138	0.6917	0.0852	-2.1582	0.3333	2.8499	0.3440	8.2842
7500	284074	145	0.4331	0.0831	-3.2765	0.7071	3.7096	0.7120	5.2104
9000	315680	147	0.3413	0.0825					
shear zones									
Distance buffer(m)		npixbd	Wp	stdWp	Wn	stdWn	C	stdC	sigC
0	5008	4	0.8811	0.5002	-0.0163	0.0836	0.8974	0.5070	1.7695
500	54423	49	1.0010	0.1429	-0.2748	0.1010	1.2758	0.1750	7.2907
1000	**101082**	80	0.8720	0.1118	-0.5275	0.1222	1.3995	0.1660	8.4497
1500	**142125**	**110**	**0.8496**	**0.0954**	**-0.9939**	**0.1644**	**1.8435**	**0.1900**	**9.6988**
3000	233438	139	0.5872	0.0848	-2.1653	0.3536	2.7525	0.3640	7.5696
4000	257811	141	0.4242	0.0842	-2.2109	0.4083	2.6351	0.4170	6.3208
5000	317228	143	0.3088	0.0836	-2.3511	0.5000	2.6599	0.5070	5.2470
6000	348796	145	0.2277	0.0831	-2.7579	0.7071	2.9856	0.7120	4.1935
6500	**362071**	147	0.2041	0.0825					
Alteration zones									
Distance buffer(m)	npixb	npixbd	Wp	stdWp	Wn	stdWn	C	stdC	sigC
0	80151	65	0.8963	0.1241	-0.3847	0.1104	1.2810	0.1660	7.7123
500	**103443**	**80**	**0.8487**	**0.1118**	**-0.5206**	**0.1222**	**1.3693**	**0.1660**	**8.2674**
1000	126627	90	0.7642	0.1054	-0.6117	0.1325	1.3760	0.1690	8.1272
1500	148890	100	0.7076	0.1000	-0.7319	0.1459	1.4395	0.1770	8.1382
2000	170009	109	0.6611	0.0958	-0.8703	0.1622	1.5314	0.1880	8.1294
3000	211205	121	0.5485	0.0909	-1.0868	0.1961	1.6353	0.2160	7.5658
4000	248981	133	0.4785	0.0867	-1.5288	0.2673	2.0073	0.2810	7.1432
5000	280230	139	0.4043	0.0848	-1.9137	0.3536	2.3181	0.3640	6.3750
7500	338879	144	0.2496	0.0834	-2.4511	0.5774	2.7007	0.5830	4.6293
10000	381419	146	0.1451	0.0828	-3.0308	1.0000	3.1759	1.0030	3.1651
12500	412452	146	0.0668	0.0828	-2.3452	1.0000	2.4120	1.0030	2.4038
15000	432621	147	0.0259	0.0825					
Foliation and s-fabric									
Distance buffer(m)	npixb	npixbd	Wp	stdWp	Wn	stdWn	C	stdC	sigC
0	14864	4	0.2086	0.5001	-0.0065	0.0836	0.2151	0.5070	0.4242
1000	202198	93	0.3276	0.1037	-0.3928	0.1361	0.7203	0.1710	4.2097
2000	**259712**	**120**	**0.2766**	**0.0913**	**-0.8191**	**0.1925**	**1.1458**	**0.2130**	**5.3782**
3000	296774	131	0.2864	0.0874	-1.1116	0.2500	1.3980	0.2650	5.2787
4000	325687	136	0.2309	0.0858	-1.2667	0.3015	1.4976	0.3130	4.7775
5000	350336	138	0.1725	0.0851	-1.2325	0.3333	1.4050	0.3440	4.0844
6000	399304	138	0.1115	0.0851	-0.9622	0.3334	1.0737	0.3440	3.1204
9000	426215	142	0.0247	0.0839	-0.5269	0.4473	0.5517	0.4550	1.2123
12000	438069	142	-0.0187	0.0839	0.7697	0.4474	-0.7884	0.4550	-1.7320
15000	442398	147	0.3413	0.0825					
Granite-greenstone contact									
Distance buffer(m)	npixb	npixbd	Wp	stdWp	Wn	stdWn	C	stdC	sigC
0	1982	1	0.4215	1.0003	-0.0024	0.0828	0.4239	1.0040	0.4223
1000	39110	20	0.4350	0.2237	-0.0541	0.0887	0.4891	0.2410	2.0325
2000	**74555**	**42**	**0.5318**	**0.1543**	**-0.1527**	**0.0976**	**0.6845**	**0.1830**	**3.7491**
3000	105521	48	0.3178	0.1444	-0.1240	0.1005	0.4418	0.1760	2.5112
4000	133521	56	0.2366	0.1337	-0.1219	0.1048	0.3585	0.1700	2.1103
5000	158340	64	0.1996	0.1250	-0.1306	0.1098	0.3302	0.1660	1.9847
10000	**255855**	**121**	**0.3567**	**0.0909**	**-0.8740**	**0.1961**	**1.2307**	**0.2160**	**5.6939**
15000	332369	132	0.1820	0.0871	-0.9020	0.2582	1.0840	0.2720	3.9781
20000	412559	137	0.0479	0.0855	-0.4953	0.3163	0.5432	0.3280	1.6579
25000	427043	147	0.0390	0.0825					
Magnetic lineaments									
Distance buffer(m)	npixb	npixbd	Wp	stdWp	Wn	stdWn	C	stdC	sigC
0	6078	1	0.6994	1.0001	-0.0071	0.0828	0.7064	1.0040	0.7039
1500	214229	70	0.0131	0.1195	-0.0121	0.1140	0.0252	0.1650	0.1526
3000	**322823**	**127**	**0.1726**	**0.0888**	**-0.6964**	**0.2236**	**0.8689**	**0.2410**	**3.6116**
4500	377708	139	0.1058	0.0848	-1.0096	0.3536	1.1154	0.3640	3.0674
6000	406292	145	0.0751	0.0831	-1.8319	0.7071	1.9070	0.7120	2.6785
7500	422997	146	0.0417	0.0828	-1.9401	1.0000	1.9817	1.0030	1.9749
9000	432995	146	0.0183	0.0828	-1.2941	1.0000	1.3124	1.0030	1.3079
10500	438388	147	0.0127	0.0825					

npixb = No. of pixels where pattern is present

npixbd = No. of gold deposits in pattern

Entries in bold represent optimal spatial association

Note: for the granite-greenstone contact, the lower value of Sig C (3.7491) is chosen because of the assumption that not all the gold deposits are spatially associated with the granite-greenstone contact and that the distance for the highest value of Sig C at 10000m is too great for the granite-greenstone contact to have an effect on the spatial location of gold deposits.